UNIVERSITY OF RIJEKA

FACULTY OF BIOTECHNOLOGY AND DRUG DEVELOPMENT

Nada Birkić

Sepsis associated acute lung injury: role of lipid mediators and TRP channels

DOCTORAL THESIS

Rijeka, 2026

UNIVERSITY OF RIJEKA

FACULTY OF BIOTECHNOLOGY AND DRUG DEVELOPMENT

Nada Birkić

Sepsis associated acute lung injury: role of lipid mediators and TRP channels

DOCTORAL THESIS

Mentor: Associate professor Christian A. Reynolds, PhD

Rijeka, 2026

SVEUČILIŠTE U RIJECI
FAKULTET BIOTEHNOLOGIJE I RAZVOJA LIJEKOVA

Nada Birkić

Sepsom uzrokovana akutna ozljeda pluća: uloga lipidnih medijatora i TRP kanala

DOKTORSKI RAD

Mentor: Izv. prof. dr. sc. Christian A. Reynolds

Rijeka, 2026

Mentor: Associate professor Christian A. Reynolds, PhD

Doctoral thesis was defended ---- at the University of Rijeka, Faculty of Biotechnology and drug development, in front of Evaluation Committee:

1. prof. Jasminka Giacometti, PhD
2. prof. Ivana Munitić, PhD
3. prof. Morana Jaganjac, PhD

Acknowledgement

This work was supported by Croatian Science Foundation grants UIP-2020-02-2476 and DOK-2021-02-7992.

Abstract

Sepsis is a dysregulated systemic response to infection and remains a leading cause of mortality worldwide. Among its complications, sepsis associated lung injury (sALI) is the most frequent and closely linked to poor clinical outcomes. Beyond cytokine-driven inflammation, accumulating evidence suggests lipid mediators (LMs) as underappreciated drivers of pulmonary barrier failure in sALI. LMs are known modulators of transient receptor potential (TRP) channels expressed in non-neuronal lung cells. In endothelial and epithelial compartments, activation of TRP channels elevates intracellular Ca^{2+}, increases microvascular permeability, impairs alveolar fluid clearance, and promotes pulmonary edema. While cytokine driven inflammation in sepsis has been extensively studied, the role of LMs, particularly those derived from polyunsaturated fatty acids (PUFA), remains insufficiently defined. The aim of this dissertation was therefore to characterize LM dynamics in a rat model of intraperitoneal sepsis-fecal peritonitis (FP) in different time points (6h, 24h, 48h), determine their association with biochemical markers of lung injury, and evaluate their potential to modulate TRPV1 through *in silico* analyses.

A targeted liquid chromatography-tandem mass spectrometry (LC-MS/MS) method was optimized for the quantification of >100 structurally diverse LMs. Chromatographic refinement enabled baseline separation of critical regioisomers, while scheduled MRM acquisition enhanced sensitivity for low abundant analytes. Despite extensive optimization, only a subset of LMs was consistently quantified in plasma and lung tissue, reflecting their intrinsically low endogenous levels.

Using this method, we observed a rapid and selective systemic shift in linoleic acid (LA) derived LMs following FP. Plasma concentrations of LA derived 12,13-DiHOME and 9,10-DiHOME increased markedly at 6 h and 24 h, with partial normalization by 48 h. Similar early increase was detected for 13-oxoODE and 9,10-DiHODE, whereas other quantified LMs remained comparatively stable. Lung tissue LMs did not differ significantly across groups. Despite the absence of pulmonary edema, myeloperoxidase (MPO) expression increased at 6 h and 24 h following FP, indicating early neutrophil activation. Notably, plasma 12,13-DiHOME strongly correlated with lung MPO levels, linking systemic LA derived lipid dysregulation to early pulmonary inflammatory signaling.

To assess whether circulating LMs possess structural capacity to modulate transient potential vanilloid 1 (TRPV1) channel, molecular docking and molecular dynamics simulations were performed for 13 endogenous LMs previously reported to influence its activity. Docking validation with capsaicin in both open and closed channel conformations confirmed methodological accuracy. Most tested LMs formed stable

interactions within the vanilloid pocket, engaging key residues such as Tyr511 and Ser512. Several LMs demonstrated binding energies comparable to or stronger than capsaicin, supporting the notion that some LMs may act as endogenous TRPV1 modulators relevant to sepsis associated inflammation.

In summary, this work provides a comprehensive characterization of LM responses in experimental sepsis, demonstrating that systemic LA derived lipid shifts occur rapidly, precede overt lung injury, and correlate with biochemical markers of neutrophil activation. The findings highlight 12,13-DiHOME as promising early biomarker of septic inflammatory dysregulation and reveal structural compatibility between endogenous LMs and TRPV1. Together, these data establish a mechanistic framework linking LM dysregulation to early inflammatory pathways in sALI and lay the groundwork for future translational applications in sepsis diagnostics and pathophysiology.

Key words: Lipid mediators; LC-MS/MS; Sepsis associated lung injury; Fecal peritonitis; TRPV1

Sažetak

Sepsa je disregulirani sustavni odgovor na infekciju i jedan je od vodećih uzroka smrti u svijetu. Među njezinim komplikacijama, najčešće se javlja sepsom uzrokovano oštećenje pluća (sALI), koje je usko povezano s lošim kliničkim ishodima. Osim upale posredovane citokinima, sve je više dokaza da su lipidni medijatori (LM-ovi) nedovoljno prepoznati posrednici poremećaja plućne barijere u sALI. Poznato je da LM-ovi moduliraju aktivnost kanala prolaznih receptorskih potencijala (TRP) koji su izraženi u ne-neuronskim stanicama pluća. U endotelnim i epitelnim stanicama, aktivacija TRP kanala dovodi do porasta unutarstanične koncentracije Ca^{2+} te povećanja mikrovaskularne permeabilnosti, narušavanja alveolarnog klirensa tekućine i poticanja razvoja plućnog edema. Iako je uloga citokina u sepsi intenzivno proučavana, uloga LM-ova, osobito onih nastalih iz polinezasićenih masnih kiselina (PUFA) još uvijek nije dovoljno razjašnjena. Cilj ove disertacije stoga je karakterizirati promjene LM-ova u štakorskom modelu intraperitonealne sepse-fekalnom peritonitisu (FP) u različitim vremenskim točkama (6 h, 24 h, 48 h), odrediti njihovu povezanost s biokemijskim markerima oštećenja pluća te ispitati njihov potencijal za modulaciju TRPV1 ionskog kanala korištenjem *in silico* pristupa.

Razvijena je i optimizirana ciljana metoda tekućinske kromatografije spregnute sa spektrometrijom masa (LC–MS/MS) za kvantifikaciju više od stotinu strukturno različitih LM-ova. Kromatografske postavke omogućile su razdvajanje ključnih regioizomera, dok je uporaba zakazane MRM (*eng. scheduled MRM*) metode povećala osjetljivost za analite prisutne u vrlo niskim koncentracijama. Unatoč sveobuhvatnoj optimizaciji, samo je manji dio ciljanih LM-ova dosljedno kvantificiran u plazmi i plućnom tkivu, što odražava njihovu prirodno nisku endogenu zastupljenost.

Primjenom ove metode pokazano je da FP izaziva brzu i selektivnu sistemsku promjenu LM-ova izvedenih iz linolne kiseline (LA). Koncentracije 12,13-DiHOME i 9,10-DiHOME u plazmi značajno su porasle nakon 6 i 24 sata, uz djelomičan povratak prema početnim vrijednostima nakon 48 sati. Sličan rani porast zabilježen je za 13-oxoODE i 9,10-DiHODE, dok su ostali LM-ovi ostali relativno stabilni. U plućnom tkivu nisu utvrđene značajne razlike između septičnih i kontrolnih životinja. Unatoč izostanku plućnog edema, ekspresija mijeloperoksidaze (MPO) bila je značajno povišena 6 i 24 sata nakon indukcije sepse, što ukazuje na ranu aktivaciju neutrofila. Važno je istaknuti da je koncentracija 12,13-DiHOME u plazmi snažno korelirala s razinama MPO u plućnom tkivu, povezujući sistemsku disregulaciju LA izvedenih LM-ova s ranom upalnom aktivacijom pluća.

Kako bi se procijenilo posjeduju li cirkulirajući LM-ovi strukturni kapacitet za modulaciju TRPV1 kanala, provedene su molekulska dokiranja i simulacije molekulske dinamike za 13 endogenih LM-ova za koje je ranije pokazano da utječu na aktivnost TRPV1. Validacija metodologije provedena je dokiranjem kapsaicina u otvorenu i zatvorenu konformaciju TRPV1, što je potvrdilo pouzdanost simulacija. Većina ispitivanih LM-ova tvorila je stabilne interakcije unutar vaniloidnog džepa, uključujući ključne aminokiseline poput tirozina 511 (Tyr511) i serina 512 (Ser512). Nekoliko LM-ova pokazalo je energije vezanja usporedive ili čak povoljnije od kapsaicina, što podupire hipotezu da određeni LM-ovi mogu djelovati kao endogeni modulatori TRPV1 te potencijalno doprinijeti upalnim signalnim putovima relevantnima za sepsu i sALI.

Zaključno, ovaj rad pruža sveobuhvatnu karakterizaciju LM odgovora u eksperimentalnoj sepsi, pokazujući da se sistemske promjene LA izvedenih medijatora javljaju rano, prethode vidljivom oštećenju pluća i koreliraju s biokemijskim pokazateljima aktivacije neutrofila. Posebno se ističe 12,13-DiHOME kao mogući rani biomarkeri disregulacije u sepsi, dok strukturna kompatibilnost LM-ova s TRPV1 upućuje na nove mehanističke veze između lipidne signalizacije i upalnih putova. Ovi nalazi pružaju temelj za buduću translacijsku primjenu LM profila u ranom otkrivanju i dubljem razumijevanju sALI patofiziologije.

Ključne riječi: Lipidni medijatori; LC-MS/MS; Sepsom inducirano oštećenje pluća; Fekalni peritonitis; TRPV1

Contents

1.Introduction

Sepsis associated lung injury (sALI) is the most frequent and severe organ complication of sepsis, yet the biochemical mechanisms linking systemic inflammation to the onset of pulmonary dysfunction remain poorly defined. Lipid mediators (LMs), particularly those derived from polyunsaturated fatty acids (PUFAs), are increasingly recognized as key regulators of vascular permeability, immune cell activation, and inflammatory signaling, but their contribution to the development of sALI has not been adequately investigated. The present dissertation focuses on characterizing changes in the LM profile in a rat model of fecal peritonitis (FP) and determining their relationship to biochemical indicators of lung injury. The purpose and objectives of this research were to quantify LMs using a targeted liquid chromatography-tandem mass spectrometry (LC-MS/MS) method, define their temporal dynamics, examine their association with molecular markers of lung injury and investigate their potential interaction with the transient receptor potential vanilloid 1 (TRPV1) ion channel through *in silico* modeling. Given that dietary linoleic acid (LA) availability profoundly influences LM biosynthesis, we additionally examined how modulation of LA intake affects systemic LM profiles in rats to understand how baseline dietary status may shape LM responses to sepsis.

1.1. Sepsis

Sepsis is a severe life-threatening condition caused by a dysregulated host response to infection, often resulting in acute organ dysfunction and high mortality rates (Singer et al., 2016). The understanding of sepsis leads back to ancient medicine when the term sepsis was first introduced by Hippocrates in the fourth century B.C. describing a process of decay or decomposition of organic matter (Majno, 1991). Roman physicians later identified redness, swelling, fever, pain, and loss of function as the cardinal signs of inflammation (Stone, 2017), which remain clinically relevant today. In 1914, Schottmueller further characterized sepsis as a systemic host response to pathogenic microorganisms in the bloodstream, leading to widespread inflammation (Huang et al., 2019). Subsequent advances in microbiology, immunology, and intensive care have established sepsis as a complex, multifactorial condition.

Sepsis can be triggered by an infection starting anywhere in the body caused by wide spectrum of pathogens including bacteria, viruses, parasites and fungi (Huang et al., 2019). However, a causative organism can be identified in only two-thirds of patients, leaving a substantial proportion without identified pathogen (Rudd et al., 2020). A global study published in 2020 reported that sepsis affects approximately

49 million people annually and causes 11 million deaths, accounting for 20% of all global mortality (Rudd et al., 2020). Although the incidence of sepsis decreased between 1990 and 2017, it continues to impose a substantial healthcare and economic burden, particularly in low-income countries (Rudd et al., 2020). In addition to its high incidence and mortality, recent evidence shows that sepsis survivorship is associated with poor long-term outcomes, including cognitive impairment, stress-related and depressive disorders and an increased risks of dementia and cardiovascular events. Moreover, sepsis survivors experience higher rates of hospital readmission due to acute renal failure, recurrent infections and sepsis, as well as excess late mortality that cannot be explained by prior health status (Prescott et al., 2019).

Among the affected organs, the lungs are particularly vulnerable with pneumonia representing the leading cause of sepsis worldwide (Mayr et al., 2014). Moreover, sepsis is the most common cause of acute lung injury (ALI) often referred to as sALI (Rubenfeld et al., 2005; Sun et al., 2023). This condition is characterized by disruption of the alveolar-capillary barrier leading to impaired gas exchange and can rapidly progress to the most severe manifestation of the ALI spectrum, acute respiratory distress syndrome (ARDS) (Shi et al., 2022).

1.1.2. Sepsis pathophysiology

At the molecular level, sepsis is initiated by recognition of pathogen-associated molecular patterns (PAMPs), such as lipopolysaccharide (LPS), and damage-associated molecular patterns (DAMPs), released from injured or necrotic cells. These signals are detected by pattern recognition receptors (PRRs), e.g. toll-like receptors and NOD-like receptors expressed on innate immune cells including macrophages, neutrophils, and dendritic cells (H. Kumar et al., 2009; S. Kumar et al., 2013; Takeuchi & Akira, 2010). Engagement of PRRs activates NF-κB and other transcription factors, driving the production of inflammatory cytokines including tumor necrosis factor-α (TNF-α) and interleukin-1 (IL-1). Some PRRs also assemble inflammasome complexes which mediate caspase-1 dependent cleavage of pro-IL-1β and pro-IL-18 into their active cytokines (Lamkanfi & Dixit, 2014). Extensive cell death and microbial toxins together with mentioned proinflammatory mediators further exacerbate the release and recognition of DAMPs (Chousterman et al., 2017). This establishes a self-amplifying cascade of immune activation leading to hyperinflammatory phase characterized by a cytokine storm (Van Der Poll et al., 2017). The hyperinflammatory response promotes neutrophil adhesion to the endothelium, activates complement and the coagulation cascade, and induces

microthrombus formation, ultimately causing endothelial dysfunction, microvascular injury, and multi-organ failure (Van der Poll et al., 2021; Ward, 2004).

Under physiological conditions, immune activation is localized and followed by tissue repair and restoration of homeostasis (Van Der Poll et al., 2017). In sepsis, however, compensatory anti-inflammatory mechanisms are rapidly engaged (Hotchkiss & Karl, 2003). Anti-inflammatory cytokines such as IL-10 and transforming growth factor-β (TGF-β), together with regulatory T cells and myeloid derived suppressor cells, suppress effector functions to limit tissue injury (Delano & Ward, 2016). Although protective in the short term, this counter-regulation frequently overshoots, resulting in profound immunosuppression. Immunosuppression occurs alongside persistent inflammation and impairs both innate and adaptive immune responses, predisposing patients to secondary and nosocomial infections with worse long-term outcomes (Hotchkiss et al., 2013). Antigen presenting cells (APC) display reduced antigen-presenting capacity and endotoxin tolerance, neutrophils exhibit impaired chemotaxis and reduced production of reactive oxygen species (ROS) and cytokines leading to bacterial persistence and infectious complications. Extensive apoptosis of dendritic cells, T cells, and B cells further compromises immune function (Delano & Ward, 2016). Myeloid cells show decreased proinflammatory but increased anti-inflammatory cytokine production, notably IL-10 (Grailer et al., 2014). Splenocytes from deceased patients demonstrate marked loss of $CD4^+$ and $CD8^+$ lymphocytes, and lymphopenia during sepsis strongly correlates with secondary infections and poor long-term survival. Together, these alterations underpin a chronic immunosuppressive state that drives recurrent infections, viral reactivation, increased hospital readmissions, and diminished survival in sepsis survivors (Boomer et al., 2011).

1.1.3. Diagnostic criteria

To improve clinical recognition, international consensus conferences have repeatedly revised the definition of sepsis. Earlier conferences classified sepsis into sepsis, severe sepsis, and septic shock (Bone et al., 1992; Levy et al., 2003). First, sepsis was defined as infection accompanied by the systemic inflammatory response syndrome (SIRS; Table 1), while severe sepsis indicated additional organ dysfunction, hypoperfusion, or hypotension. Septic shock represented the most advanced stage, characterized by persistent hypotension despite adequate fluid resuscitation, often accompanied by perfusion abnormalities and high mortality (Bone et al., 1992; Levy et al., 2003). Although widely adopted, this stepwise classification was criticized for limited specificity and poor prognostic accuracy, which prompted further revisions.

The most recent and widely accepted definition, *Sepsis-3*, was published in 2016 by the Society of Critical Care Medicine (SCCM) and the European Society of Intensive Care Medicine (ESICM) (Singer et al., 2016). Sepsis is now defined as “life-threatening organ dysfunction caused by a dysregulated host response to infection”. This definition emphasizes that the syndrome results not only from the infection itself but from maladaptive host responses leading to organ failure. Notably, the term “severe sepsis” was removed, while the definition of septic shock was refined to include profound circulatory and metabolic abnormalities. Clinically, septic shock is now identified in patients requiring vasopressors to maintain a mean arterial pressure of ≥ 65 mmHg, with serum lactate > 2 mmol/L despite adequate fluid resuscitation (Singer et al., 2016).

In parallel, several scoring systems were introduced to improve recognition and prognostication. First described SIRS criteria (Bone et al., 1992) focused on signs of systemic inflammation but lacked specificity, as many non-infectious conditions can mimic described features. The Sequential Organ Failure Assessment (SOFA; Table 2) score was subsequently adopted to quantify organ dysfunction (Levy et al., 2003), while the simplified quick SOFA (qSOFA; Table 3) was proposed as a rapid bedside tool outside of intensive care, using three clinical parameters, hypotension, tachypnea, and altered mentation (Singer et al., 2016). Although qSOFA was intended to flag patients at risk of poor outcomes, its predictive validity has been questioned. Experts argue that qSOFA may have low sensitivity, leading to delayed recognition and treatment in some patients. Professional societies in the field, therefore, recommend applying SOFA, qSOFA, and SIRS in combination for risk stratification and monitoring, rather than using them as stand-alone diagnostic tools (Singer et al., 2016).

Overall, these evolving criteria reflect both the complexity of sepsis and the persistent challenges in achieving early and reliable diagnosis. The ongoing debates highlight the dynamic nature of the field, where definitions must continually adapt to emerging evidence and clinical realities.

Table 1. Criteria for systemic inflammatory response syndrome (SIRS). SIRS is present when ≥ 2 of the following criteria are met in the context of suspected or proven infection. Table adapted from Bone et. al, 1992.

Criterion	Threshold
Body temperature	> 38 °C or < 36 °C
Heart rate	> 90 beats/min
Respiratory rate	> 20 breaths/min or *$PaCO_2$ < 32 mmHg (4.3 kPa)
White blood cell count	> 12,000 /mm³ or < 4,000 /mm³ or > 10% immature forms

*$PaCO_2$, partial pressure of arterial carbon dioxide

Table 2. Description of Sequential Organ Failure Assessment (SOFA) scoring system. Scores from 0 to 4 are assigned for each of the six organ systems, with a higher score indicating worse organ dysfunction. Table adapted from Vincent et al., 1996.

		Score				
	Variable	**0**	**1**	**2**	**3**	**4**
Respiratory system	*PaO_2/FiO_2 (mmHg)	≥ 400	< 400	< 300	< 200	< 100
Coagulation system	Platelets ($\times 10^9$/L)	≥ 150	< 150	< 100	< 50	< 20
Hepatic system	Bilirubin (mg/dL)	< 1.2	1.2 - 1.9	2.0 - 5.9	6.0 - 11.9	≥ 12.0
Cardiovascular system (dose in µg/kg/min)	Hypotension/ vasopressors	**MAP > 70 mmHg	**MAP < 70 mmHg	Dopamine ≤ 5 or dobutamine (any dose)	Dopamine > 5 or epinephrine/ norepinephrine ≤ 0.1	Dopamine > 15 or epinephrine/ norepinephrine > 0.1
Central nervous system	***Glasgow Coma Scale (GCS)	15	13 - 14	10 - 12	6 - 9	< 6
Renal system	Creatinine (mg/dL) Urine output	< 1.2	1.2 - 1.9	2.0 - 3.4	3.5 - 4.9	≥ 5.0

	-	-	-	< 500 mL/day	< 200 mL/day

*PaO2, partial pressure of oxygen; FiO2, fraction of inspired oxygen

**MAP, mean arterial pressure

***Glasgow Coma Scale scores range from 3–15; higher score indicates better neurological function

Table 3. Criteria for the quick Sequential Organ Failure Assessment (qSOFA) score. qSOFA is used as a bedside tool to identify patients with suspected infection at increased risk of poor outcomes. A score ≥ 2 suggests high risk. Table adapted from Singer et al., 2016.

Criterion	Threshold
Respiratory rate	≥ 22 breaths/min
Systolic blood pressure	≤ 100 mmHg
Altered mentation	Altered mentation (GSC < 15)

1.1.4. Sepsis therapy

Sepsis management remains largely supportive, as no pharmacological therapy has consistently improved survival. Current management consists of infection control, hemodynamic stabilization, modulation of the host response and supportive care for organ function (Evans et al., 2021; Vincent, 2022). Infection control requires prompt administration of broad-spectrum antibiotics, ideally after cultures are obtained, and timely source control through drainage, debridement, or removal of infected devices. Hemodynamic management involves individualized fluid resuscitation, typically with crystalloids, followed by vasopressor therapy if hypotension persists. Adjunctive therapies remain limited, low-dose corticosteroids are recommended in refractory septic shock, and vasopressin may be used as a second-line vasopressor with potential renal benefits. Other interventions, such as extracorporeal blood purification or high-dose vitamin C, have not consistently demonstrated survival benefit. Organ support, including mechanical ventilation, oxygen supplementation and renal replacement therapy, is provided when respiratory or renal failure occurs (Vincent, 2022).

1.1.5. Rodent models of sepsis

Experimental models of sepsis differ in their ability to reproduce key pathophysiological features of the human disease (Cai et al., 2023). Sepsis in rodents can be generally developed by exogenous infusion of a toxin such as LPS (toxemia models) and infusion of pathogen or enabling the release of endogenous pathogens (polymicrobial infection models). The toxemia model, based on administration of LPS (systemic administration, typically intraperitoneal injection; single injection or continuous infusion), is widely used due to its simplicity and reproducibility and primarily reflects an acute inflammatory response, but does not fully mimic clinical sepsis. In contrast, polymicrobial models such as fecal slurry injection (intraperitoneal injection of a fecal suspension) or cecal ligation and puncture (CLP) (surgical ligation of the cecum followed by puncture to allow leakage of fecal content) induce intra-abdominal infection, progressive organ dysfunction, and more closely resemble the clinical course of abdominal sepsis. CLP is one of the regularly used and well-accepted sepsis models, however, there are several limitations of the model, including the difficulty in controlling cecal content release as well as inter- and intra-experimental variability in severity and mortality (Cai et al., 2023). Furthermore, several therapies developed based on the promising results obtained using CLP could not be translated to the clinic (Dejager et al., 2011).

In contrast to CLP, FP models enable induction of a polymicrobial intra-abdominal infection with a precisely controlled infectious burden (dose and concentration

controlled fecal slurry injection), resulting in high reproducibility and reduced inter-operator variability. FP induces diffuse peritonitis, systemic inflammation, and progressive multi-organ dysfunction, thereby capturing key pathophysiological features of human abdominal sepsis (Gonnert et al., 2011).

1.2. Sepsis associated acute lung injury (sALI)

Organ failure is a hallmark of sepsis and reflects the systemic consequences of a dysregulated host response. The kidneys, cardiovascular system and liver are frequently affected, however the lungs represent the most injured organ, and sepsis is the leading cause of sALI (V. Kumar, 2020). Presence of sALI and its severe manifestation ARDS, are associated with worse clinical outcomes in sepsis patients (Shi et al., 2022). Epidemiological data indicate that sepsis underlies approximately 75% of ARDS cases (Bellani et al., 2016), with sepsis-induced ARDS showing higher mortality compared to ARDS of other etiologies (Chen et al., 2019; Stapleton et al., 2005).

Efficient gas exchange in the respiratory system relies on the integrity of the alveolar-capillary barrier, composed of alveolar epithelial cells type 1 and type 2 (AT1 and AT2), the pulmonary microvascular endothelium, and the intervening interstitium (Y. Wang et al., 2018; West, 2009). sALI arises from disruption of this barrier through either direct pulmonary insults (e.g., pneumonia) or indirect injury originating outside the lung (Bellani et al., 2016). In direct sALI, the epithelium is the primary site of damage, characterized by activation of alveolar macrophages, neutrophil infiltration, and abundant release of pro-inflammatory cytokines and LMs (Herold et al., 2015). In indirect sALI, inflammatory mediators circulate to distant sites of the body, including lungs, compromising the alveolar-capillary barrier (Englert et al., 2019). Disruption of this barrier is initiated by pathogen-driven activation of alveolar macrophages and a cascade of inflammatory mediators, including cytokines and bioactive LMs (X. Zhou & Liao, 2021). Recruited neutrophils release proteases, ROS, and neutrophil extracellular traps, all contributing to epithelial and endothelial injury (Sun et al., 2023). Complement activation, further amplifies inflammation and promotes coagulopathy (Ward, 2004). Concurrent endothelial activation triggers intravascular coagulation and formation of microthrombi, impairing pulmonary microcirculation and worsening gas exchange (Simmons & Pittet, 2015). Additionally, programmed cell death pathways release DAMPs, perpetuating innate immune activation and barrier dysfunction (Hotchkiss et al., 2016).

The clinical and histological evolution of sALI is commonly described in three stages. In initial, exudative stage, infiltration of inflammatory cells increases alveolar

epithelial and endothelial permeability, resulting in leakage of protein-rich fluid into the alveolar spaces. The accumulation of fluid neutralizes pulmonary surfactant and increases alveolar surface tension, thereby reducing lung compliance. As a result, some parts of the lungs collapse while others remain more open, which on a chest X-ray looks like patchy shadows on both lungs. When patients are put on mechanical ventilation, the healthier areas may become overstretched while the stiffer ones stay underinflated, causing an uneven distribution of air. Because blood still flows through poorly ventilated areas, it does not get enough oxygen, leading to severe low blood oxygen levels (hypoxemia) (Varisco, 2011). In the second, proliferative phase, the lung responds to the initial damage with overactive tissue repair. Fibroblasts and fibroblast-like cells formed from injured epithelium drive tissue growth (G. Zhou et al., 2009) however, increased fibroproliferative response can worsen lung injury (Quesnel et al., 2010; Sanders et al., 2007). In third, fibrotic phase, the lung may either remodel and recover or progress to fibrosis. Successful remodeling leads to near normal lung function within months (Peters et al., 1989). On the other hand, failure to terminate the fibroproliferative response leads to persistent myofibroblast activity, disordered tissue remodeling, and progression to pulmonary fibrosis, which is associated with chronic respiratory impairment and increased late mortality (Varisco, 2011).

Despite growing evidence of bioactive LMs contributing to secondary lung injury in sepsis, cytokines remain the most extensively studied mediators of sepsis. Excessive release of pro-inflammatory cytokines, including TNF-α, IL-1β, and IL-6, results in endothelial activation, increased vascular permeability, and propagation of tissue damage (Qiao et al., 2024). In the lungs, these cytokines recruit neutrophils and macrophages, prolong their activation, and amplify oxidative and proteolytic injury. The extent of cytokine release correlates with severity of clinical outcomes. For instance, elevated IL-6 levels are associated with higher mortality (Shimazui et al., 2025; Varga et al., 2025), while TNF-α and IL-1β directly impair alveolar barrier function (Ganter et al., 2008; Tang et al., 2014). Although anti-inflammatory cytokines such as IL-10 are upregulated in parallel, they are often insufficient to counterbalance the overwhelming pro-inflammatory cytokine storm (J. Zhang et al., 2025).

1.2.1. sALI diagnosis and treatment

Importantly, various biomarker validation studies and numerous clinical trials specifically targeting ALI/ARDS, have failed to identify effective therapies, largely because study cohorts combine highly heterogeneous etiologies of lung injury, including penetrating traumas, aspiration of gastric contents, pneumonia, and

systemic infection under the umbrella of ALI/ARDS. Pooling such diverse conditions together obscures endotype specific drivers, producing inconsistent findings, limiting therapeutic translation, and leading to calls for increased endotyping studies in this area (Abraham, 2016). There is currently no method for early identification of those at greatest risk of sALI and only treatment options currently available are mechanical ventilation and oxygen supplementation. However, these interventions are often insufficient and can aggravate lung damage if not precisely applied.

Multiple studies have demonstrated that the plasma metabolomic profile of critically ill ALI/ARDS patients differs between survivors and non-survivors (Dalli et al., 2017; Langley et al., 2013; Rogers et al., 2014). However, it is unknown to what extent plasma metabolic profiling reflects the biology of disease progression. At least 6 prior studies have carried out plasma metabolic profiling in ARDS cohorts (Dalli et al., 2017; Izquierdo-Garcia et al., 2018; Rogers et al., 2021; Singh et al., 2015; Stringer et al., 2011; Viswan et al., 2019) and several have identified lipid molecules as key metabolites associated with ALI/ARDS. It is not surprising that metabolomic profiles of individuals with ALI secondary to local or systemic infection may differ drastically from those with ALI secondary to trauma or aspiration even when clinical phenotypes overlap. Such heterogeneity aligns with the broader endotyping paradigm proposed for ARDS, where identification of biologically distinct endotypes has been shown to explain divergent outcomes and heterogeneous responses to therapy (Calfee et al., 2014; Sinha et al., 2020).

Consistent with the idea that sALI may represent a pathophysiologically distinct form of ALI with specific molecular drivers, clinical trials investigating pharmacological interventions for specifically treating sALI have been performed, with limited success (Table 4).

Although the full pathophysiology of sALI remains incompletely understood, preclinical sepsis models consistently reproduce key features of the condition, including leukocyte infiltration, pulmonary edema, and impaired gas exchange (Table 5).

Table 4. Summary of clinical trials investigating pharmacological interventions for treating sALI/ARDS.

Study Title	Key Findings	Reference
A phase I trial of low-dose inhaled carbon monoxide in sepsis-induced ARDS	Patients who received inhaled carbon monoxide (iCO) had lower circulating mtDNA levels, suggesting a potential role in reducing DAMP-induced inflammation and limiting cellular damage in sepsis-induced ARDS. Precise administration of low-dose iCO is feasible, well-tolerated, and appears to be safe in patients with sepsis-induced ARDS.	(Fredenburgh et al., 2018)
Effect of aspirin on development of ARDS in at-risk patients presenting to the emergency department: The LIPS-A randomized clinical trial	In the LIPS-A randomized clinical trial, early administration of aspirin did not significantly reduce the incidence of ARDS in at-risk patients, including those with sepsis, compared to placebo.	(Kor et al., 2016)
Effect of ganciclovir on IL-6 levels among cytomegalovirus-seropositive adults with critical illness: A randomized clinical trial	Ganciclovir did not significantly affect IL-6 levels in cytomegalovirus (CMV)-seropositive adults with sepsis-associated respiratory failure but reduced CMV reactivation, shortened mechanical ventilation duration, and increased ventilator-free days.	(Limaye et al., 2017)

Rosuvastatin for sepsis-associated acute respiratory distress syndrome	Despite benefits in preclinical models, a randomized clinical trial of rosuvastatin versus placebo in sepsis-induced ARDS failed to show a difference in 60-day mortality and was stopped early for futility.	(JD et al., 2014)
Randomized clinical trial of a combination of an inhaled corticosteroid and beta agonist in patients at risk of developing the acute respiratory distress syndrome	This phase IIa study supports the safety and feasibility of initiating early inhaled budesonide/formoterol in patients at high risk of ARDS. Despite baseline imbalances between groups, treated patients showed improvement in the S/F* ratio as a surrogate measure of oxygenation. These preliminary findings justify evaluation in a larger, adequately powered trial focused on clinically meaningful endpoints, including ARDS prevention and reduced need for mechanical ventilation.	(Festic et al., 2017)

*S/F - the ratio of peripheral oxygen saturation (SpO_2), measured by pulse oximetry, to the fraction of inspired oxygen (FiO_2)

Table 5. Experimental rodent models of extrapulmonary sepsis and associated pulmonary outcomes.

Study	Extrapulmonary sepsis model	Species	Pulmonary outcomes measured	Main observation in lung pathology
(Peralta et al., 1993)	Cecal ligation and puncture (CLP)	Rat	Lung MPO, BAL protein, leukocyte oxidative activity in lungs	20× lung MPO rise 6 h post CLP procedure
(Stamme et al., 1999)	Fecal peritonitis (FP)	Mouse	BAL cytokines (TNF, IFN-γ), lung MPO, static lung compliance, BAL eicosanoids	Dose-dependent pulmonary inflammation accompanied by decreased lung compliance
(Fisher et al., 2012)	Fecal peritonitis	Mouse	Lung MPO, histology score, neutrophil infiltration, lung cytokines, wet/dry ratio, BAL protein, alveolar fluid clearance	Pulmonary injury marked by inflammation, edema, and loss of epithelial barrier function caused by FP
(Muniz et al., 2015)	Cecal ligation and puncture	Mouse	Lung leukocyte infiltration	Increased leukocyte infiltration into lungs after CLP procedure

(L. Zhang et al., 2018)	Colon ascendens stent peritonitis	Rat	Lung metabolic changes	Lung shows various metabolite shifts during sepsis
(Fallon et al., 2021)	Cecal peritonitis (CP)	Mouse (neonates)	Pulmonary edema, neutrophil influx, lung MPO	Marked increase in all measured pulmonary outcomes 24 h after CP procedure
(Bastarache et al., 2022)	Cecal peritonitis	Mouse	BAL cells, total BAL protein, wet/dry ratio	CP alone induces mild pulmonary alterations, whereas its combination with hyperoxia results in a pronounced acute lung injury
(Sharma et al., 2024)	Fecal peritonitis	Mouse (young vs aged)	Histological assessment of lung injury, MPO, cytokines in lung tissue homogenates	Elevated MPO and lung cytokine levels (IL-6, IL-10), higher histological injury scores after FP procedure
(Dibekoğlu et al., 2025)	Fecal peritonitis	Rat	Histopathological analysis, arterial blood gas analysis, arterial oxygen pressure and carbon dioxide pressure	Lung injury and impaired gas exchange caused by FP

1.3. Eicosanoids and related lipid mediators

While cytokines have long been considered a hallmark of systemic inflammation, eicosanoids and related LMs have received comparatively less attention. Yet, growing evidence highlights their crucial role in shaping the immune response. LMs (e.g. eicosanoids) are endogenous chemical signals that orchestrate responses to infection (Dennis & Norris, 2015). These bioactive LMs are derived from PUFAs, and LM signaling, like cytokine signaling, is extremely complex. Recent advances in mass spectrometry (MS) have enabled quantitative identification of numerous novel lipid species and LMs have emerged as important regulators of vascular permeability, interstitial edema, and impaired lung compliance. LMs and their diet-derived PUFA precursors contribute to both pro- and anti-inflammatory states across a wide range of diseases, including ARDS (Funk, 2001; Stephenson et al., 2017).

1.3.1. Polyunsaturated fatty acids (PUFA)

Fatty acids (FA) are major sources of energy and functional components of biological membranes in living organisms (Hulbert et al., 2014). They are made of hydrocarbon chains ending with a carboxyl group (-COOH) and occur in a wide variety of molecules such as oils, waxes, sterols, triglycerides (TG), and phospholipids (PL) (Guillou et al., 2010). PL are fundamental building blocks of cell membranes (Figure 1), and they consist of FA esterified to a glycerol backbone at the sn-1 and sn-2 positions, and a polar phosphate head group, attached at sn-3 position (Narváez-Rivas & León-Camacho, 2015). FA are generally classified according to the number of double bonds in their hydrocarbon chain as follows: saturated fatty acids (SFA) contain only single carbon-carbon bonds, monounsaturated fatty acids (MUFA) contain one double bond, while polyunsaturated fatty acids (PUFA) contain two or more double bonds (Wallis et al., 2002).

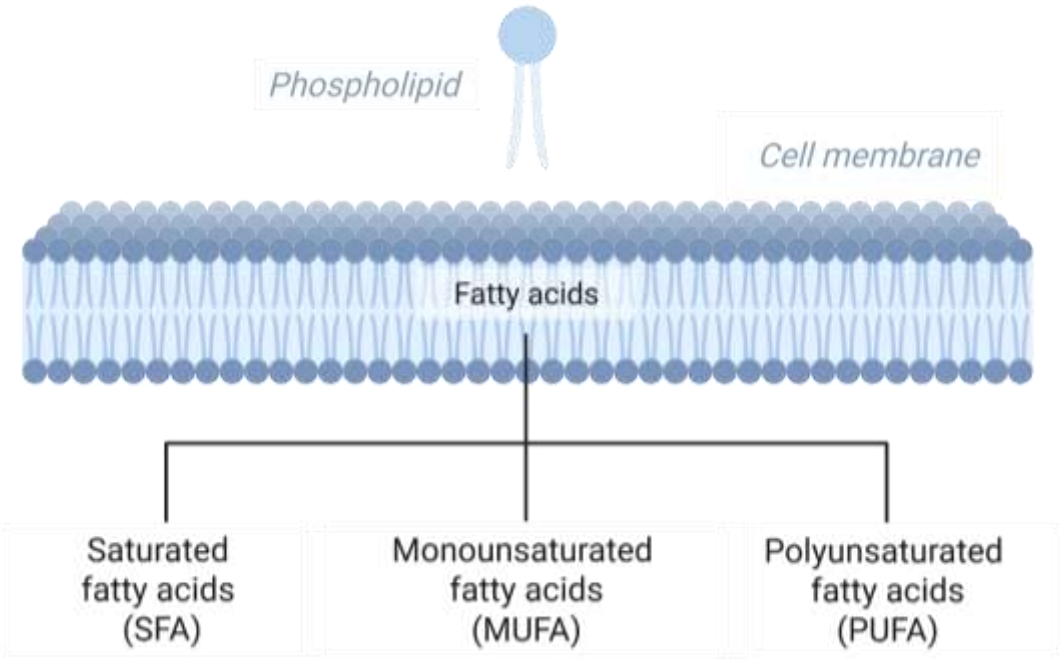

Figure 1. Structural organization of fatty acids within the phospholipid bilayer of the cell membrane. Phospholipids, the primary components of biological membranes, consist of a hydrophilic head and two hydrophobic fatty acid tails. These fatty acids can be classified according to their degree of saturation into saturated fatty acids, monounsaturated fatty acids, and polyunsaturated fatty acids, each contributing differently to membrane fluidity, flexibility, and overall biophysical properties.

PUFA are broadly divided into two main families, omega-3 and omega-6, which are named according to the position of the first double bond in their hydrocarbon chain, counted from the terminal methyl end (Figure 2). In most PUFA, the double bonds occur in a *cis* configuration and are regularly spaced at three-carbon intervals, meaning that each double bond is separated by a methylene group (-CH_2-). This structural regularity allows PUFA to be described simply by indicating the total number of carbon atoms, the number of double bonds, and the position of the first double bond closest to the terminal methyl carbon (Wallis et al., 2002).

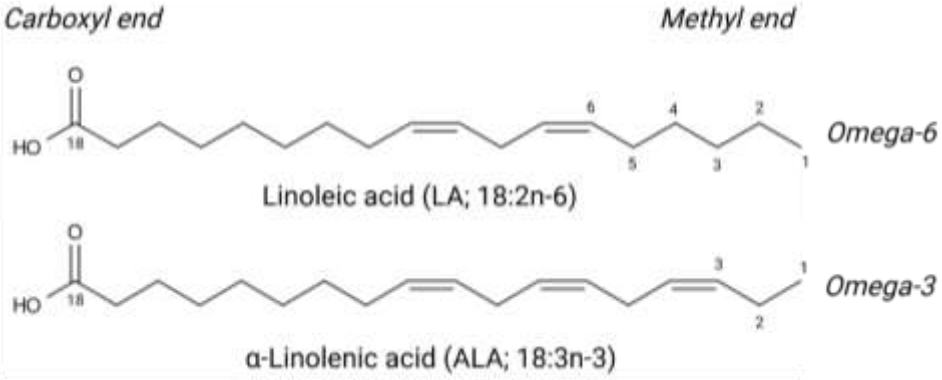

Figure 2. Nomenclature of essential PUFA, linoleic acid (18;2n-6) and α-linolenic acid (18;3n-3). The first number indicates the total number of carbon atoms (18), the number after the colon represents the number of double bonds, and the n-6 / n-3 refers to the position of the first double bond counted from the methyl (omega) end of the chain.

The essential PUFAs alpha linolenic acid (ALA; 18:3n-3) and linoleic acid (LA; 18:2n-6), and their long-chain derivatives, eicosapentaenoic acid (EPA; 20:5n-3), docosahexaenoic acid (DHA; 22:6n-3) and arachidonic acid (AA; 20:4n-6), are the major enzyme substrates for pro- and anti-inflammatory LM production. Sources of omega-6 FA include vegetable oils such as corn, safflower, and soybean oil, whereas the primary sources of omega-3 FA are oily fish such as salmon and tuna (Marszalek & Lodish, 2005). Both LA and ALA are considered essential FA in mammals because they meet two key criteria: animals cannot synthesize them *de novo* from other FA, and they play crucial roles in maintaining physiological functions. Therefore, they must be obtained through the diet, serving as precursors for the biosynthesis of their long-chain PUFA derivatives (Guillou et al., 2010; Simopoulos A P, 1999). Before agricultural revolution, human beings consumed a diet relatively low in PUFA and containing a roughly equal ratio of ALA:LA (Simopoulos A P, 1999), while the modern diet contains an abundance of LA, which accounts for > 85–90% of dietary PUFA (Blasbalg et al., 2011; Simopoulos A P, 1999). This has led some to hypothesize that dietary LA content may directly influence inflammation.

Recent studies using murine models have shown that direct administration of the AA and DHA can reverse biochemical alterations and physiological effects produced by essential FA deficiency. Accordingly, AA and DHA may also be regarded as “conditionally essential” FA (Le et al., 2013).

Once ingested, PUFA are incorporated into cell membranes through the esterification of their carboxyl groups with the hydroxyl groups of glycerol in PL. Upon hormonal stimulation or activation by growth factors acting on membrane receptors, the enzyme phospholipase A2 (PLA2) is activated and releases PUFA esterified at the sn-2 position of PL. Once liberated into the cytoplasm, these molecules serve as substrates for the biosynthesis of signaling compounds and LMs that exhibit diverse biological activities (Schmitz & Ecker, 2008).

PUFA can undergo oxygenation to generate numerous bioactive LMs (Brash, 1999). Among the best-studied classes of oxygenated mediators are the eicosanoids. Term *eicosanoid* refers to fatty acids containing 20 carbon atoms (from the Greek *eíkosa*), although in practice, the term is often used more broadly to also include shorter and longer PUFA derived metabolites with similar structures (Astarita et al., 2015; Buczynski et al., 2009). Eicosanoids and related LMs for the purpose of this thesis will be all together called LMs.

LMs are produced through enzymatic oxidation of PUFAs by four families of enzymes: cyclooxygenases (COX), lipoxygenases (LOX), epoxygenases and hydroxylases (CYP) (Figure 3) (Dennis & Norris, 2015). While COX products have historically dominated the field, since they collectively elicit the cardinal signs of inflammation including fever, swelling, redness, and pain (Dennis & Norris, 2015), hundreds of additional bioactive LMs are generated during infection (Dalli et al., 2017; Norris et al., 2014). Substantial epoxygenase metabolites can be produced by CYP P450 isoforms and accumulation of these metabolites is associated with respiratory distress and lung injury (Jia-Ning et al., 1988; Kosaka et al., 1994; Sevanian et al., 1979; Takayuki Ozawa et al., 1988; Zheng et al., 2001). Recent evidence indicates that accumulation of specific CYP derived LMs, the dihydroxy metabolites of LA (LA-DiHOMEs; 9,10-DiHOME and 12,13-DiHOME), directly contribute to lung injury and pulmonary dysfunction (Hildreth et al., 2020).

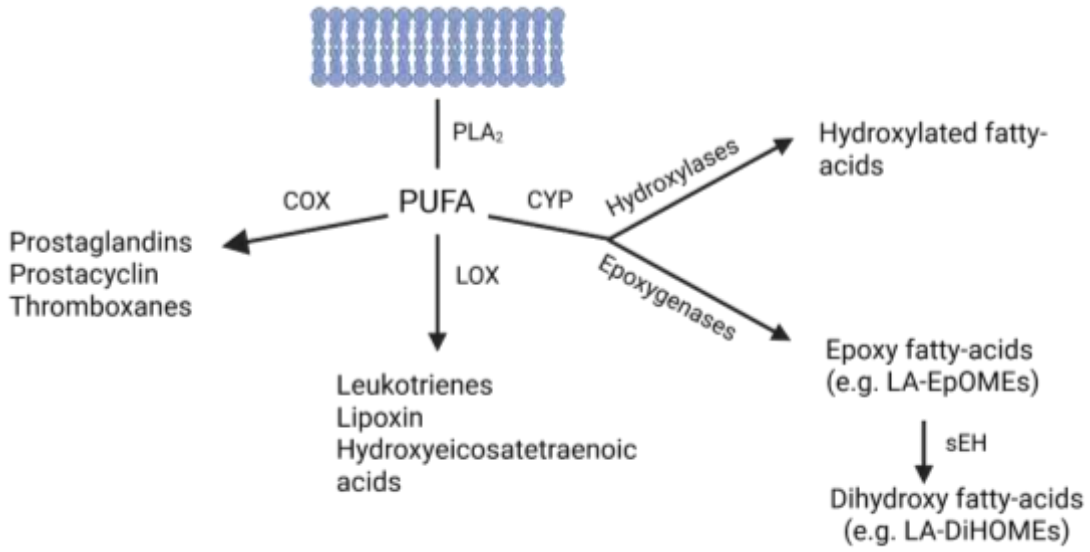

Figure 3. PUFA derived lipid mediator networks: enzymatic pathways and functional classes. Membrane phospholipids are hydrolyzed by PLA_2 to release PUFAs, which serve as substrates for three major enzymatic routes. The COX pathway generates prostanoids (prostaglandins and thromboxanes); the LOX pathway yields leukotrienes and hydroxy-eicosanoids and provides precursors for specialized pro-resolving mediators (e.g., lipoxins, resolvins, protectins, maresins); and the CYP P450) pathway forms epoxyeicosatrienoic acids (EETs) and ω-hydroxylated products (e.g., 20-HETE), sEH converting epoxides to corresponding diols (DHETs).

1.3.2. Lipid mediators in sALI

The involvement of CYP P450 derived LMs in sALI was first suggested in burn victims, where a circulating toxic factor originating from damaged skin was associated with late mortality, ARDS, and sepsis (Aoyama et al., 1982). Subsequent rodent burn studies isolated this compound (Suzuki et al., 1981), which was later identified as 9,10-epoxy-octadecenoic acid (9,10-EpOME) (Yokoo et al., 1986).

Furthermore, the term ″eicosanoid storm″ has been introduced to describe the massive release of eicosanoids and related LMs such as octadecanoids and docosanoids during infection and inflammation that parallel the well-known cytokine storm (Dennis & Norris, 2015). LMs are bioactive signaling lipids derived from PUFAs. The essential PUFAs, ALA and LA, and their long-chain derivatives,

eicosapentaenoic acid (EPA; 20:5n-3), DHA and AA are the major enzyme substrates for pro and anti-inflammatory LM production (Melissa Gabbs et al., 2015). LMs derived from COX and LOX pathways, such as prostaglandins and leukotrienes, are well-established drivers of inflammation and represent classical pharmacological targets exemplified by non-steroidal anti-inflammatory drugs (NSAIDs) and leukotriene receptor antagonists (Dennis & Norris, 2015). However, beyond these traditional targets, other LM producing pathways have gained increasing attention. In the case of sALI, various CYP-derived LMs have been implicated in sepsis-associated endothelial dysfunction, vascular leakage, and lung injury.

LA is the primary ω-6 PUFA obtained in the diet and is one of the most abundant FA found in the lipids of cell membranes in individuals consuming a Western diet (Simopoulos A P, 1999). In the CYP pathway, LA is coverted to epoxy-metabolites (LA-EpOMEs), namely 9(10)-EpOME and its regioisomer 12(13)-EpOME, which are then rapidly hydrolyzed by epoxide hydrolases (sEH) to the corresponding dihydroxy metabolites, 9(10)-DiHOME and 12(13)-DiHOME (LA-DiHOMEs) (Figure 4). These LA-EpOMEs are formed in tissues and are called leukotoxins because they produce their documented toxic effects against leukocytes (Kosaka et al., 1994; Takayuki Ozawa et al., 1988; Zheng et al., 2001). In addition to vasodilatory effects, they are also believed to exert toxicity on alveolar epithelial cells and cardiovascular tissues (Chiamvimonvat et al., 2007; Zheng et al., 2001). Experimental models have shown that CYP-derived LA metabolites can induce severe lung injury, promoting pulmonary capillary leak, interstitial edema, and impaired lung compliance (Jia-Ning et al., 1988; Kosaka et al., 1994; Sevanian et al., 1979; Takayuki Ozawa et al., 1988; Zheng et al., 2001).

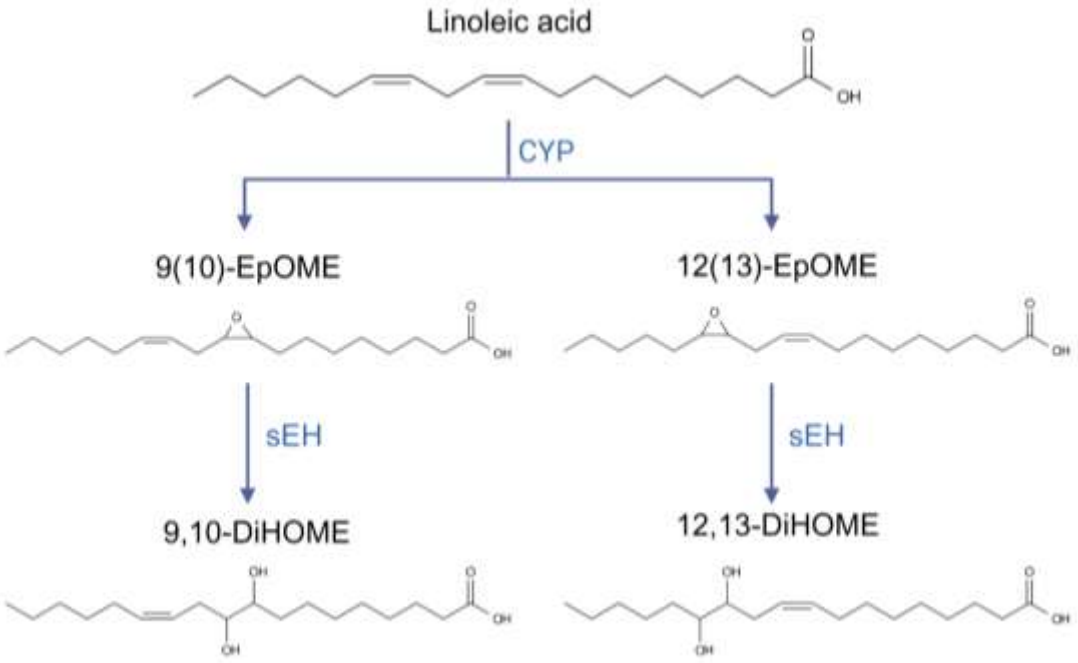

Figure 4. Metabolic conversion of linoleic acid to EpOMEs and DiHOMEs. Linoleic acid is oxidized by CYP P450 enzymes to form the epoxide regioisomers 9(10)- EpOME and 12(13)-EpOME, which are subsequently hydrolysed by sEH to their corresponding diols, 9,10-12,13-DiHOME and 12,13-DiHOME.

Consistent with these preclinical findings, clinical studies support a pathogenic role for LA-DiHOMEs in human ALI. A large retrospective cohort study of sepsis patients reported that the global profiling of 970 distinct metabolites in plasma could not fully differentiate patients with early sepsis with ARDS from those without ARDS, however, the LA-DiHOME, 12,13-DiHOME, was one of 43 metabolites, which included drugs related to intubation and mechanical ventilation (i.e., rocuronium, pantoprazole), that were higher in patients with ARDS, and one of 29 metabolites that were associated with disease severity based on Simplified Acute Physiology Score (SAPS) II (Rogers et al., 2021). Similarly, two independent studies have reported markedly elevated LA-DiHOME levels in COVID-19 patients with ARDS (Karu et al., 2022; McReynolds et al., 2021)

1.4. TRP channels and their pulmonary relevance

Expeditious, accurate recognition and intervention have been cited as one of the greatest barriers to compliance with the recommended standard of care for sALI (Burney et al., 2012; Kuo et al., 2012; Tsangaris et al., 2005). There has been slow but incremental progress in identifying biomarkers that (i) may directly contribute to the pathophysiology of ARDS, (ii) have utility in diagnosis and monitoring, and (iii) are potential therapeutic targets (Calfee et al., 2014). The lipid biomarkers discussed in this thesis may be poised to delineate a unique ALI/ARDS endotype, guide clinical intervention, and potentially serve as novel therapeutic targets. Among the emerging biochemical pathways linking LMs to sALI, the transient receptor potential (TRP) channels have recently gained substantial attention. These non-selective cation channels are expressed in non-neuronal lung tissue and directly modulated by bioactive LMs (Table 6).

Table 6. TRP channels and lipid mediators known to modulate their activity.

TRP Channel	Lipid mediator	Effect	Experimental model	Reference
TRPV1	9,10-DiHOME, 12,13-DiHOME, 9(10)-EpoME, 12(13)-EpOME	Activate	*In vitro*: Whole-cell patch-clamp and Ca^{2+} imaging in CHO-TRPV1 and rat trigeminal ganglion neurons *In vivo*: Mouse burn injury model	(Green et al., 2016)
	9-HODE, 13-HODE, 9-oxoODE, 13-oxoODE	Activate	*In vitro*: Ca^{2+} imaging, whole-cell and single cell patch-clamp, in trigeminal ganglion and CHO-TRPV1 cells *In vivo*: Intraplantar injection produced TRPV1-dependent nociceptive behavior and heat hyperalgesia (absent in $TRPV1^{-/-}$ mice)	(Patwardhan et al., 2009, 2010)
	20-HETE	Activate	*In vitro*: Whole cell patch- clamp, Ca^{2+} imaging in dorsal root ganglion (DRG) neurons and HEK cells	(Wen et al., 2012)
	5-HETE, 12-HPETE, 15-HPETE, 15-HETE,	Activate	*In vitro*: Whole-cell patch-clamp on cultured DRG neurons and VR1-transfected HEK cells	(Wook Hwang et al., 2000)

LTB4			
LXA4	Inhibit	*In vitro*: Ca^{2+} imaging in DRG cells In vivo: TiO_2-induced arthritis mice model	(Saraiva-Santos et al., 2023)
RvE1	Inhibit	*In vitro*: Ca^{2+} imaging, whole-cell patch-clamp in DRG neurons *Ex vivo*: Patch-clamp in spinal cord slices In vivo: Intrathecal RvE1 administration	(Z. Z. Xu et al., 2010)
RvD2	Inhibit	*In vitro*: Whole-cell patch-clamp recordings in DRG neurons *Ex vivo*: Spinal cord slices *In vivo*: Intrathecal RvD2 administration	(Park, Xu, et al., 2011)
Maresin 1	Inhibit	*In vitro*: Whole-cell patch-clamp in TG neurons *Ex vivo*: Patch-clamp in trigeminal nucleus slices *In vivo*: intraplantar MaR1 administration	(Park, 2015; Serhan et al., 2012)

	Neuroprotectin D1	Inhibit	*In vitro*: Whole-cell patch-clamp in DRG neurons *Ex vivo*: Mouse spinal cord slices *In vivo*: intrathecal NPD1 administration in mice	(Park, Lü, et al., 2011)
TRPV2	13-HODE	Activate	*In vitro*: Ca^{2+} imaging in HEK-293 cells overexpressing rat TRPV2	(De Petrocellis et al., 2012)
TRPV3	RvD1	Inhibit	*In vitro*: Ca^{2+} imaging and whole-cell patch-clamp in HEK293T-TRPV3 and HaCaT keratinocytes *In vivo*: Reduction of TRPV3-mediated heat and chemical pain behaviors	(Bang et al., 2010)
	17R-RvD1	Inhibit	*In vitro*: Ca^{2+} imaging and whole-cell patch-clamp in HEK293T-TRPV3 and HaCaT cells *In vivo*: Intraplantar injection of 17R-RvD1 reversed CFA-induced heat hyperalgesia and FPP-evoked pain	(Bang et al., 2012)
TRPV4	5,6-EpETrE, 8,9-EpETrE	Activate	*In vitro*: Ca^{2+} imaging and whole-cell/single-cell patch-clamp in TRPV4-	(Watanabe et al., 2003)

			transfected HEK-293 cells and primary mouse aortic endothelial cells	
	RvD1	Inhibit	*In vitro*: Ca^{2+} imaging and whole-cell patch-clamp TRPA1 transfected HEK293T cells and DRG neurons	(Bang et al., 2010)
TRPA1	9,10-DiHOME, 12,13-DiHOME, 9(10)-EpoME, 12(13)-EpOME	Activate	*In vitro*: Whole-cell patch-clamp and Ca^{2+} imaging in transfected CHO-TRPA1 cells and rat TG neurons	(Green et al., 2016)
	9-HODE, 13-HODE	Activate	*In vitro*: Ca^{2+} imaging and patch-clamp	(De Petrocellis et al., 2012)
	5,6-EpETrE	Activate	*In vitro*: Ca^{2+} imaging in mouse DRG neurons *Ex vivo*: Patch-clamp in spinal cord slices *In vivo*: Intrathecal 5,6-EpETrE caused TRPA1- dependent mechanical allodynia in mice (absent in $TRPA1^{-/-}$ mice)	(Sisignano et al., 2012)
	LXA4	Inhibit	*In vitro*: calcium imaging in DRG cells *In vivo*: TiO_2-induced arthritis model in mice	(Saraiva-Santos et al., 2023)

RvD1	Inhibit	*In vitro*: Ca^{2+} imaging and whole-cell patch-clamp in TRPA1-expressing HEK293T and DRG neurons *In vivo*: Intradermal RvD1 alleviates TRPA1 channel-mediated acute nociception in mice	(Bang et al., 2010)

TRP channels are a family of ion channels that regulate calcium (Ca^{2+}) and sodium (Na^{+}) influx in response to mechanical, thermal and chemical stimuli (Caterina et al., 1997; Tominaga et al., 1998). They are classified into six subfamilies: TRPC (canonical), TRPV (vanilloid), TRPM (melastatin), TRPA (ankyrin), TRPP (polycystin), and TRPML (mucolipin) (Yue & Xu, 2021). TRP channels consist of intracellular N- and C-termini, six membrane-spanning helices (S1–S6), and a pore-forming loop between S5 and S6 (Cao et al., 2013). In the lungs, TRP channels are implicated in regulating endothelial permeability, immune cell recruitment, and cytokine production (Prandini et al., 2016; Weissmann et al., 2012).

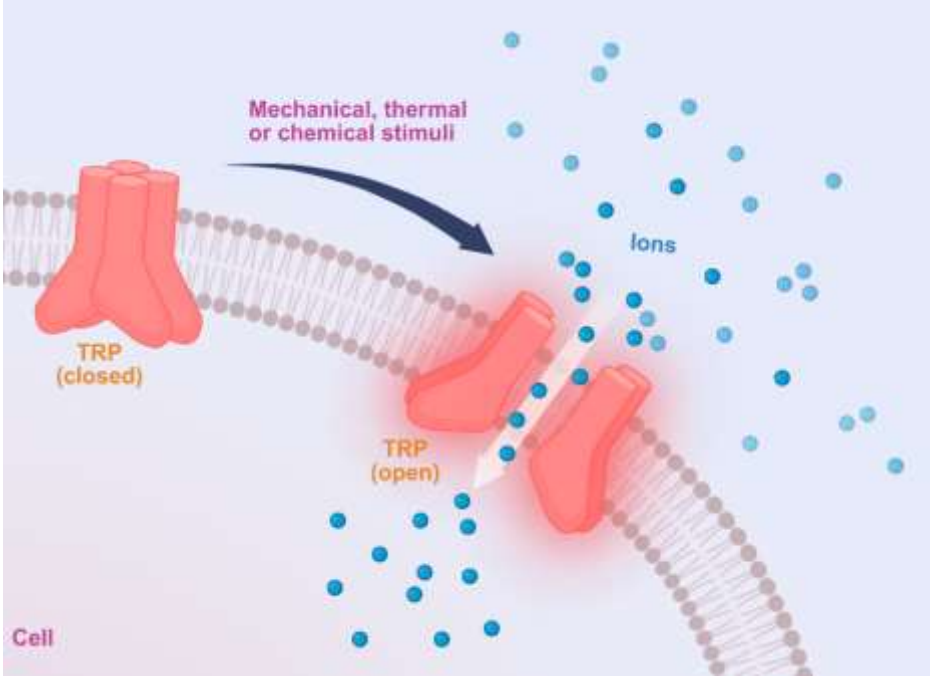

Figure 5. Schematic representation of TRP channel activation. TRP channels transition from a closed to an open state in response to mechanical, thermal, or chemical stimuli enables cation influx across the plasma membrane.

TRP channels are expressed in various non-neuronal lung cells including bronchial epithelial cells, airway smooth muscle cells, AT1) and AT2 cells, alveolar macrophages, precapillary arterial smooth muscle cells and endothelial cells. Dysregulation of these channels can contribute to the pathogenesis of respiratory diseases, including ALI/ARDS by promoting inflammation and reducing cell barrier function. In lung pathophysiology, particular focus has been on TRPA, TRPC, and

TRPV channels which are modulated by inflammatory LMs. Their location and function in non-neuronal lung tissue are reviewed in Table 7.

Table 7. TRP channels expressed in non-neuronal (lung) tissue and their location and function.

TRP Channel	Location in non-neuronal (lung) tissue	Key roles in lungs
TRPA1	Bronchial epithelial cells, alveolar epithelial cells, fibroblasts, macrophages, neutrophils	Upregulated by inflammatory cytokines in human lung epithelium; responds to chemical irritants/oxidants; contributes to airway inflammation, cough/bronchoconstriction (Belvisi & Birrell, 2017; Luostarinen et al., 2023; Müller et al., 2022; M. Xu et al., 2019)
TRPC1	Lung microvascular endothelial cells	Loss of TRPC1 disrupts adherens junction and induces endothelial hyperpermeability (Tauseef et al., 2016)
TRPC6	Pulmonary arterial smooth muscle cells, lung endothelial cells, alveolar macrophages	Regulates Ca^{2+} dependent vascular tone; contributes to vascular permeability (Jain et al., 2021; Weissmann et al., 2012)
TRPV1	Bronchial fibroblasts, lung epithelial cells, arterial smooth muscle cells, macrophages, neutrophils	Detects inhaled toxicants, inflammatory; promotes neurogenic inflammation and bronchoconstriction (Dietrich, 2019)
TRPV4	Alveolar epithelial cells, lung endothelial cells, airway smooth muscle cells, macrophages	Regulates endothelial barrier function, contributes to vascular permeability and lung edema (Schaller et al., 2024; Sonkusare & Laubach, 2022)

TRPM2	Macrophages	ROS sensor influencing cytokine/chemokine production (Mortadza et al., 2015; Rajan et al., 2024)

TRP family members described in table 7 have been directly implicated in lung injury progression. The involvement of these channels in pathogenesis of sALI is substantiated by experimental studies demonstrating that their pharmacological or genetic inhibition can attenuate pulmonary edema and barrier dysfunction.

Notably, TRPC6 contributes to vascular tone regulation and neutrophil chemotaxis, with its overactivation increasing endothelial permeability and pulmonary edema (Damann et al., 2009; Lindemann et al., 2013). Moreover, selective TRPC6 inhibition, for example with larixyl derivatives, has been shown to mitigate pulmonary edema (Weissmann et al., 2012). Similarly, TRPC6 deletion confers lung protection in experimental rodent models of sepsis (Tauseef et al., 2012; M. Wang et al., 2023).

TRPV4, discovered in 2000, is an osmosensitive and heat-sensitive channel found in various tissues, including airway smooth muscle cells and endothelial cells. TRPV4 plays a crucial role in lung physiology by regulating vascular tone, ciliary movement, and pulmonary barrier function. TRPV4 activation disrupts the alveolar barrier, contributing to lung edema and acute lung injury. It also plays a role in regulating blood flow in the pulmonary vasculature (Alvarez et al., 2006).

TRPA1's role in the non-neuronal lung tissue is less understood, with most research focusing on its presence in neuronal tissues where it’s co-expressed with TRPV1 channel. As TRPA1 is activated by inflammatory mediators such as histamine and prostaglandins it’s believed that it can mediate airway inflammation. In vitro experiments have shown that hyperoxia induced increase in intracellular Ca2+ was absent in TRPA1-/- non neuronal cells from tracheae, bronchi, and alveoli compared to the wild type cells. Despite evidence of non-neuronal activation of TRPV1 in airway inflammation, other functions of this channel are still poorly understood (Nassini et al., 2012).

Finally, TRPV1, the first cloned member of the vanilloid family, which is best known for its role in sensory neurons, is also found in lung epithelial cells, where it detects toxic inhalants and regulates inflammation. TRPV1, amplifies neurogenic inflammation and cytokine release in the lung microenvironment when activated by toxic inhalants or inflammatory mediators (M. Xu et al., 2019). It has also been implicated in asthma and chronic obstructive pulmonary disease (COPD), and TRPV1 antagonists have shown promise in reducing airway hyperresponsiveness and inflammation in experimental models of asthma.

1.4.1. Lipid mediators and their modulation of TRP channels

The interaction of inflammatory LMs with TRP channels has most widely been studied in the context of inflammatory pain conditions, due to the predominate expression of these channels on sensory nerves. Table 6. summarizes know LM-TRP channel interactions associated with the activation, inhibition, or sensitization of nociception. While the influence of LMs on nociception via interaction with TRP channels has been well characterized, recent evidence suggests that LM-TRP cannel interactions exert important pathophysiological roles in non-neuronal tissues (e.g. the lung).

The AA derivatives 12-HpETE, 15-HpETE, 5-HETE, 15-HETE and LTB4, activate TRPV1 channel with similar potencies as it's natural agonist capsaicin, and this activation is blocked by capsazepine, a TRPV1 antagonist (Wook Hwang et al., 2000). Another AA metabolite, 20-HETE, not only activates but sensitizes TRPV1 (Wen et al., 2012b). Interestingly, ω-3 PUFA derivatives such as 20-HEPE (from EPA) and 22-HDoHE (from DHA) display higher efficacy in TRPV1 activation in vitro than 20-HETE yet fail to induce pain behaviors in murine models.

LA derived LMs, 9-HODE, 13-HODE, 9-oxoODE and 13-oxoODE also activate TRPV1 leading to acute pain and thermal hyperalgesia (Patwardhan et al., 2010). In vivo, these effects are abolished in TRPV1-deficient mice or by pharmacological antagonists (Patwardhan et al., 2010). In addition, both 9-HODE and 13-HODE were reported to activate TRPA1, while 13-HODE has been reported to activate TRPV2 (De Petrocellis et al., 2012). The epoxy- and dihydroxy- metabolites of CYP-LA metabolism, 9, 10-DiHOME, 12,13-DiHOME, 9(10)-EpOME and 12(13)-EpOME activate both TRPV1 and TRPA1 *in vitro* and *in vivo* (Green et al., 2016).

Interestingly, administration of ketoconazole, a general CYP inhibitor, significantly reduced LA-derived DiHOMEs and EpOMEs concentrations in neuronal tissues in a burn injury pain model. Both ketoconazole treatment and TRPV1/TRPA1 antagonism reversed post-burn hypersensitivity, supporting the role of CYP-generated LMs in TRPV1/TRPA1 activation and pain sensitization (Green et al., 2016). Interestingly, three clinical studies have suggested that ketoconazole may be effective in preventing the development of lung injury in high-risk critically ill patients (G J Slotman et al., 1988; M Yu & G Tomasa, 1993; Sinuff et al., 1999). However, the use of ketoconazole as a treatment for inflammatory respiratory disease was not widely adopted after the Ketoconazole and Respiratory Management in Acute Lung Injury and ARDS (KARMA) Trial, found no significant benefit in a large multicenter clinical trial (Thompson, 2000). However, the KARMA Trial enrolled patients with

very heterogeneous lung injury etiologies including, those resulting from penetrating trauma, or aspiration of gastric contents.

Recent studies have shown that various pro-inflammatory LMs activate TRPV1 with similar potencies as capsaicin, and this activation is blocked by capsazepine, a TRPV1 antagonist (Hwang et al., 2000). Given that capsazepine blocks the activation of TRPV1 by capsaicin, this suggests these LM ligands might bind the channel in a similar manner as capsaicin. Moreover, TRPV4 is, for instance, modulated by PUFA metabolites including epoxyeicosatrienoic acids (EETs) (Watanabe et al., 2003). TRPV4 activation by EETs increases endothelial permeability and promotes alveolar edema (Alvarez et al., 2006; Jian et al., 2008).

In contrast to these pro-inflammatory LMs, various anti-inflammatory LMs may act as potent endogenous inhibitors of TRP channels. Notably, resolvin D1 (RvD1) inhibits TRPA1, TRPV3, and TRPV4, attenuating agonist-induced acute pain and reversing hypersensitivity in inflamed tissues (Bang et al., 2010). Resolvin D2 (RvD2) emerges as a potent inhibitor of both TRPV1 and TRPA1, abolishing inflammation-induced synaptic plasticity and reversing both acute and chronic inflammatory pain. Resolvin E1 (RvE1), in turn, selectively inhibits TRPV1 and reduces TRPV1-driven pain behaviors (Park, Xu, et al., 2011). Importantly, maresin 1 (MaR1), a DHA derived LM produced by macrophages, also dose-dependently inhibits TRPV1, blocks capsaicin-induced responses, and reduces both inflammation and chemotherapy induced neuropathic pain (Serhan et al., 2012).

Although, various LMs are known to influence nociception via interaction with TRP channels, recent evidence suggests that TRP roles go beyond that. Non-neuronal TRP channels in the lung epithelium and endothelium are directly modulated by LMs, thereby linking LM signaling to barrier integrity.

1.4.2. Therapeutic implications of TRP channel modulation in sALI

TRP channel modulation presents a promising therapeutic strategy for treating sALI. Channels like TRPV1 and TRPV4 play critical roles in regulating inflammation and vascular permeability, making them key targets in addressing the pathophysiological mechanisms underlying sALI. Inhibitors of TRPV1 and TRPV4, for instance, have shown protective effects in experimental models by reducing calcium influx, which in turn mitigates the inflammatory response and lung damage.

One potential therapeutic approach is the use of TRP channel inhibitors in combination with LM targeting, such as COX and LOX inhibitors. This combined strategy may provide synergistic benefits by simultaneously controlling inflammation and reducing lung injury. Additionally, modulating specialized TRP channels offers

the advantage of minimizing side effects that are typically associated with broader anti-inflammatory drugs.

TRPV4 has been identified as a critical regulator of lung endothelial barrier function. The TRPV4 blocker GSK2193874 has demonstrated efficacy in reducing lung edema in various experimental models, including those of sepsis, myocardial infarction, and acid aspiration. By preventing the stretch-induced activation of TRPV4, which results in increased endothelial permeability and capillary leakage, GSK2193874 holds potential as a therapeutic agent for pulmonary edema. Studies in TRPV4-deficient mice further support this approach, showing significant reductions in lung injury compared to controls.

TRPC6 also plays an important role in the development of lung edema. Its activation by lipopolysaccharides in septic patients, through the Toll-like receptor 4 pathway, leads to increased endothelial permeability and vascular dysfunction. Inhibiting TRPC6, particularly with selective blockers such as larixyl derivatives, has shown promise in reducing lung ischemia-reperfusion-induced edema (LIRE), which is a major cause of primary graft failure in lung transplantation. The inhibition of TRPC6 also limits calcium influx and endothelial damage caused by platelet-activating factor, further reducing pulmonary edema.

Moreover, a key element in targeting TRP channels for therapeutic purposes is preventing the conversion of EpOMEs to the more toxic DiHOMEs, which are associated with increased vascular permeability and lung injury. Inhibiting soluble epoxide hydrolase (sEH), the enzyme responsible for this conversion, could provide an additional therapeutic approach for mitigating lung damage in sALI.

2. Thesis aims and hypothesis

sALI arises from a dysregulated host response to infection and remains a major contributor to morbidity and mortality in sepsis. Mounting evidence indicates that bioactive LMs, particularly derived from LA, accumulate during systemic infection and contribute to secondary pulmonary injury through endothelial barrier disruption and increased vascular leak. In parallel, TRP channels have emerged as potential downstream effectors of lipid-mediated injury pathways. Since LMs and TRP channels both regulate inflammatory signaling and vascular permeability, their interplay may represent a mechanistic axis linking systemic inflammation to lung injury. Given that modern diets are enriched in LA, identifying modifiable lifestyle factors that influence inflammation are of a great value to the society.

Based on these observations, in this thesis we propose that LM profiles in rodent model of FP directly contribute to secondary lung injury by influencing TRP channels activity. Additionally we hypothesize that dietary interventions alter baseline concentration of plasma LMs based on the diet content (either high or low in LA). To test this hypotheses, we combined targeted LC-MS/MS method, *in vivo* experimental sepsis modeling, and computational chemistry approaches. Furthermore, we developed two rodent diets in which standard corn oil was replaced by two different custum made trygliceride blends.

The specific aims and hypotheses were following:

1. Optimizing a comprehensive targeted MS method for LM profiling. LMs represent a various structurally similar molecules with low endogenous abundance and high oxidation potential, necessitating sensitive and selective analytical approaches. To enable simultaneous separation and quantification of 100 LMs originating from COX, LOX, CYP pathways, we aimed to establish a targeted LC-MS/MS workflow. We hypothesised that a highly optimized multiple reaction monitoring (MRM) method together with improved sample preparation strategies and optimized liquid chromatography (LC) separation would enable reliable detection and quantification of a broad LM panel in both plasma and lung tissue.

2. Testing whether LA derived LMs contribute to pulmonary edema in a FP rodent model of sepsis. Given that LA-derived epoxides (EpOMEs) and their diol metabolites (DiHOMEs) accumulate during systemic infection and experimentally induce vascular leak and lung dysfunction, we aimed to determine whether these LMs are elevated *in vivo* during sepsis and whether their levels correlate with pulmonary edema formation. We hypothesized that septic rats would exhibit

significantly increased concentrations of LA derived LMs in plasma and lung tissue, and that these elevations would associate with increased wet/dry lung weight ratios indicative of edema.

3. Investigating TRPV1 channel interactions with LMs using computational chemistry. TRPV1, a well-characterized cation channel activated by heat, protons, and capsaicin, is increasingly recognized as a mediator of inflammatory barrier dysfunction. Previous studies suggest that LMs may modulate TRPV1 channel and downstream signaling pathways relevant to lung injury. We hypothesized that selected LMs including LA-DiHOMEs interact with the vanilloid binding pocket of TRPV1 in a manner comparable to, or distinct from, capsaicin, thereby providing a mechanistic basis for TRPV1 activation in sALI.

4. Testing how dietary intervention affects baseline profile of circulating LMs using custom made rodent diets. Given that modern diets are disproportionately enriched in LA, we aimed to determine how dietary FA composition shapes the circulating LM profile. We hypothesized that rats fed a high LA diet would exhibit substantial increases in circulating pro-inflammatory omega-6 LA and AA derived LMs, accompanied by reductions in omega-3 derived anti-inflammatory metabolites. To test this, we quantified plasma LM profiles in male and female rats raised on custom triglyceride-based diets enriched either in LA or in oleic acid (OA; control diet), from weaning through nine weeks of age.

3. Materials and Methods

3.1. Targeted LC-MS/MS lipidomic analysis

All analytical solvents were purchased from VWR Chemicals (Lutterworth, UK) unless stated otherwise. All analytical lipid standards and isotope-labeled internal standards (IS) were obtained from Cayman Chemical (Ann Arbor, MI, USA) as individuals or as a part of a mixture. Quantitative analysis of LMs in the collected plasma and tissue samples was carried out using an Acquity UPLC I-Class system (Waters, Milford, MA, USA) coupled to a Xevo TQD triple quadrupole mass spectrometer (Waters, Milford, MA, USA) equipped with an electrospray ionization (ESI) source. Data acquisition and processing were performed using TargetLynx software (Waters, Milford, MA, USA). Chromatographic separation was achieved on an Accura Triart C18 analytical column (150 × 2.1 mm, 1.9 µm, 12 nm pore size; YMC Co., Ltd., Kyoto, Japan) maintained at 45 °C. The mobile phase consisted of solvent A [0.1% ammonium acetate (Sigma-Aldrich, St. Louis, MO, USA) in water/methanol/acetonitrile (85:10:5, v/v)] and solvent B [0.1% ammonium acetate in water/methanol/acetonitrile (5:90:5, v/v)]. A linear gradient elution was applied as follows: 0–8 min, 50% to 80% B; 8–15 min, 80% to 95% B; 15–20 min, isocratic at 95% B; 20–21 min, return to 50% B; 21–26 min, isocratic at 50% B. The flow rate was 0.2 ml/min, the injection volume was 5 µl, and the autosampler was maintained at 10 °C. The mass spectrometer was operated in negative electrospray ionization (ESI-) mode using a scheduled MRM method. The following source parameters were applied: capillary voltage, 2.5 kV; source temperature, 150 °C; cone gas flow, 600 L/h; desolvation gas flow, 150 L/h; desolvation temperature, 450 °C. Nitrogen was used as both desolvation and collision gas.

3.1.1. Multiple reaction monitoring method optimization

MRM parameters were established by optimizing commercially obtained lipid standards. Because several standards were supplied as mixtures and shared identical precursor ions, direct injection could not be reliably used for optimization. Instead, all transitions were optimized on the column. For each standard and internal standards, a precursor ion and a characteristic product ion were selected to define MRM transition. Cone voltage (the source potential controlling ion transmission and in-source fragmentation) and collision energy (CE: the collision cell potential that drives gas-phase fragmentation with a neutral gas) were tested across predefined ranges using 5 µL injections, and the settings yielding the highest signal intensity were retained. Adjusting the cone energy helps optimize signal stability and intensity, as different compounds may require specific cone voltages to maximize ion production without causing excessive fragmentation. Adjusting the CE,

fragmentation is controlled and produces characteristic product ions, which are essential for compound identification and quantification in tandem mass spectrometry. As the final MRM panel comprised >100 precursor-product ion transitions, data were acquired in scheduled MRM mode to optimize dwell time and ensure enough points across each chromatographic peak. For each transition, the acquisition window was set as experimentally determined retention time (Rt) ± 0.5 min. Final precursor- product ion transitions and their optimized voltages are summarized in Table 9 and Table 10.

3.1.1.1. Lipid quantification

Absolute quantification was performed for analytes matching isotopically labeled IS available (Prostaglandin E1-d4, 15-HETE-d8, 9,10-DiHOME-d4, 12,13-DiHOME-d4, 9(10)-EpOME-d4 and 12(13)-EpOME-d4). For all other analytes, a surrogate internal-standard approach was applied: each analyte was assigned to the most appropriate deuterated IS based on the nearest retention time. The full analyte to IS assignment is provided in Table 11. A fixed amount of an IS mix was added to all calibration standards and to every sample to be used for normalization, recovery, and relative (or absolute) quantitation of each analyte. Calibration standards were prepared as a serial dilution of a master mix of the purchased lipid standards and injected in triplicate (5 µL). For each analyte, a calibration curve was constructed. Sample concentrations were obtained by interpolating their peak area on the corresponding calibration curve and applying any dilution factors and are reported as ng/mL for plasma and ng/mg tissue for lung samples.

Table 8. MRM parameters for MS/MS analysis of lipids. Shown are lipid standards, scan mode, m/z precursor, cone voltage, m/z fragment values, CE, retention times (Rt), linearity and lower limit of detection (LLOQ).

Lipid	Mode	*m/z* precursor ion	Cone /V	m/z fragments	CE/eV	Rt/min	Linearity /R2	Linear range (ng/mL)	LOQ (ng/mL)
8-iso PGF2α	-	353.2	26	193.1	27.00	3.3	0.991	27.7-250	27.70
TXB1	-	371.2	25	171.0	11.00	3.5	0.993	3.08-250	3.08
TXB3	-	367.2	24	195.2	11.00	3.6	0.992	3.08-250	3.08
TXB2	-	369.2	25	195.1	15.00	3.7	0.999	3.08-250	3.08
PGF2α	-	353.2	20	193.1	24.00	3.8	0.998	3.08-250	3.08
PGE3	-	349.2	26	269.1	16.00	4.1	0.992	3.08-250	3.08
8-iso PGE2	-	351.2	25	271.1	17.00	4.3	0.999	27.7-250	27.70
PGD3	-	349.2	25	269.1	15.00	4.6	0.985	9.25-250	9.25
PGE2	-	351.2	25	271.1	17.00	4.9	0.993	3.08-250	3.08
PGD2	-	351.2	20	271.1	12.00	5.3	0.997	9.25-250	9.25

PGE1	-	353.2	20	273.2	11.00	5.4	0.996	9.25-250	9.25
PGD1	-	353.3	25	317.3	14.00	5.4	0.994	3.08-250	3.08
Δ12-PGJ2	-	332.9	25	188.9	17.00	5.6	0.991	27.7-250	27.70
PGB2	-	333.2	25	174.9	20.00	5.7	0.994	9.25-250	9.25
17,18-DiHETE	-	335.2	26	247.1	16.00	8.0	0.991	9.25-250	9.25
14,15-DiHETE	-	335.2	30	207.1	16.00	8.2	0.993	3.08-250	3.08
11,12-DiHETE	-	335.2	30	167.1	16.00	8.4	0.997	3.08-250	3.08
12,13-DiHOME	-	313.1	40	183.1	21.00	8.5	0.995	3.08-250	3.08
9,10-DiHOME	-	313.1	36	200.9	20.00	8.6	0.991	3.08-250	3.08
8,9-DiHETE	-	335.2	32	185.0	18.00	8.9	0.992	9.25-250	9.25
14,15-DiHET	-	337.2	28	207.1	18.00	9.1	0.994	3.08-250	3.08
19.20-DiHDPA	-	361.2	28	273.2	15.00	9.3	0.998	83.3-250	83.30
13-HOTrE-gamma	-	293.2	25	193.1	11.00	9.3	0.997	27.7-250	27.70
9-HOTrE	-	293.3	25	171.1	13.00	9.4	0.995	9.25-250	9.25

16,17-DiHDPA	-	361.2	30	233.1	15.00	9.4	0.991	27.7-250	27.70
13-HOTrE	-	293.2	25	195.1	20.00	9.4	0.998	27.7-250	27.70
11,12-DiHET	-	337.2	30	167.1	18.00	9.5	0.990	9.25-250	9.25
13,14-DiHDPA	-	361.2	30	193.1	19.00	9.5	0.982	27.7-250	27.70
18-HEPE	-	317.2	28	259.1	12.00	9.6	0.985	27.7-250	27.70
5,6-DiHETE	-	335.2	26	145.1	20.00	9.7	0.995	27.7-250	27.70
15-HEPE	-	317.2	25	219.1	14.00	9.8	0.985	27.7-250	27.70
10,11-DiHDPA	-	361.2	30	153.2	17.00	9.8	0.993	27.7-250	27.70
11-HEPE	-	317.2	30	167.1	14.00	9.9	0.991	3.08-250	3.08
8-HEPE	-	317.2	30	155.1	13.00	10.1	0.991	27.7-250	27.70
8,9-DiHET	-	337.2	30	185.1	14.00	10.1	0.925	83.3-250	83.30
19-HETE	-	319.2	28	275.1	13.00	10.2	0.996	83.3-250	83.30
9-HEPE	-	317.2	18	149.1	12.00	10.3	0.917	83.3-250	83.30
15-OxoETE	-	317.2	20	219.1	15.00	10.3	0.876	83.3-250	83.30

13-OxoODE	-	293.2	32	178.6	22.00	10.3	0.991	9.25-250	9.25
20-HETE	-	319.2	16	275.1	15.00	10.4	0.995	83.3-250	83.30
7,8-DiHDPA	-	361.2	30	127.1	18.00	10.5	0.984	27.7-250	27.70
17(18)-EpETE	-	317.2	28	259.1	9.00	10.5	0.992	9.25-250	9.25
13-HODE	-	295.2	32	195.1	18.00	10.5	0.992	3.08-250	3.08
9-OxoODE	-	293.2	32	185.1	20.00	10.6	0.989	27.7-250	27.70
9-HODE	-	295.2	36	171.1	17.00	10.6	0.994	3.08-250	3.08
20-HDHA	-	343.2	20	241.1	11.00	10.6	0.987	27.7-250	27.70
5-HEPE	-	317.2	25	115.1	16.00	10.7	0.986	3.08-250	3.08
14(15)-EpETE	-	317.2	28	207.0	10.00	10.7	0.991	27.7-250	27.70
15-HETE	-	319.2	25	219.2	12.00	10.8	0.987	9.25-250	9.25
11(12)-EpETE	-	317.2	28	167.1	10.00	10.8	0.998	9.25-250	9.25
5,6-DiHET	-	337.2	30	145.1	16.00	10.9	0.998	27.7-250	27.70
17-HDHA	-	343.2	25	201.1	14.00	10.9	0.997	83.3-250	83.30

16-HDHA	-	343.2	26	233.1	15.00	10.9	0.984	27.7-250	27.70
13-HDHA	-	343.2	26	193.1	14.00	11.0	0.994	27.7-250	27.70
11-HETE	-	319.2	25	167.1	17.00	11.0	0.990	3.08-83.3	3.08
8(9)-EpETE	-	317.2	26	155.1	11.00	11.1	0.994	9.25-250	9.25
5-OxoETE	-	317.2	26	203.1	19.00	11.1	0.968	27.7-250	27.70
14-HDHA	-	343.2	26	161.1	15.00	11.1	0.999	27.7-250	27.70
12-HETE	-	319.2	26	179.1	14.00	11.2	0.984	3.08-83.3	3.08
10-HDHA	-	343.2	25	153.1	15.00	11.2	0.967	9.25-250	9.25
8-HETE	-	319.2	25	155.1	13.00	11.4	0.991	9.25-250	9.25
12(13)-EpOME	-	295.1	32	194.8	15.00	11.4	0.991	27.7-250	27.70
11-HDHA	-	343.2	25	121.1	14.00	11.4	0.998	27.7-250	27.70
9-HETE	-	319.2	30	151.1	11.00	11.6	0.987	27.7-250	27.70
19(20)-EpDPA	-	343.2	30	241.1	10.00	11.6	0.999	27.7-250	27.70
14(15)-EET	-	319.2	30	219.1	9.00	11.6	0.993	3.08-250	3.08

9(10)-EpOME	-	295.1	30	170.7	15.00	11.7	0.995	9.25-250	9.25
7-HDHA	-	343.2	26	141.1	10.00	11.7	0.994	27.7-250	27.70
8-HDHA	-	343.2	30	189.1	15.00	11.8	0.993	9.25-250	9.25
16(17)-EpDPA	-	343.2	26	274.4	10.00	11.9	0.991	83.3-250	83.30
13(14)-EpDPA	-	343.2	30	193.1	10.00	12.0	0.996	27.7-250	27.70
5-HETE	-	319.2	30	115.1	16.00	12.1	0.980	9.25-250	9.25
10(11)-EpDPA	-	343.2	30	153.1	10.00	12.1	0.991	9.25-250	9.25
11(12)-EET	-	319.2	28	167.1	12.00	12.2	0.993	3.08-250	3.08
8(9)-EET	-	319.2	28	155.1	10.00	12.4	0.993	27.7-250	27.70
7(8)-EpDPA	-	343.2	30	112.8	19.00	12.5	0.992	27.7-250	27.70
4-HDHA	-	343.2	25	101.1	15.00	12.5	0.995	9.25-250	9.25

Table 9. MRM parameters developed for LC-MS/MS analysis. Shown are deuterated IS used for normalization of quantified data, scan mode, m/z precursor, cone voltage, m/z fragment values, CE and Rt.

Deuterated internal standard	Mode	*m/z* precursor ion	Cone /V	*m/z* fragments	CE/V	Rt /Min
PGE1-d4	-	357.2	25	277.1	15	5.0
12,13-DiHOME-d4	-	317.1	38	185.0	20	8.5
9,10-DiHOME-d4	-	317.1	36	202.9	20	8.6
15-HETE-d8	-	327.2	25	226.1	12	10.8
12(13)-EpOME-d4	-	299.1	36	197.9	18	11.4
9(10)-EpOME-d4	-	299.1	30	171.9	17	11.7

Table 10. List of lipid mediators and their corresponding internal standards used for quantification.

PGE1-d4	12,13-DiHOME-d4	9,10-DiHOME-d4	15-HETE-d8	12(13)-EpOME-d4	9(10)-EpOME-d4
8-iso PGF2α	17,18-DiHETE	9,10-DiHOME	7,8-DiHDPA	11(12)-EpETE	9(10)-EpOME
TXB1	14,15-DiHETE	8,9-DiHETE	17,18-EpETE	5,6-DiHET	7-HDHA
TXB3	11,12-DiHETE	14,15-DiHET	13-HODE	17-HDHA	8-HDHA
TXB2	12,13-DiHOME	19.20-DiHDPA	9-OxoODE	16-HDHA	16(17)-EpDPA
PGF2α		13-HOTrE-gamma	9-HODE	13-HDHA	13(14)-EpDPA
PGE3		9-HOTrE	20-HDHA	11-HETE	5-HETE
8-iso PGE2		16,17-DiHDPA	5-HEPE	8(9)-EpETE	10(11)-EpDPA
PGD3		13-HOTrE	14(15)-EpETE	5-oxoETE	11(12)-EET
PGE2		11,12-DiHET	15-HETE	14-HDHA	8(9)-EET
PGD2		13,14-DiHDPA		12-HETE	7(8)-EpDPA
PGE1		18-HEPE		10-HDHA	4-HDHA
PGD1		5,6-DiHETE		8-HETE	
Δ12-PGJ2		15-HEPE		12(13)-EpOME	
PGB2		10,11-DiHDPA		11-HDHA	
		11-HEPE		9-HETE	
		8-HEPE		19(20)-EpDPA	

	8,9-DiHET	14(15)-EET
	19-HETE	
	9-HEPE	
	15-OxoETE	
	13-OxoODE	
	20-HETE	

3.2. Rats

All rat protocols and procedures employed in this study received ethical approval from the Ministry of Agriculture of the Republic of Croatia (Approval No. KLASA: UP/I-322-01/20-01/63; URBROJ:525-10/0543-21-4; HR-POK-024 from 2nd of March 2021) and Ethics Committees of the Medical School of the University of Rijeka (Approval No. EP 317/2021 from 26th of February 2021) and were performed in accordance with the ARRIVE guidelines.

Male and female Sprague Dawley rats (Charles River Laboratories, Wilmington, MA, USA) were purchased at 7 weeks of age. Two male-female pairs were further bred within the animal facility at the Medical School of the University of Rijeka to generate experimental litters, whereas all other rats were used directly in the experimental protocols. Animals were group-housed under controlled conditions (24 °C; 12-h light/dark cycle) with free access to food and water.

At 9 or 12 weeks of age animals were anesthetized using isoflurane and plasma and tissue samples were collected as part of a terminal procedure and stored at − 80 °C until further analysis. Inclusion of two age groups was based on experimental design: 12 weeks represented the standard age for the sepsis model, whereas 9-week-old rats were included in the dietary study because parallel experiments (data not included in this thesis) required this earlier age as optimal

3.2.1. Dietary intervention

Male and female littermates (n = 23) from three pregnant Sprague Dawley female rats (Charles River Laboratories, Wilmington, Massachusetts), where used in dietary intervention experiment. At the time of weaning, animals were randomized to receive one of two custom AIN-76A rodent diets (Bio-Serv, Flemington, New Jersey) each containing 5.1% fat. In these diets, the standard corn oil was replaced with one of two custom triglyceride blends to precisely control the FA composition and eliminate variability inherent to natural oils. The high LA formulation consisted of 18.5% tripalmitin (palmitic acid), 18.5% triolein (oleic acid), 60% trilinolein (linoleic acid), and 3% trilinolenin (α-linolenic acid). The high oleic acid (low LA) formulation consisted of 18.5% tripalmitin, 75% triolein, 3.5% trilinolein, and 3% trilinolenin. An overview of the relative proportions of the FA species in the two experimental diets is provided in Table 8. These diets were administered exclusively to rats subjected to the dietary intervention experiment. All other animals used for the purpose of this dissertation were maintained on the standard Mucedola 4RF21 diet (Mucedola S.R.L., Settimo Milanese, Italy).

Table 11. Relative proportions of the fatty acid species in the two experimental diets. High omega-6 oil was one rich in LA, whereas low omega-6 oil was one rich in in oleic acid (low LA oil).

	High omega-6 oil	Low omega-6 oil
Fat, % Kcal	12.5%	12.5%
Fatty acid composition (%Kcal from)		
C18:2 ω6 Linoleic acid	7.41%	0.46%
C18:3 ω3 α-linolenic acid	0.46%	0.46%
Total Polyunsaturated fatty acids	7.87%	0.93%
Total Saturated fatty acids	2.31%	2.31%
Total Monounsaturated fatty acids	2.31%	9.26%

3.2.2. Sepsis induction

At 12 weeks of age, rats were randomized to receive either an intraperitoneal injection of 30 % fecal slurry to induce sepsis or sterile saline, which served as vehicle control. Inclusion of two age groups was based on experimental design: 12 weeks represented the standard age for the sepsis model, whereas 9-week-old rats were included in the dietary study because parallel experiments (data not included in this thesis) required this earlier age as optimal. A 30% fecal slurry was freshly prepared on the day of induction using feces collected from several animals of the same batch, suspended in sterile saline, and filtered through a series of mesh strains to remove large particulates. Each animal was weighed, and 2 ml/kg of fecal slurry or sterile saline was administered intraperitoneally in the left lower abdominal quadrant using a 22G needle.

3.2.3. Plasma and organ collection

At 6, 24, and 48 h post-injection, animals were anesthetized with 5% isoflurane (Vetpharma Animal Health, Barcelona, Spain) (3 L/min) in a gas chamber for 2 min, weighed, and euthanized by decapitation using a guillotine. Trunk blood was collected into 50 mL Falcon tubes containing 1000 IU of heparin (25,000 IU/5 ml; Belupo,

Koprivnica, Croatia) and subsequently transferred into 6 ml K_2EDTA tubes (Becton Dickinson, Franklin Lakes, NJ, USA), followed by centrifugation at 800 x g for 10 min to obtain plasma which was further stored at −80 °C until LC-MS/MS analysis. The animal was placed in the dorsal position, the skin and peritoneum were opened, and lungs were excised. One lung lobe was used for wet/dry weight ratio determination while the remaining lobe was stored at −80 °C until LC-MS/MS analysis.

3.2.4. Wet/dry ratio determination

Immediately after excision, one lung lobe was weighed in triplicate to obtain wet weight, dried in an incubator at 75 °C for 7 days, and subsequently reweighed in triplicate to obtain the dry weight. Mean wet and dry values were then used to calculate the wet/dry ratio (wet weight/dry weight).

3.2.5. Sample preparation for LC-MS/MS analysis

3.2.5.1. Plasma protein precipitation

Plasma samples (500 µl) were spiked with an IS mix (5 ng each of prostaglandin E1-d4, 15-HETE-d8, 9,10-DiHOME-d4, 12,13-DiHOME-d4, 9(10)-EpOME-d4 and 12(13)-EpOME-d4) and diluted to 1.5 mL with 15% methanol in water. Samples were centrifuged at 20,000 × g for 5 min at 4 °C for protein precipitation, and 1 ml of the supernatant was applied to solid-phase extraction (SPE) cartridges (see section 3.2.5.3).

3.2.5.2. Lung tissue homogenization

Approximately 15 to 20 mg of lung tissue was weighed, finely minced with a scalpel, and transferred into 1.5 ml Eppendorf tubes containing 1.25 ml of homogenization buffer prepared by combining aqueous 1× PBS (Sigma-Aldrich, St. Louis, MO, USA) with a 1 mg/ml of butylated Hydroxytoluene (BHT) (Sigma-Aldrich, St. Louis, MO, USA) in methanol (VWR Chemicals, Lutterworth, UK) and adjusting the mixture to a final 15% (v/v) methanol. Glass beads (425–600 µm; Sigma-Aldrich, St. Louis, MO, USA) were added, and the samples were homogenized on ice with Sonopuls ultrasonic homogenizer (Bandelin electronic, Berlin, Germany) three times for 30 s at an amplitude of 76 with 10 s rest intervals between cycles. Following homogenization, samples were centrifuged at 20 000 x g for 5 min at 4 °C, and 1 ml of the supernatant was spiked with an IS mix and applied to solid-phase extraction (SPE) cartridges.

3.2.5.3. Solid-phase extraction

Precipitated plasma and lung homogenate were purified on C18 SPE cartridges (30 mg sorbent, 1 mL; Strata-X; Phenomenex, Torrance, CA, USA) using a Chromabond SPE vacuum manifold (Macherey-Nagel, Düren, Germany). The cartridges were preconditioned with 1 ml methanol followed by 1 mL 15% methanol in water. The diluted, IS-spiked samples were applied to the cartridge, washed with 2 mL of 15% methanol and

2 mL hexane (Honeywell Riedel-de Haën, Seelze, Germany), and dried under vacuum for 30 s. The cartridge was eluted with 0.5 ml methanol containing 0.1% formic acid (Honeywell Riedel-de Haën, Seelze, Germany) directly into 1.5 mL LC–MS autosampler vials. The eluate was dried under a gentle stream of nitrogen, and the residue was immediately reconstituted with 50 µL of methanol and injected into LC-MS.

3.2.6. Protein analysis

3.2.6.1. Protein extraction from lung tissue

Proteins for Western blotting were extracted from lung tissue by homogenization. Approximately 20 mg of tissue was weighed and transferred into 1.5 ml Eppendorf tubes containing 250 µL of ice-cold 1x PBS. Glass beads were added, and the samples were homogenized on ice three times for 30 s at an amplitude of 76 with 10 s rest intervals between cycles. Following homogenization, samples were centrifuged at 1000 x g for 5 min at 4 °C and supernatant was transferred to another Eppendorf tube. For protein quantification, 10 µL of each supernatant was diluted 20-fold in 1× PBS, and dilutions were applied in triplicate onto a 96-well plate. Commercial Bradford reagent (Thermo Fisher Scientific, USA) was added (100 µL per well), and absorbance was measured at 595 nm using an Infinite M200 Pro monochromator microplate reader (Tecan, Switzerland). The final protein concentration was calculated by multiplying the obtained value by the dilution factor 20. Based on the determined concentrations, each sample was adjusted to a final concentration of 5000 µg/mL in 1× PBS in total volume of 100 µL and 33 µL of 4x Laemmli buffer was added. Samples were then frozen at -20°C until sodium dodecyl sulphate-polyacrylamide gel electrophoresis (SDS-PAGE) analysis.

3.2.6.2. SDS-PAGE and western blot analyses

Samples were heated for 5 min at 95 °C before 10 µL of each was loaded on the 10% polyacrylamide gels. For protein size identification, a protein ladder marker (Roti-Mark TRICOLOR) was loaded onto the gel. For internal control, a pooled sample prepared by mixing equal aliquots of 6 h sepsis samples were included on each gel. The gels were run at 70 V in 1x SDS running buffer until samples were compressed to separating gel, and then the currency was increased to 120 V until the loading dye from Laemmli buffer reached the end of the gel. All gels were transferred to nitrocellulose membranes using Mini PROTEAN Tetra System (Bio-Rad) in 1x transfer buffer at 0.35 A for 75 min. Transfer sandwiches consisted of a sponge, Whatman paper (GE Healthcare, UK), membrane and a gel. Following transfer, membranes were stained with Ponceau S solution to visualize protein bands, and subsequently destained by washing with TBS. After destaining, membranes were blocked with 5% dry milk prepared in 1x TBS for 30 min at room temperature to prevent nonspecific antibody binding then incubated with primary antibodies over night at 4°C. The next day, membranes were washed three times for 10 min with 1x TBS-T and probed with secondary HRP-conjugated antibody probing

solutions for 1 h at room temperature. Membranes were then washed three times for 10 min with 1x TBS-T and visualized with ECL Prime detection reagents (Amersham), SuperSignal West pico or Supersignal West femto detection reagents (Thermo-fischer) depending on signal intensity, using ChemiDocTM imaging system (Bio-Rad).

3.2.6.3. Western blot densitometric analyses and relative quantification

Densitometric analyses were done using Fiji ImageJ software (National Institutes of Health). Obtained protein levels were normalized to loading (GAPDH) and internal control. Protein quantification from biochemical fractionation is shown as a fold change difference from a control sample.

Table 12. Buffer composition for SDS PAGE and western blot.

Buffer name	Final composition
1x SDS running buffer	25 mM Tris pH 8.3 192 mM glycine 0.1% SDS
1x Transfer buffer	25 mM Tris 192 mM glycine 20% methanol
1x TBS	150 mM NaCL 10 mM Tris-HCl pH 8.0
1x TBS-Tween	150 mM NaCL 10 mM Tris-HCl pH 8.0 0.05% Tween-20
Blocking buffer	5% dry milk in 1x TBS
Antibody probing solution	5% dry milk in 1x TBS
Ponceau S solution	0.1% Ponceau S (Panacea Biotec, India) 1% acetic acid

Table 13. Gels for SDS-PAGE.

Gels	Final composition
Stacking	5% acrylamide 125 mM Tris-HCl pH 6.8 0.1% SDS 0.1% APS 0.1% TEMED
Resolving (10%)	10% acrylamide 375 mM Tris-HCl pH 8.8 0.1% SDS 0.1% APS 0.1% TEMED

Table 14. List of primary antibodies for Western blot.

Antigen	Host	Catalog number	Manufacturer	Dilution
CD16	Rabbit	MA5-36143	Thermo-scientific	1:1000
GAPDH	Mouse	MAB374	Chemicon	1:1000
Myeloperoxidase	Goat	AF3667	R&D Systems	1:2000

Table 15. List of secondary antibodies for Western blot

Antibody	Conjugate	Catalog number	Manufacturer	Dilution
Anti-goat	HRP	805-035-180	Jackson ImmunoResearch	1:2000
Anti-mouse	HRP	7076	Cell signaling	1:2000
Anti-rabbit	HRP	7074	Cell signaling	1:2000

All reagents used in SDS-PAGE and western blot analyses were purchased from Carl Roth if not stated differently.

3.3. Computational methods

Molecular mechanisms underlying the interaction of LMs with the TRPV1 channel were studied using a combination of computational methods described in fallowing sections.

3.3.1. System preparation

Coordinates of LM molecules were obtained from the PubChem database. Three-dimensional conformations of the ligands were generated in Open Babel and further energy minimized using Avogadro software. The structure of the rat TRPV1 channel (PDB ID: 7LP9) was downloaded from the Protein Data Bank. Since the original structure lacked extracellular residues in the region Lys603–Gly624, these were reconstructed using the MODELER plugin in UCSF Chimera. Ligands and the protein were prepared for docking using the Dock Prep function in Chimera, applying the AMBER ff99SB force field for the protein and AM1-BCC charges for the ligands. Molecular docking was carried out with AutoDock Vina, placing each ligand into the vanilloid binding pocket of a single TRPV1 monomer. LA and AA were additionally docked as negative controls, since they do not activate the channel.

3.3.2. Membrane system setup

The tetrameric TRPV1 channel was oriented according to the Orientations of Proteins in Membranes (OPM) database and embedded in a model lipid bilayer generated using CHARMM-GUI. The bilayer was designed to mimic the cholesterol-rich cellular environment and was composed of 53% cholesterol, 22% POPC, 10% POPE, 6% sphingomyelin, 5% POPS, 2% POPI, and 1% POPA. The protein-ligand-membrane

system was solvated in a water box (210 × 210 × 225 Å) filled with TIP3P water molecules and neutralized with 0.15 M NaCl.

3.3.3. Molecular dynamics simulations

All molecular dynamics simulations were performed using GROMACS v.2021.3 and the CHARMM36m force field. Ligand topologies and parameters were generated using the CHARMM General Force Field (CGenFF). After building the system, stepwise energy minimizations were performed with positional restraints applied to different parts of the system, and the LINCS algorithm was used to constrain bond lengths. Temperature was maintained at 310 K (37 °C) and pressure at 1 bar during equilibration with Berendsen coupling. The equilibration phase lasted 200 ns to allow the system to stabilize, after which production simulations of 100 ns were carried out in the NPT ensemble, using the Nose–Hoover thermostat and the Parrinello–Rahman barostat. Electrostatic interactions were calculated with the particle mesh Ewald (PME) method and a 12 Å cutoff. All simulations were repeated in triplicate to ensure reproducibility.

3.3.4. Data analysis

Simulation trajectories were visualized and inspected in VMD software. Root-mean-square deviation (RMSD) and root-mean-square fluctuation (RMSF) analyses were performed within GROMACS. Binding free energies between ligands and TRPV1 were calculated using the gmx_MMPBSA tool, which applies the Molecular Mechanics Poisson–Boltzmann Surface Area (MM-PBSA) approach implemented in AmberTools21. Ligand–residue interactions were further analyzed and visualized using LigPlot v.2.2.5. All numerical and statistical analyses of the obtained data were performed in RStudio v.1.4.1106.

3.4. Statistics

Statistical analysis was done using GraphPad Prism Software 8.0.1 and R-studio v.4.1.2. Since all data met the criteria for normal distribution, statistical analyses were performed by Student’s T-test or ANOVA. A p-value of < 0.05 was considered statistically significant: * $p < 0.05$; ** $p < 0.01$; *** $p < 0.001$; **** $p < 0.0001$.

4. Results

4.1. LC-MS/MS method optimization for lipid mediator quantification

To enable reliable quantification of structurally similar LMs, LC and MRM parameters were systematically optimized. Chromatographic conditions were refined to achieve baseline separation of key regioisomeric pairs, ensuring accurate assignment of precursor-product ion transitions. On-column optimization of cone voltage and CE further improved signal intensity of LMs in the panel. Together, these optimizations resulted in reproducible detection of LMs in plasma and lung tissue samples.

4.1.1. Liquid chromatography optimization

LC conditions were optimized to achieve retention and separation of structurally related LMs. Several gradient profiles and mobile phase compositions were tested (data not shown), and the final method employed a mobile phase system consisting of solvent A (0.1% ammonium acetate in water/methanol/acetonitrile, 85:10:5, v/v) and solvent B (0.1% ammonium acetate in water/methanol/acetonitrile, 5:90:5, v/v). The optimized linear gradient provided improved peak shape and sufficient resolution of regioisomeric pairs. Rt were reproducible under these conditions, and no co-elution was observed among regioisomeric pairs such as LA-EpOMEs and LA-DiHOMEs (Figure 6). The final method operated at a flow rate of 0.2 mL/min with a 5 µL injection volume and autosampler temperature maintained at 10 °C.

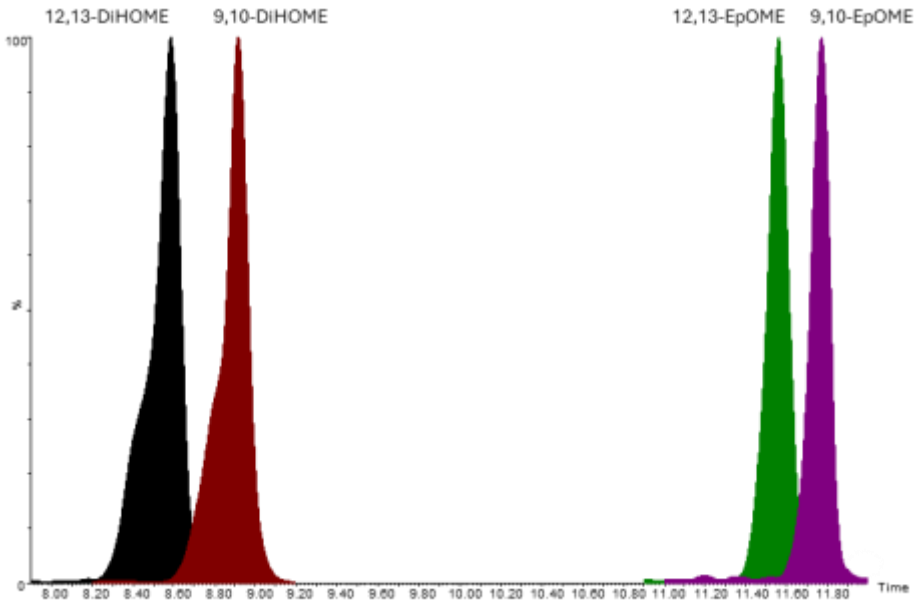

Figure 6. Chromatographic separation of linoleic acid derived regioisomers. Chromatogram shows baseline separation of the two regioisomeric LM pairs, LA-

DiHOMEs (ΔRT = 0.3 min) and LA-EpOMES (ΔRT = 0.3 min). Peaks are sharp and symmetrical with no evidence of co-elution within either regioisomeric pair. LA-DiHOMEs elute at approximately 8 min, whereas LA-EpOMEs elute at approximately 11 min. The optimized gradient and mobile phase composition provide sufficient resolving power to distinguish structurally similar LMs, which is essential for correct MRM transition assignment and accurate downstream quantification.

4.1.2. Scheduled MRM method optimization

Optimization of MRM transitions yielded reproducible precursor-product ion pairs for all LMs included in our panel. Systematic variation of cone voltage and CE demonstrated that increasing CE above analyte specific values caused excessive fragmentation, whereas lower values reduced sensitivity. The optimized combination of energies provided maximal precursor ion transmission, stable generation of characteristic product ions, and minimal in-source fragmentation.

In our LM panel, optimal cone voltages ranged from 18 to 40 V, whereas CE varied between 9 and 27 eV (Table 9). The LA derived metabolite, 12,13-DiHOME exhibited the highest signal intensity at cone voltages of 40 V and CE of 21 eV. Representative chromatograms for 12,13-DiHOME illustrate the gain in signal at the chosen cone and CE settings (Figure 7; Figure 8). The same optimization procedure was applied to every individual LM.

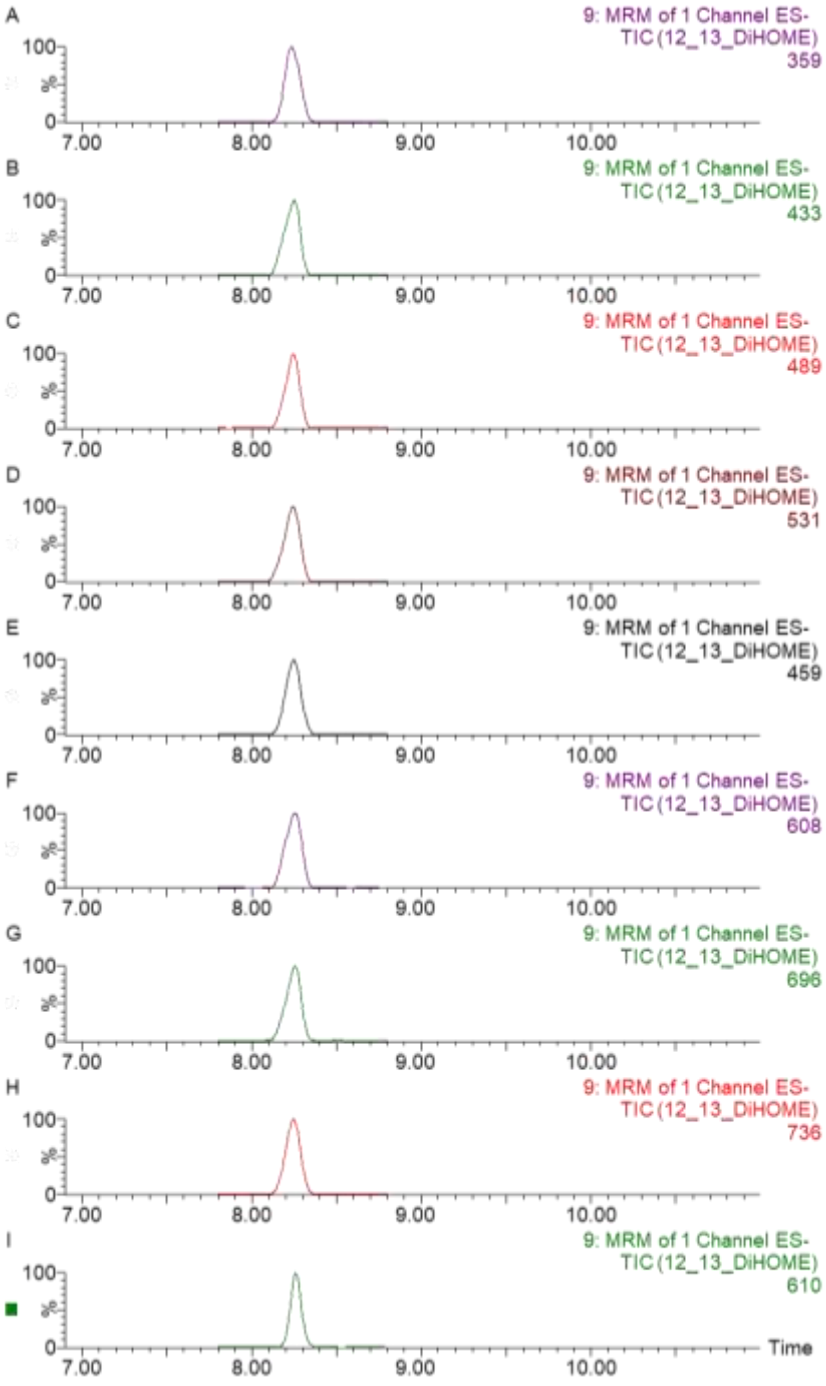

Figure 7. Cone voltage optimization for 12,13-DiHOME. Extracted ion chromatograms show repeated injections of the 12,13-DiHOME standard acquired with a cone voltage series from 5 V (A) to 45 V (I). The intensity of the precursor ion was monitored for each setting, and the cone voltage that provided the highest signal without inducing excessive in-source fragmentation was selected. For 12,13-DiHOME, the optimal cone voltage was 40 V (H; intensity: 736). The same optimization procedure was applied to all other LM standards.

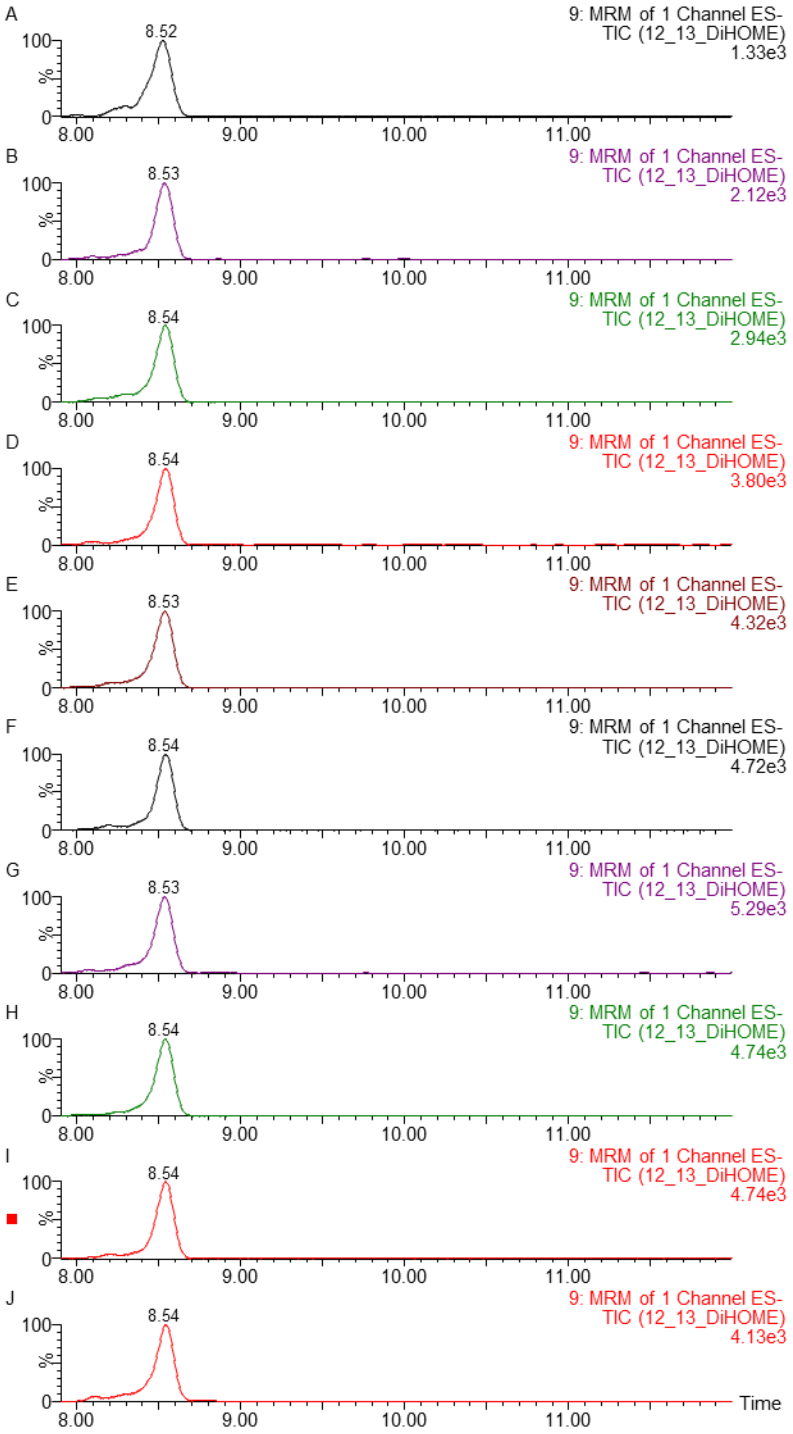

Figure 8. Collision energy optimization for 12,13-DiHOME. Optimal CE yields the most abundant and stable product ion for quantification without inducing excessive fragmentation. Extracted ion chromatograms show repeated injection of the 12,13-DiHOME standard acquired with a CE series from 15 V (A) to 24 V (J). For 12,13-DiHOME the optimal CE was 21 V (G; intensity: 5.29 x 10^3). The same optimization procedure was applied to all other LM standards.

A scheduled MRM method was employed because many analytes had to be monitored within a single LC-MS/MS run. In a traditional (unscheduled) MRM method, each transition (precursor-product ion pair) is monitored continuously across the entire chromatographic run, regardless of when the compound is expected to elute. In a scheduled MRM method, each transition is monitored during a specific time window around the compound's expected retention time (RT ± 0.5 min). Scheduling increases the dwell time for each monitored transition, thereby enhancing signal intensity and sensitivity. This approach is particularly useful when monitoring numerous MRM transitions in a single run. An example of the scheduled MRM method and the corresponding acquisition windows is shown in Figure 9 and 10.

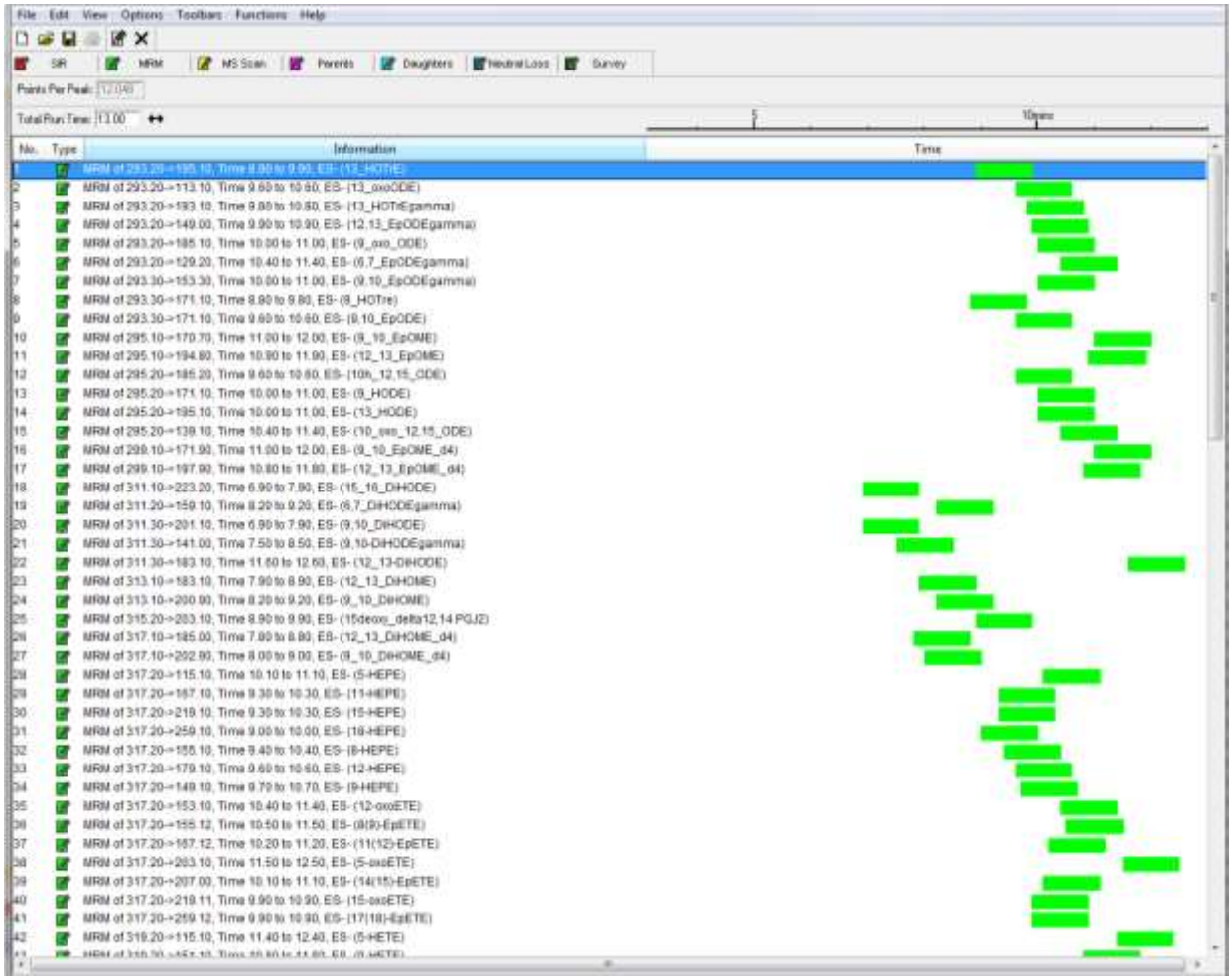

Figure 9. Scheduled MRM acquisition windows for the lipid mediator panel. The figure shows a section of the scheduled MRM method in MassLynx, generated using parameters listed in Table 9. Each green bar represents the retention time interval during

which a specific precursor-product ion pair is acquired. The structured distribution of acquisition windows ensures adequate dwell time across more than 100 transitions and prevents signal dilution that would occur in an unscheduled MRM method.

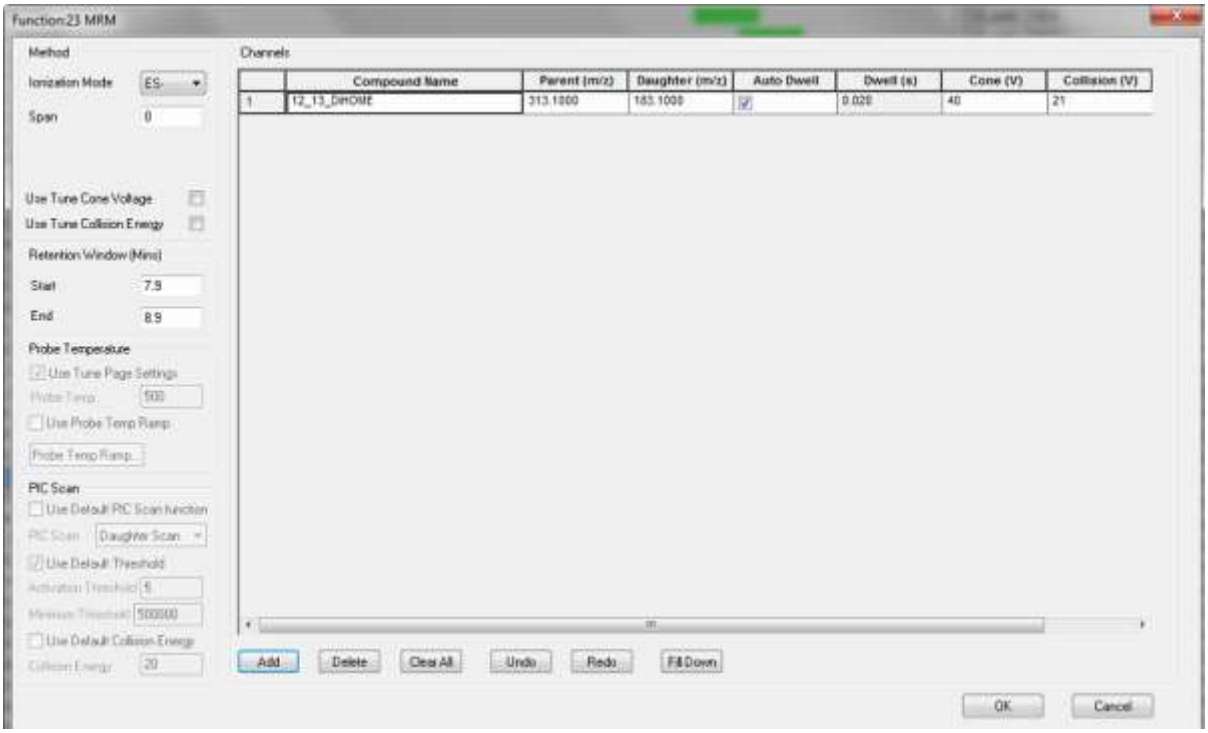

Figure 10. Optimized and scheduled MRM parameters for the quantification of 12,13-DiHOME. The example displays the final MRM transition used in the analytical method, including the precursor-product ion transition (m/z 313.1 → 183.1), optimized cone voltage (40 V), CE (21 eV), and dwell time (0.020 s). The transition was scheduled within a defined Rt window of 7.9 - 8.9 min to increase dwell time and improve sensitivity during LC-MS/MS analysis.

4.1.3. Calibration curves construction and quantification of lipid mediators

Calibration curves for each LM were constructed using pre-purchased standards. A mixed stock solution containing all available standards was prepared and diluted serially to generate a set of calibration levels covering the expected linearity range. Each calibration level was injected in triplicate, and peak area (or peak area ratio to the corresponding IS) was plotted against nominal concentration. Linear regression with appropriate weighting was applied to obtain the calibration curve for each analyte, and only curves with coefficients of determination (R^2) ≥ 0.98 were accepted for quantification (Figure 11).

These calibration curves were then used to determine analyte concentrations in plasma and lung tissue samples based on their measured signal response.

For semi-absolute quantitative analysis, several deuterated LM standards were used as IS. Deuterated standards closely mimic the physicochemical behavior of their non-deuterated analogues during extraction, chromatographic separation, ionization, and detection, and they co-elute with the target analytes. As a result, they experience the same matrix effects and variations in ionization efficiency, enabling correction for signal suppression or enhancement and for losses during sample preparation. In this study, six different deuterated IS were distributed across the chromatographic run (Table 11), and each analyte was assigned to the nearest IS according to Rt. Analyte responses were normalized to the corresponding IS, and recoveries were corrected accordingly to provide accurate and reproducible quantification.

Limits of detection (LOD) and quantification (LOQ) were determined using signal to noise ratios of 3:1 and 10:1, respectively. The linearity range for the calibration curves spanned from 3.08 to 250 ng/mL for the majority of LMs. Extraction recoveries for IS ranged between approximately 70% and 120% (data not shown). Matrix effect was minimized through chromatographic separation and IS normalization, which corrects for ion suppression or enhancement.

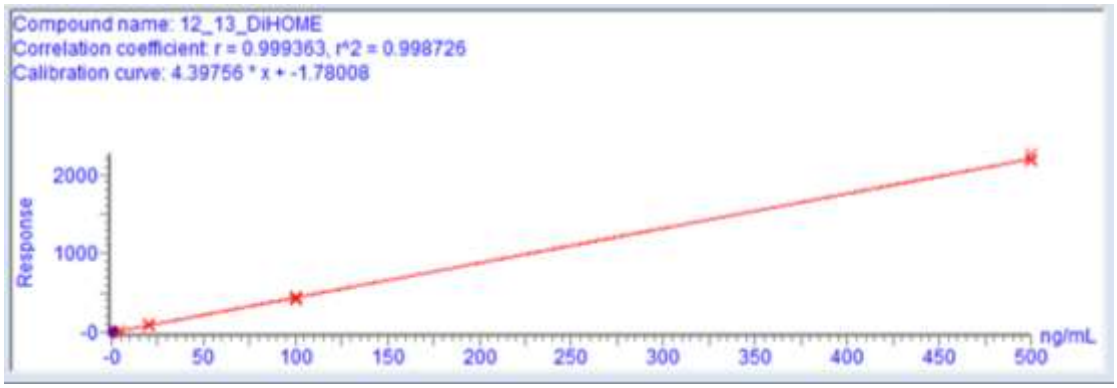

Figure 11. Example of a calibration curve for 12,13-DiHOME generated in TargetLynx. Pure standards for each LM were pre-purchased. A mixed stock solution containing all available standards was prepared and serially diluted to construct calibration levels covering the expected LM linearity. Each level was injected in triplicate, and the resulting calibration curve was used to quantify analytes in plasma and lung tissue samples based on their measured responses. The same procedure was applied to all LM standards.

4.2. Rodent model of fecal peritonitis

FP was successfully induced in all experimental animals, and all rats survived until the planned experimental endpoints (6 h, 24 h, and 48 h). No unexpected adverse events were observed. Animals were monitored throughout the experiment for general appearance, posture and activity, and no severe clinical deterioration was noted prior to terminal procedure. At each time point, rats were deeply anesthetized and subsequently sacrificed in accordance with approved ethical guidelines. Body weight did not differ markedly between experimental groups or time points (Table 15). A small but statistically significant reduction in body weight was observed in male rats at 24 h ($p < 0.05$), whereas all other within-group changes between baseline and sacrifice were not significant.

4.2.1. Lung edema assessment (wet/dry ratio)

Wet/dry lung weight ratio was first analyzed separately in male and female rats (data not shown). In males, a significant reduction in wet/dry ratio was observed at 6 h compared with vehicle ($p < 0.05$), whereas no statistically significant time-dependent changes were detected in females. Because no consistent sex-dependent pattern emerged, data from males and females were pooled for the main analysis. In the pooled dataset, wet/dry ratio was modestly but significantly reduced at 6 and 24 h compared with vehicle, while values 48 h did not differ from vehicle controls, indicating absence of overt lung water accumulation at the examined time points (Figure 12).

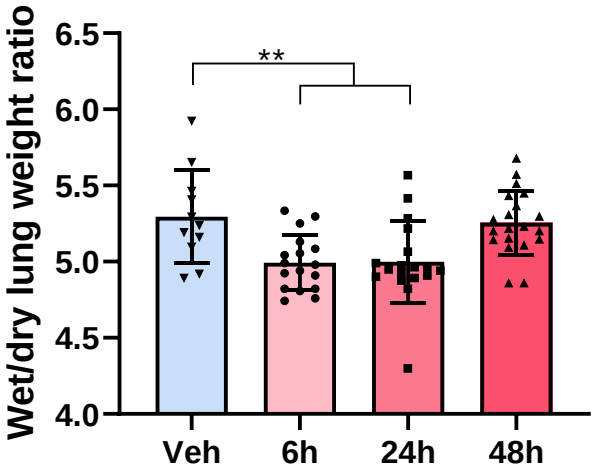

Figure 12. Wet/dry lung weight ratio following fecal peritonitis. Wet/dry ratios were measured in vehicle treated rats and at 6 h, 24 h, and 48 h after induction of FP. Bars show pooled data from male and female animals; sex-stratified analyses did not reveal a consistent sex-dependent pattern (data not shown). A significant reduction in wet/dry ratio was observed at 6 and 24 h compared with vehicle, whereas no significant differences

were detected at 48 h. Data are presented as mean ± SD; each point represents an individual animal. ** $p < 0.01$.

Table 16. Body weights (g) of male and female rats in the vehicle group and at 6, 24, and 48 h after fecal peritonitis induction (mean ± SD). Body weight was recorded immediately before the procedure (baseline) and at the time of terminal sampling (at sacrifice). Data are shown separately for male and female rats. p-values represent within-group comparisons between baseline and sacrifice. ns, not significant. N denotes the number of rats per group.

			Veh			6h			24h			48h		
			Mean ± SD	**p-value**	**N**	**Mean ± SD**	**p-value**	**N**	**Mean ± SD**	**p-value**	**N**	**Mean ± SD**	**p-value**	**N**
Weight	**Males**	**Baseline**	434.63 ± 23.70	ns	8	445.00 ± 30.68	ns	8	424.00 ± 29.80	**p < 0.05**	9	430.44 ± 28.91	ns	9
		At sacrifice	438.63 ± 22.25			443.75 ± 23.69			395.33 ± 23.58			415.56 ± 37.16		
	Females	**Baseline**	257.78 ± 19.77	ns	9	353.00 ± 15.53	ns	9	248.44 ± 15.58	ns	9	261.50 ± 18.35	ns	10
		At sacrifice	253.67 ± 15.35			250.44 ± 14.88			236.11 ±14.31			254.40 ± 17.95		

4.2.2. Quantification of plasma lipid mediators

Using the optimized scheduled MRM method, different LMs were quantified in plasma samples collected at 6 h, 24 h, and 48 h after induction of FP. LMs are present in biological samples at extremely low endogenous concentrations due to their short half-lives and rapid enzymatic turnover. Despite sample pre-concentration and the use of a sensitive LC-MS/MS method, many analytes remained below the LOD/LOQ in plasma samples. Therefore, quantitative analyses were restricted to LMs consistently detected above the LOQ. For all detectable analytes, concentrations were determined using calibration curves generated from authentic standards and normalized to deuterated IS to correct extraction variability and matrix effects. Table 16 summarizes the mean plasma concentrations ± SD of all detectable LMs in male and female rats. These values formed the basis for downstream statistical analyses.

All preliminary statistical analyses were performed separately in male and female rats (data not showed). Although some metabolites showed sex-specific variability in absolute concentrations, the overall direction and pattern of changes induced by FP were comparable between sexes. Because no consistent or biologically meaningful sex-dependent differences were observed, data from male and female rat data were pooled for all subsequent LM analyses to increase statistical power and reduce variability.

Table 17. Plasma concentrations (ng/ml) of lipid mediators in male and female rats following fecal peritonitis at 6 h, 24 h, 48 h and vehicle controls (mean ± SD). Values represent analytes consistently detected above LOQ. N indicates the number of animals per group.

Sex	Group	13-OxoODE	9-OxoODE	13-HOTrE	12,13-EpOME	9,10-EpOME	9-HODE	13-HODE
MALE	FP 6h (N=8)	1.5942 ± 0.4987	1.9446 ± 0.3152	4.0094 ± 2.9805	9.5379 ± 8.7156	1.2115 ± 1.0128	4.4142 ± 3.7277	18.7004 ± 10.9108
	FP 24h (N=9)	1.8823 ± 0.6335	2.3225 ± 0.9063	2.7678 ± 2.5040	7.5265 ± 4.3752	1.5824 ± 0.6807	4.1435 ± 1.6567	12.4696 ± 4.3431
	FP 48h (N=10)	0.6824 ± 0.6791	1.0133 ± 0.8393	0.2733 ± 0.1350	2.9657 ± 2.0365	0.5724 ± 0.5223	2.4767 ± 2.4370	6.3485 ± 5.4663
	Vehicle (N =8)	1.2527 ± 0.6259	0.9894 ± 0.8849	2.1033 ± 2.4675	6.1979 ± 4.0515	1.1461 ± 0.5482	3.1875 ± 1.7871	8.0756 ± 6.4910
FEMALE	FP 6h (N=9)	1.9411 ± 1.3689	1.6223 ± 1.2168	2.5898 ± 2.4187	6.7963 ± 6.6063	1.2554 ± 0.7526	8.2569 ± 10.4388	20.8566 ± 26.7614
	FP 24h (N=9)	1.6011 ± 0.6054	2.5362 ± 1.5302	3.8679 ± 4.1377	6.6391 ± 3.0931	1.5076 ± 0.9478	4.2419 ± 2.2070	11.8406 ± 7.0723
	FP 48h (N=10)	1.6206 ± 0.8684	1.1269 ± 0.8908	2.9180 ± 3.3947	4.5445 ± 2.7151	0.7217 ± 0.8909	4.1005 ± 2.5136	7.7079 ± 8.4427

Vehicle (N =9)	1.4158 ± 0.7868	0.9554 ± 1.0627	2.3584 ± 2.8533	6.7152 ± 4.7495	0.9601 ± 0.8334	3.3530 ± 1.9238	8.6406 ± 8.0987

Sex	Group	9,10-DiHODE	12,13-DiHOME	9,10-DiHOME	12-HETE	18-HEPE	15-HEPE	5-HEPE
MALE	FP 6h (N=8)	5.5363 ± 3.0893	29.2000 ± 15.9826	14.1267 ± 4.3318	30.6568 ± 18.1587	1.4363 ± 0.6643	1.1584 ± 0.6148	0.9088 ± 0.5396
	FP 24h (N=9)	3.4156 ± 2.5839	23.4126 ± 14.6805	10.7235 ± 4.4599	7.7252 ± 5.3735	1.4337 ± 0.5759	1.7044 ± 0.8705	0.4137 ± 0.1986
	FP 48h (N=10)	0.8840 ± 0.6487	12.0850 ± 7.1740	4.0600 ± 2.0945	1.8763 ± 1.7983	<LOQ	<LOQ	<LOQ
	Vehicle (N =8)	1.6850 ± 0.6849	6.1783 ± 4.2170	4.3367 ± 1.7360	6.1813 ± 8.3385	1.1753 ± 0.6595	1.5803 ± 1.7310	0.4580 ± 0.2759
FEMALE	FP 6h (N=9)	2.9725 ± 1.5195	19.3348 ± 15.9799	10.4960 ± 6.5042	18.6856 ± 32.9659	2.0395 ± 1.4456	1.6929 ± 1.2032	0.4644 ± 0.1881
	FP 24h (N=9)	3.7591 ± 2.9411	24.9026 ± 11.3825	11.9244 ± 4.4775	30.7200 ± 34.8415	1.3946 ± 0.7321	1.1820 ± 0.7680	0.6492 ± 0.8868
	FP 48h (N=10)	1.6038 ± 0.7857	15.2170 ± 10.5446	6.6783 ± 4.1810	5.2962 ± 8.6449	1.8598 ± 1.9686	1.4234 ± 1.5729	0.3772 ± 0.1563
	Vehicle (N =9)	2.3504 ± 1.2608	9.4748 ± 5.8922	5.8556 ± 3.5717	4.1525 ± 3.6759	1.1542 ± 0.6847	1.3264 ± 1.2013	0.3941 ± 0.2553

Sex	Group	11-HETE	11(12)-EET	5-HETE	11-HEDE	11_12-DiHET
MALE	FP 6h (N=8)	2.3996 ± 2.3826	0.2043 ± 0.1810	0.7604 ± 0.3677	0.2811 ± 0.1707	0.4415 ± 0.3193
	FP 24h (N=9)	0.7214 ± 0.3429	0.4028 ± 0.4458	0.7007 ± 0.6121	0.1097 ± 0.1067	0.4167 ± 0.3062
	FP 48h (N=10)	0.6791 ± 0.6092	0.1237 ± 0.0621	0.0930 ± 0.0719	0.0466 ± 0.0251	0.1404 ± 0.0760
	Vehicle (N =8)	0.8360 ± 0.6419	0.4675 ± 0.5344	0.8608 ± 0.7271	0.1873 ± 0.1572	0.3178 ± 0.2878
FEMALE	FP 6h (N=9)	0.7612 ± 0.3895	0.2806 ± 0.2108	0.3793 ± 0.2576	0.2109 ± 0.1868	0.4397 ± 0.4777
	FP 24h (N=9)	0.7396 ± 0.3940	0.4104 ± 0.4352	0.7856 ± 0.6084	0.1024 ± 0.1370	0.5505 ± 0.3708
	FP 48h (N=10)	0.5456 ± 0.5871	0.1227 ± 0.0623	0.6779 ± 0.7844	<LOQ	<LOQ
	Vehicle (N =9)	0.6048 ± 0.4293	0.2112 ± 0.2184	0.5428 ± 0.5259	0.1270 ± 0.1365	0.3880 ± 0.3365

4.2.2.1. Early fecal peritonitis induces systemic shift in the plasma lipid mediator profile

Targeted LC-MS/MS profiling revealed pronounced time dependent alterations in male and female plasma LMs following FP. Z-score normalized heatmap demonstrates distinct patterns of LM regulation across 6 h, 24 h, and 48 h compared to vehicle controls (Figure 13). The earliest point (6 h) was characterized by a prominent accumulation of LA derived metabolites, including 9,10-DiHOME, 12,13-DiHOME, 9-OxoODE, 13-HODE, while other LMs remained comparatively stable. By 48 h, most elevated LA metabolites were partially normalized, indicating an acute plasma LM shift during early FP.

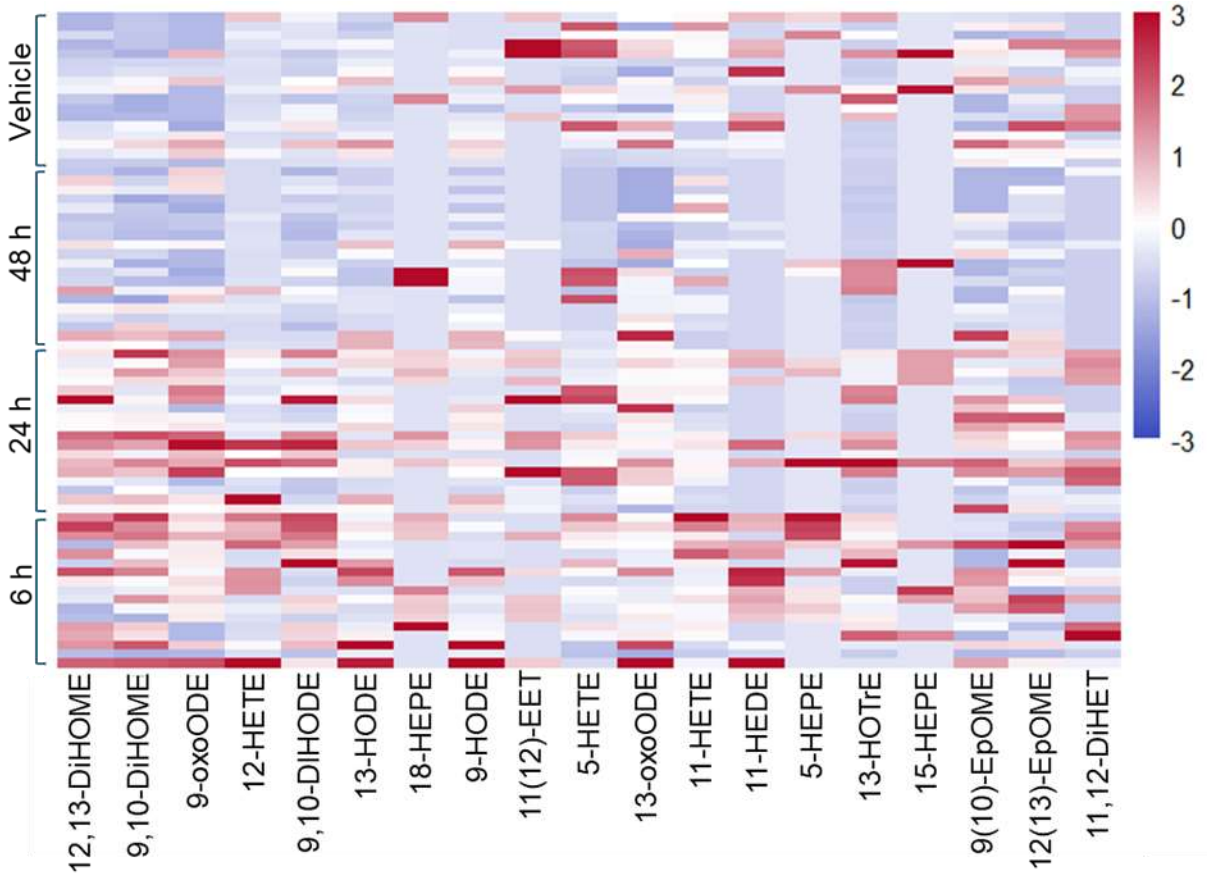

Figure 13. Temporal changes in the plasma lipid mediator profile following fecal peritonitis. Heatmap showing Z-score normalized concentrations of individual LMs at 6, 24, and 48 h relative to vehicle controls. Each column represents a distinct LM and each row a biological replicate. Red indicates relative increase, blue relative decrease. An early and coordinated rise in LA derived metabolites (e.g. DiHOMEs) is visible, indicating activation of LA metabolism during early FP.

4.2.2.2. Individual lipid mediators exhibiting significant temporal changes following fecal peritonitis

To validate the patterns observed in the global heatmap analysis, quantified LMs were examined separately. Only LMs that exhibited statistically significant temporal changes were visualized in individual concentration plots (Figure 14). Several LA derived metabolites displayed clear and reproducible concentration changes following FP. Both DiHOME regioisomers (12,13-DiHOME and 9,10-DiHOME) showed an early and robust rise at 6 h and 24 h, followed by a gradual decline toward baseline at 48. Similar early-phase increases were observed for 9,10-DiHODE and 9-OxoODE, although with lower amplitude. These metabolite-specific profiles confirm that early FP triggers a rapid and transient activation of LM pathways, consistent with the shift observed in the heatmap.

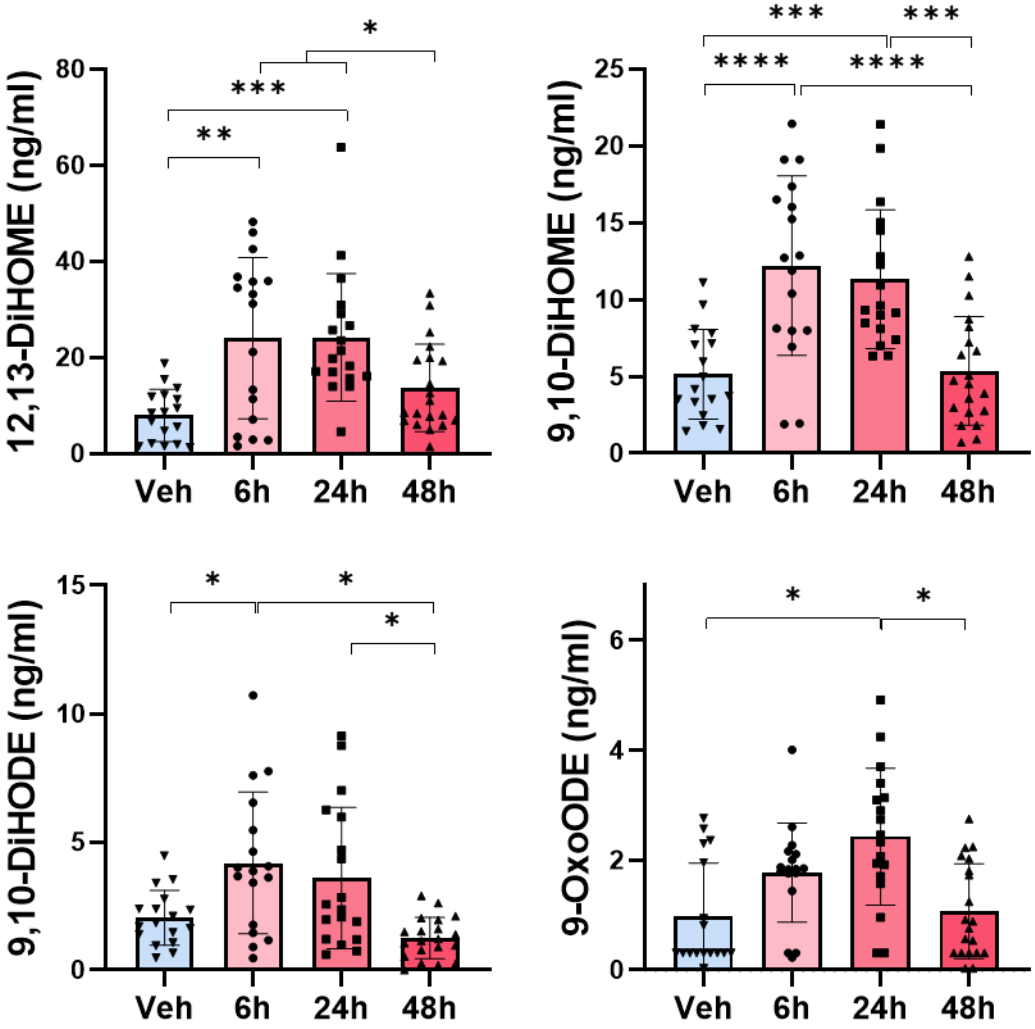

Figure 14. Concentration profiles of lipid mediators exhibiting significant temporal regulation following fecal peritonitis. Individual concentration plots are shown for LMs

that demonstrated statistically significant time-dependent changes in plasma. Data are presented for 12,13-DiHOME, 9,10-DiHOME, 9-OxoODE and 9,10-DiHODE. Each point represents an individual animal; bars indicate mean ± SD. Early after induction of FP (6 h and 24 h), both DiHOME regioisomers showed marked increases relative to vehicle controls, followed by partial normalization at 48 h. 9-OxoODE and 9,10-DiHODE metabolites exhibited similar but less pronounced temporal shifts. These profiles confirm selective activation of LA metabolism pathways during early systemic inflammation. * $p < 0.05$; ** $p < 0.01$; *** $p < 0.001$; **** $p < 0.0001$.

4.2.2.3. Plasma lipid mediator content as a predictor of sepsis

To determine which LMs were most strongly associated with fecal FP independently of sampling time, we applied a linear modelling approach that integrated measurements across all three-time intervals (6 h, 24 h, and 48 h). FP status was used as the main predictor, while time was included as a covariate to adjust for temporal variation. The resulting effect estimates were visualized using a forest plot (Figure 15), allowing a consolidated overview of directionality and magnitude of FP-associated LM changes.

Using this approach, 9,10-DiHOME, 12,13-DiHOME, 12-HETE, 9-OxoODE and 9,10-DiHODE showed significant positive associations with FP in the unadjusted model ($p < 0.05$). After further p-value adjustment using the Benjamini–Hochberg false discovery rate (FDR) at 5%, four metabolites remained statistically significant: 9,10-DiHOME, 12,13-DiHOME, 9,10-DiHODE and 9-oxoODE. Among these, 12,13-DiHOME and 9,10-DiHOME showed the largest positive effects, corresponding to 15.17 ng/mL and 6.21 ng/mL higher concentrations in FP rats compared with vehicle controls, respectively, whereas 9-oxoODE and 9,10-DiHODE exhibited more modest increases of 1.31 ng/mL and 1.60 ng/mL, respectively (Table 17).

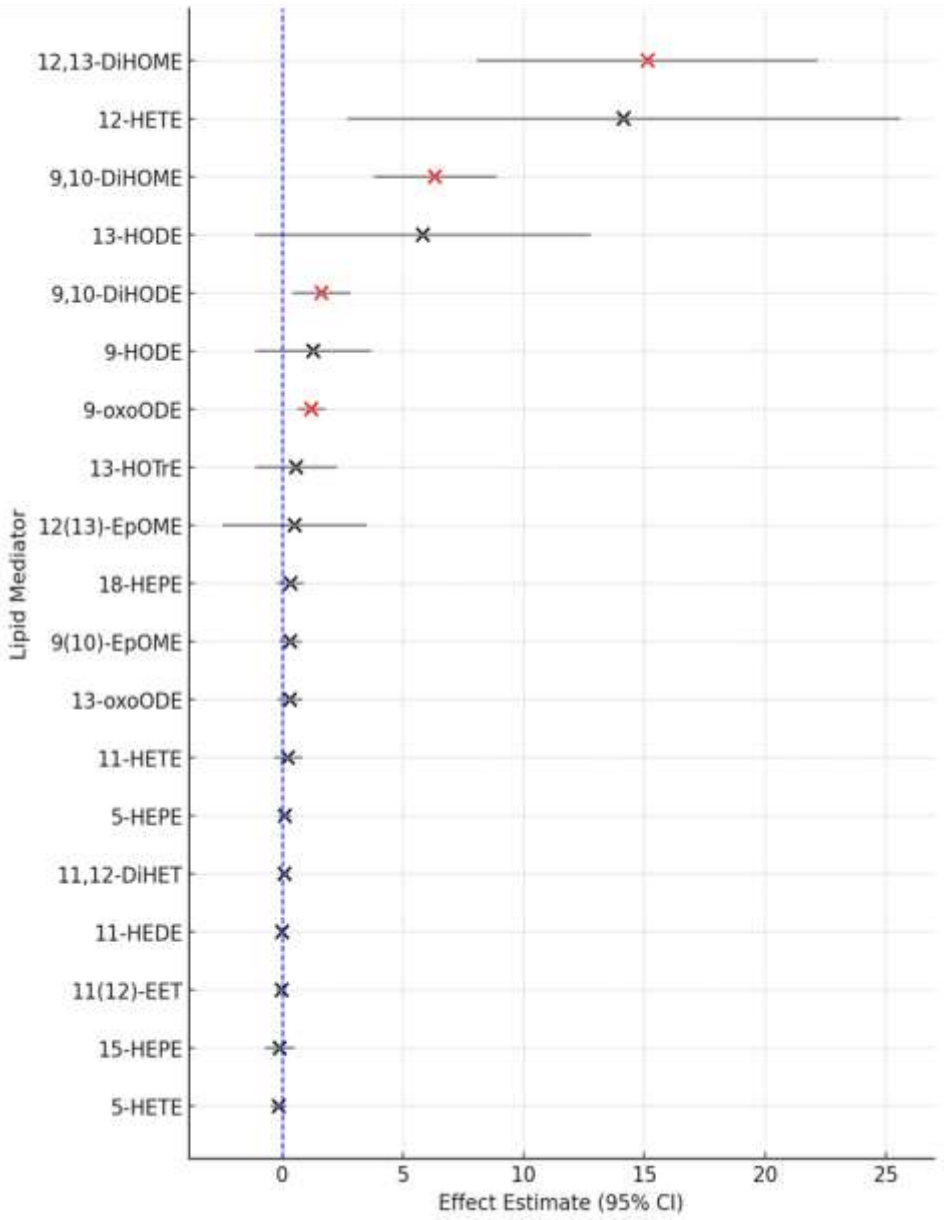

Figure 15. Lipid mediators predict fecal peritonitis status in rat models. Each LM is plotted with its effect estimate and corresponding 95% confidence interval (CI). The vertical dashed line indicates the null effect (no association). LMs marked in red remained statistically significant after p-value adjustment using the Benjamini–Hochberg false discovery rate (FDR) correction at a 5% threshold (adjusted $p < 0.05$), whereas black markers represent lipids that did not meet this criterion. Effect estimates greater than zero indicate a positive association with FP status. The largest positive effect estimates were observed for 12,13-DiHOME and 9,10-DiHOME, followed by 9,10-DiHODE and 9-oxoODE.

Table 18. Regression estimates of plasma lipid mediators differentiating septic and vehicle control rats, including Benjamini-Hochberg adjusted p-values (FDR 5%). Linear model output showing effect estimates, standard errors, 95% confidence intervals, and p-values for each LM. FP status (septic vs. vehicle) was used as the main predictor, and effect estimates represent the mean difference in concentration (ng/mL) between FP and vehicle control groups. Adjusted p-values were calculated using the Benjamini-Hochberg procedure to control the false discovery rate at 5%. Four lipid mediators including 9,10-DiHOME, 12,13-DiHOME, 9,10-DiHODE, and 9-oxoODE remained significant after adjustment (adjusted $p < 0.05$).

Lipid Mediator	estimate	std.error	p.value	adj_p	conf.low	conf.high
13-oxoODE	0.33	0.26	0.21	0.31	-0.18	0.84
9-oxoODE	1.21	0.30	**<0.001**	**<0.001**	0.62	1.79
13-HOTrE	0.58	0.87	0.50	0.58	-1.12	2.28
12(13)-EpOME	0.52	1.53	0.73	0.80	-2.47	3.52
9(10)-EpOME	0.34	0.24	0.15	0.25	-0.12	0.81
9-HODE	1.29	1.22	0.29	0.38	-1.10	3.68
13-HODE	5.83	3.54	0.10	0.18	-1.11	12.77
9,10-DiHODE	1.63	0.61	**0.01**	**0.03**	0.43	2.83
12,13-DiHOME	15.14	3.61	**<0.001**	**<0.001**	8.06	22.21
9,10-DiHOME	6.33	1.30	**<0.001**	**<0.001**	3.79	8.87
12-HETE	14.14	5.84	0.02	0.05	2.70	25.59
18-HEPE	0.35	0.29	0.23	0.32	-0.21	0.91
15-HEPE	-0.10	0.31	0.74	0.80	-0.70	0.50
5-HEPE	0.11	0.12	0.35	0.44	-0.13	0.35
11-HETE	0.24	0.30	0.43	0.51	-0.35	0.82
11(12)-EET	-0.02	0.10	0.82	0.85	-0.22	0.17

Lipid Mediator	estimate	std.error	p.value	adj_p	conf.low	conf.high
5-HETE	-0.14	0.16	0.39	0.48	-0.45	0.18
11-HEDE	0.00	0.04	0.94	0.94	-0.08	0.08
11,12-DiHET	0.10	0.09	0.29	0.38	-0.08	0.28

4.2.2.4. DiHOME/EpOME ratios and 12,13-EpOME-12,13-DiHOME contouring suggest the likelihood of sepsis

LA derived epoxides and their corresponding diols are frequently analyzed as EpOME/DiHOME or DiHOME/EpOME ratios in the literature because this balance reflects the activity sEH and the metabolic flux through the CYP-sEH pathway. To further investigate this axis in our model, we examined the relationship between 12,13-EpOME and 12,13-DiHOME (Figure 16A).

Contour modelling of plasma concentrations demonstrated that higher 12,13-DiHOME levels relative to 12,13-EpOME corresponded to a greater modelled likelihood of sepsis, with warmer contour regions representing a high DiHOME/EpOME balance (Figure 16B). This pattern suggests that elevated concentration of DiHOMEs may be a feature of the systemic inflammatory response in FP.

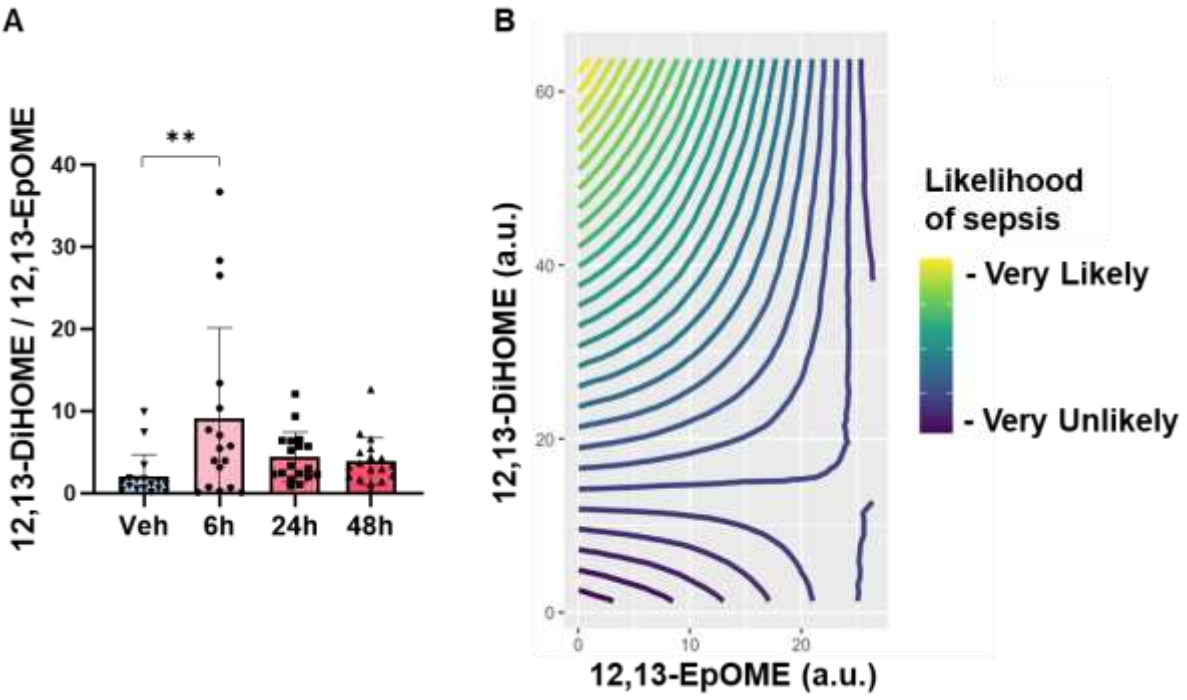

Figure 16. Plasma 12,13-DiHOME/12,13-EpOME ratio and 12,13-DiHOME-12,13-EpOME contour modelling suggest the likelihood of sepsis. (A) Plasma 12,13-DiHOME/12,13-EpOME ratio across experimental groups (vehicle control, 6 h, 24 h, 48 h). The ratio increased markedly at 6 h after FP induction and then declined toward baseline at 24 h and 48 h indicating an early imbalance between 12,13-EpOME and its downstream diol product. (B) Contour plot of plasma 12,13-EpOME (x-axis) and 12,13-DiHOME (y-axis) showing the modelled likelihood of sepsis. Warmer colors represent higher predicted likelihood. Regions with relatively high 12,13-DiHOME and lower 12,13-EpOME correspond to the greatest modelled likelihood, consistent with a shift toward DiHOME formation. ** $p < 0.01$.

Taken together, these data show that FP induces a rapid, early and highly specific systemic shift in the plasma LM profile. The most pronounced and consistent changes occurred among LA derived metabolites, particularly both DiHOMEs, whereas other LMs remained comparatively stable. Time-integrated modelling identified 12,13-DiHOME, 9,10-DiHOME, 9,10-DiHODE and 9-oxoODE as the strongest discriminators between septic and vehicle control animals after FDR correction, independent of sampling time. In addition, the elevated 12,13-DiHOME/12,13-EpOME ratio and the 12,13-DiHOME-12,13-EpOME contour surface pointed towards a shift in the EpOME–DiHOME equilibrium. Overall, these findings indicate that LA-derived LMs constitute sensitive circulating signatures of early systemic inflammation in this rat model of FP.

4.2.3. Quantification of lung tissue lipid mediators

In lung tissue, fewer LMs were detected compared with plasma detected again reflecting their low endogenous abundance. Only metabolites consistently detected above the LOQ across all experimental groups were included in subsequent analyses (Table 18).

Across all points (6 h, 24 h, 48 h), no statistically significant differences in lung tissue LM profile were observed between septic and vehicle control animals (data not shown). Although minor fluctuations were present, these changes did not reach significance and showed substantial biological variability. In contrast to plasma, where clear temporal shifts were detected, the lung LM profile remained largely stable following FP.

To determine whether LA-DiHOMEs, the most dynamic plasma metabolites, also changed in lung tissue, both DiHOME regioisomers (12,13-DiHOME and 9,10-DiHOME) were examined individually (Figure 17). Although both metabolites were detectable in most animals, no statistically significant differences were observed between septic and vehicle control rats at any time point.

Table 19. Lung tissue concentrations (ng/mg tissue) of lipid mediators in male and female rats following fecal peritonitis at 6 h, 24 h, 48 h and vehicle controls (mean ± SD). Values represent analytes consistently detected above LOQ. N indicates the number of animals per group.

Sex	Group	9,10-EpOME	12,13-EpOME	12,13-DiHOME	9,10-DiHOME	13-OxoODE	9-HODE	13-HODE
MALE	FP 6h (N=8)	0.5182 ± 0.4806	0.7737 ± 0.8509	0.0488 ± 0.0314	0.1528 ± 0.0756	0.2321 ± 0.2283	5.4187 ± 2.9492	13.6275 ± 12.5909
	FP 24h (N=9)	0.6775 ± 0.9548	0.8639 ± 0.9218	0.1230 ± 0.1008	0.1435 ± 0.0283	0.2313 ± 0.1699	4.8342 ± 1.8650	8.1091 ± 3.5726
	FP 48h (N=10)	0.5142 ± 0.4552	0.9850 ± 1.0157	0.0786 ± 0.0679	0.1415 ± 0.0317	0.4049 ± 0.2578	4.4821 ± 1.0440	8.4005 ± 1.6487
	Vehicle (N =8)	0.9811 ± 0.7897	1.1760 ± 1.0941	0.0903 ± 0.0983	0.1545 ± 0.0269	0.6563 ± 0.6507	4.3153 ± 1.5315	6.9045 ± 4.4363
FEMALE	FP 6h (N=9)	0.2172 ± 0.1826	0.3647 ± 0.4147	0.0913 ± 0.0692	0.1663 ± 0.0403	0.3150 ± 0.2208	3.4328 ± 1.4703	6.2374 ± 2.0287
	FP 24h (N=9)	0.1551 ± 0.0879	0.3377 ± 0.0644	0.1780 ± 0.1635	0.1654 ± 0.0433	0.2925 ± 0.1576	4.9978 ± 3.0313	8.5736 ± 5.0094
	FP 48h (N=10)	0.5304 ± 0.2772	0.6653 ± 0.2513	0.1272 ± 0.1147	0.1599 ± 0.0255	0.3606 ± 0.1955	3.6813 ± 1.6803	5.4985 ± 2.0326

Vehicle (N =9)	0.5179 ± 0.4348	0.9959 ± 0.6865	0.1181 ± 0.1177	0.1970 ± 0.1065	0.4133 ± 0.2649	3.6570 ± 1.6221	5.9766 ± 2.4922

Sex	Group	12-HETE	11-HETE	5-HETE	15-HEDE	11-HEDE	15-HETE	8,9-EET
MALE	FP 6h (N=8)	67.0647 ± 58.1467	21.3292 ± 24.5362	9.2406 ± 12.3072	2.8653 ± 6.2561	1.3155 ± 0.7172	14.2816 ± 19.4200	0.6814 ± 0.6616
	FP 24h (N=9)	66.0950 ± 75.3350	20.4204 ± 12.5631	10.6322 ± 14.4963	0.4676 ± 0.4674	1.4709 ± 0.9168	3.2293 ± 0.8792	1.2680 ± 1.6529
	FP 48h (N=10)	66.1512 ± 51.2394	19.8812 ± 9.5509	8.5974 ± 3.0999	0.4437 ± 0.2057	1.0465 ± 0.3584	4.8773 ± 2.7207	0.7765 ± 1.0562
	Vehicle (N =8)	44.0485 ± 32.2942	8.5602 ± 4.9781	4.0438 ± 5.1606	0.4343 ± 0.2572	0.9616 ± 0.4236	3.0580 ± 1.8884	1.0123 ± 0.7655
FEMALE	FP 6h (N=9)	109.6479 ± 84.9601	18.5218 ± 7.7947	4.8079 ± 4.7544	0.3214 ± 0.1431	1.1490 ± 0.3875	4.0301 ± 1.8374	0.5603 ± 0.5899
	FP 24h (N=9)	67.2169 ± 102.1033	20.2170 ± 12.4872	9.8111 ± 11.6909	0.4087 ± 0.1728	1.0796 ± 0.4093	5.4997 ± 2.4034	0.4171 ± 0.3503
	FP 48h (N=10)	63.5765 ± 73.8635	16.6967 ± 8.0513	6.8759 ± 6.1645	0.2223 ± 0.1560	0.8831 ± 0.3067	3.4646 ± 1.9698	0.5982 ± 1.9698
	Vehicle (N =9)	116.7039 ± 188.1931	15.9346 ± 10.8039	5.1464 ± 4.1567	0.5047 ± 0.5083	1.0219 ± 0.3500	3.1732 ± 1.3137	116.7039 ± 0.7115

Sex	Group	14,15-EET	14-HDHA
MALE	**FP 6h (N=8)**	0.0527 ± 0.0578	18.0267 ± 26.2160
	FP 24h (N=9)	0.1820 ± 0.3430	6.6622 ± 8.5754
	FP 48h (N=10)	0.1606 ± 0.1764	7.3576 ± 5.3414
	Vehicle (N =8)	0.1165 ± 0.1153	5.3283 ± 4.1867
FEMALE	**FP 6h (N=9)**	0.0575 ± 0.0762	9.2483 ± 8.0227
	FP 24h (N=9)	0.0435 ± 0.0394	14.6022 ± 17.3423
	FP 48h (N=10)	0.0467 ± 0.0603	5.0079 ± 5.6638
	Vehicle (N =9)	0.1513 ± 0.1437	16.8102 ± 23.6958

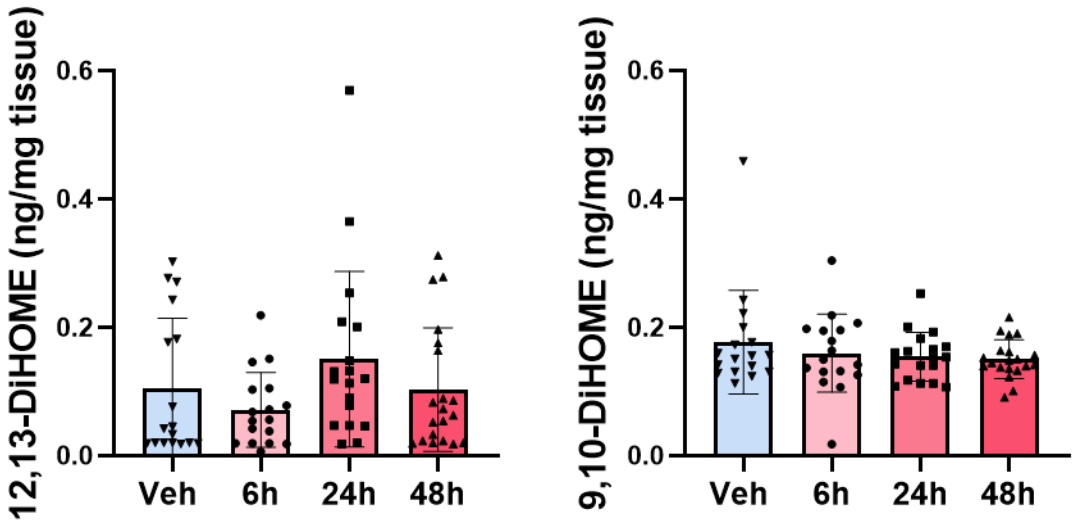

Figure 17. Lung tissue concentrations of 12,13-DiHOME and 9,10-DiHOME following fecal peritonitis. Individual data points with mean ± SD for vehicle controls, 6 h, 24 h, and 48 h groups. Although both metabolites were detectable in most animals, no statistically significant changes were observed across time points.

Unlike plasma, which displayed a clear temporal shift in LA derived metabolites, lung tissue LMs did not show coordinated or time dependent changes. This divergence suggests that circulating LMs reflect systemic inflammation more sensitively than local tissue pools.

4.2.4. Biochemical evidence of lung injury following fecal peritonitis

Although plasma LMs showed clear systemic alterations during early FP, lung tissue analyses revealed no significant changes in LM concentrations and the lung wet to dry weight ratio did not differ between septic and vehicle control animals (Table 12), indicating an absence of overt pulmonary edema within the 48 hour observation period. These findings suggest that biochemical dysregulation occurs systemically before measurable structural injury becomes detectable in lung tissue.

4.2.4.1. Neutrophil driven lung inflammation

Given that early inflammatory activation may precede fluid accumulation or morphological damage, we next quantified two established markers of neutrophil driven lung injury, MPO and CD16, to assess whether molecular signatures of pulmonary inflammation were present despite the lack of gross edema. MPO reflects the activated state and of neutrophils, whereas increased CD16 expression is indicative of enhanced neutrophil presence and recruitment into lung tissue, i.e. neutrophil infiltration.

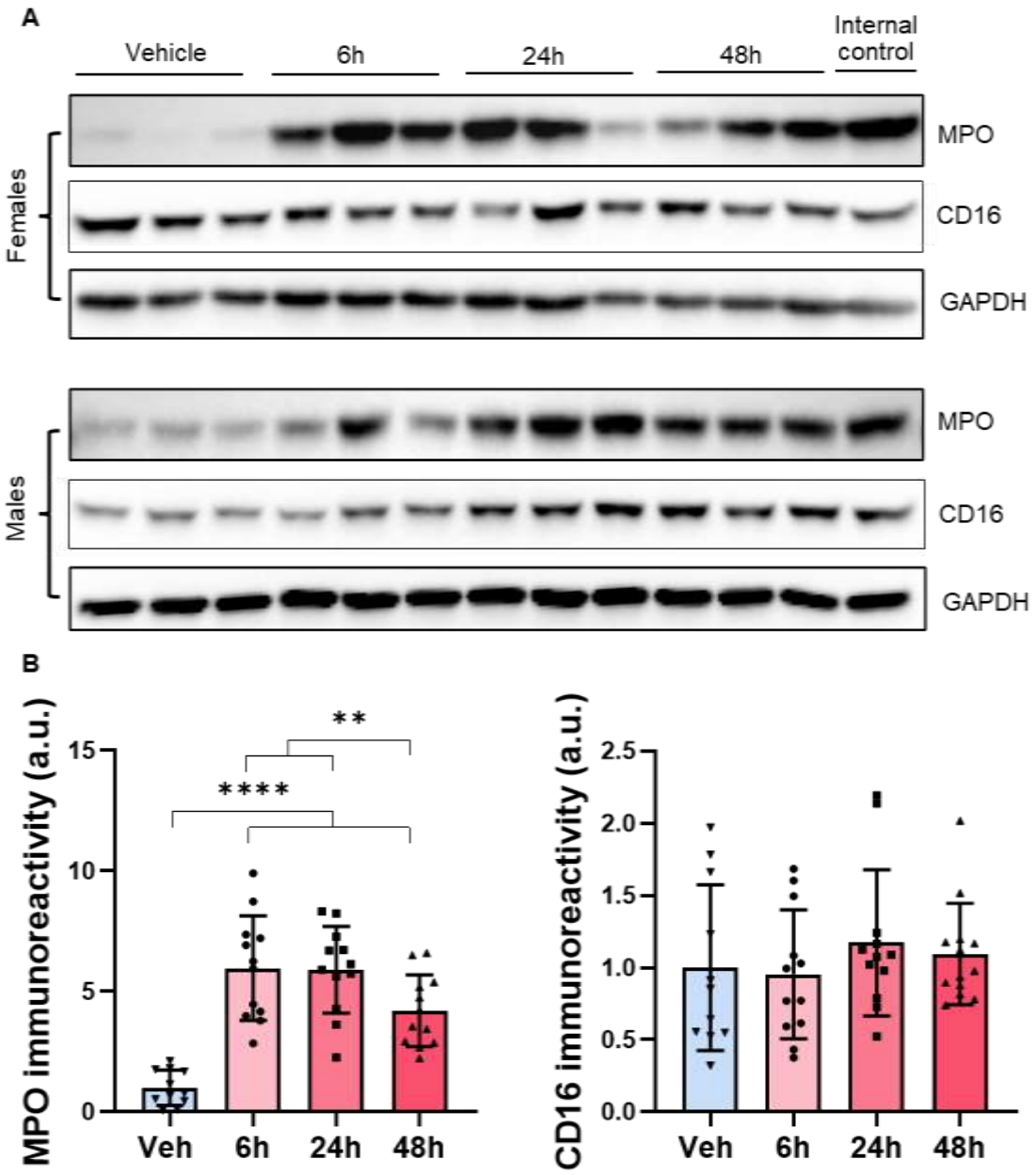

Figure 18. MPO and CD16 expression in lung tissue following fecal peritonitis. (A) Representative Western blots for MPO and CD16 from vehicle control, 6 h, 24 h, and 48 h groups. (B) Densitometric quantification of MPO and CD16 at the indicated time points. MPO, but not CD16, was significantly increased in septic animals compared with vehicle controls, indicating early neutrophil activation despite the absence of measurable pulmonary edema. CD16 levels showed a trend toward higher values but did not reach statistical significance. Data are presented as mean ± SD; each dot represents an individual animal. * $p < 0.05$; ** $p < 0.01$; *** $p < 0.001$; **** $p < 0.0001$

4.2.4.2. Plasma lipid mediators correlate with pulmonary neutrophil activation

To determine whether systemic LM alterations reflect pulmonary inflammatory activation, MPO expression in lung tissue was correlated with plasma concentrations of LMs that were significantly elevated during FP (12,13-DiHOME, 9,10-DiHOME, 9,10-DiHODE and 9-oxoODE). Linear regression analyses showed significant positive associations between MPO and 12,13-DiHOME, 9,10-DiHOME and 9-oxoODE, indicating that higher systemic levels of these LA-derived metabolites correspond to stronger neutrophil activation in the lung. In contrast, 9,10-DiHODE did not show a significant correlation with MPO, suggesting that not all LMs elevated in plasma equally reflect pulmonary inflammatory status.

This suggests that circulating DiHOMEs and related metabolites may serve as early biochemical indicators of lung-directed inflammatory processes, even in the absence of overt tissue injury.

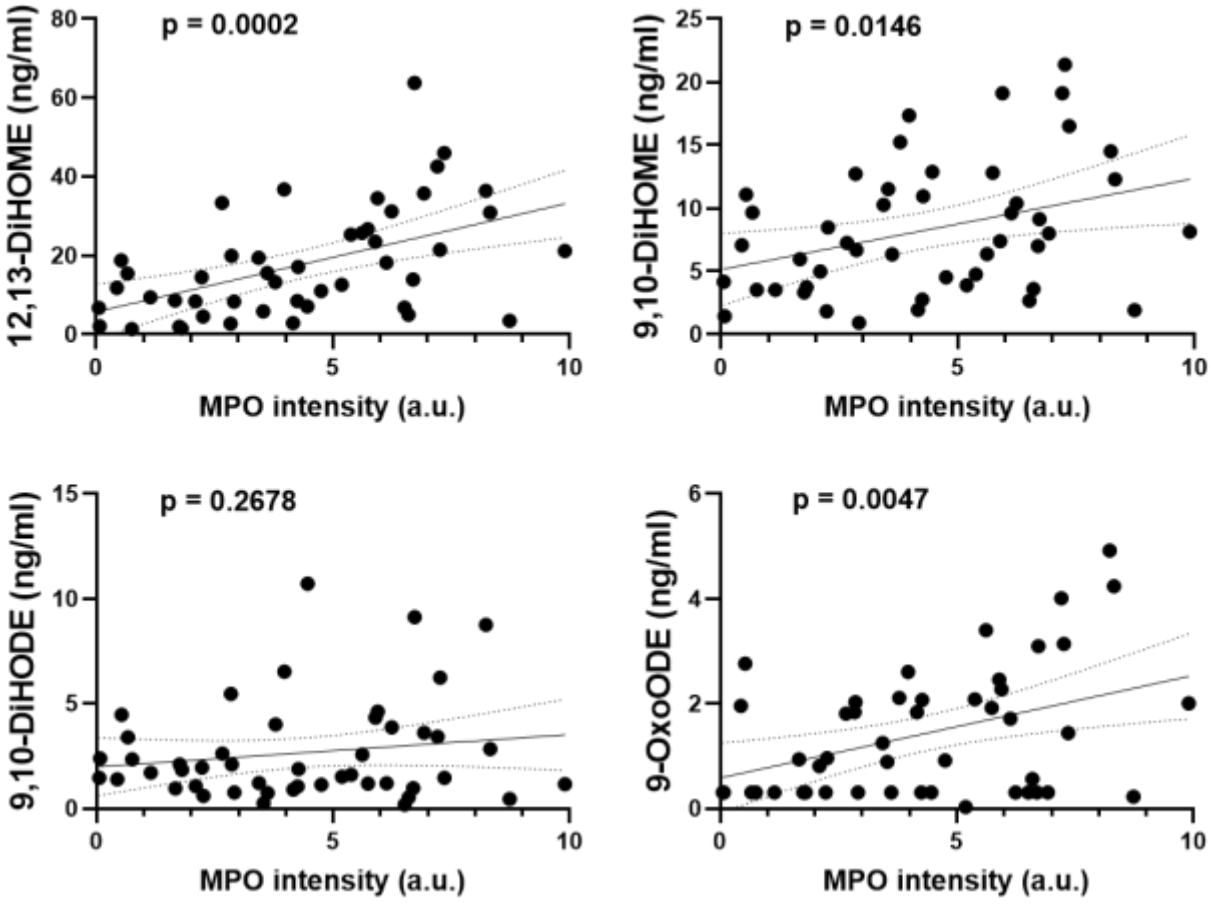

Figure 19. Correlation between lung MPO expression and plasma lipid mediators elevated in fecal peritonitis. Scatter plots with linear regression lines for MPO vs. 12,13-

DiHOME, 9,10-DiHOME, 9,10-DiHODE and 9-oxoODE. Significant positive correlations were observed for 12,13-DiHOME, 9,10-DiHOME and 9-oxoODE, whereas 9,10-DiHODE showed no significant association with MPO. Shaded areas represent 95% confidence intervals; each point represents an individual animal.

Together, our *in vivo* results demonstrate that FP induces a rapid and systemic shift in circulating LA derived LMs, most notably DiHOMEs, which emerge as sensitive early indicators of the septic state. In contrast, lung tissue LM levels remained low and unchanged, and no overt pulmonary edema developed within the 48-hour window. Nevertheless, increased MPO expression revealed early neutrophil-driven inflammatory activation in the lung, and this activation correlated strongly with plasma concentrations of elevated LA derived metabolites. These findings indicate that systemic LM responses precede measurable structural lung injury and that circulating DiHOMEs may serve as early biochemical markers linking systemic metabolic alterations to pulmonary inflammatory activation in FP.

Although both male and female rats were included in FP study, sex-stratified analyses did not reveal consistent or biologically meaningful differences in LM responses to FP. For this reason, plasma data were pooled to increase statistical power. Nonetheless, subtle sex-specific effects cannot be fully excluded and should be explored in future studies with designs powered specifically for sex comparisons.

4.3. Dietary modulation of lipid mediator profiles

4.3.1. Dietary linoleic acid content determines circulating plasma lipid mediators' profile

Among female rats, mean body weight at 9 weeks did not differ between the LA-rich and OA-rich diet groups (262.0 ± 25.5 g vs 253.3 ± 37.7 g). In males, animals fed the OA-rich diet were heavier on average than those fed the LA-rich diet at 9 weeks (376.3 ± 96.5 g vs 338.2 ± 76.1 g), although this trend did not reach statistical significance. Plasma LM profiles from all samples (N = 23) were subsequently evaluated by principal component analysis (PCA). As shown in Figure 20A, samples segregated into two distinct clusters according to diet when plotted across principal component 1 (PC1) and principal component 2 (PC2). Together, PC1 and PC2 explained 59.5% of the total variance (Figure 20B), and the relative contributions of individual LM variables to each component are summarized in Figure 20C.

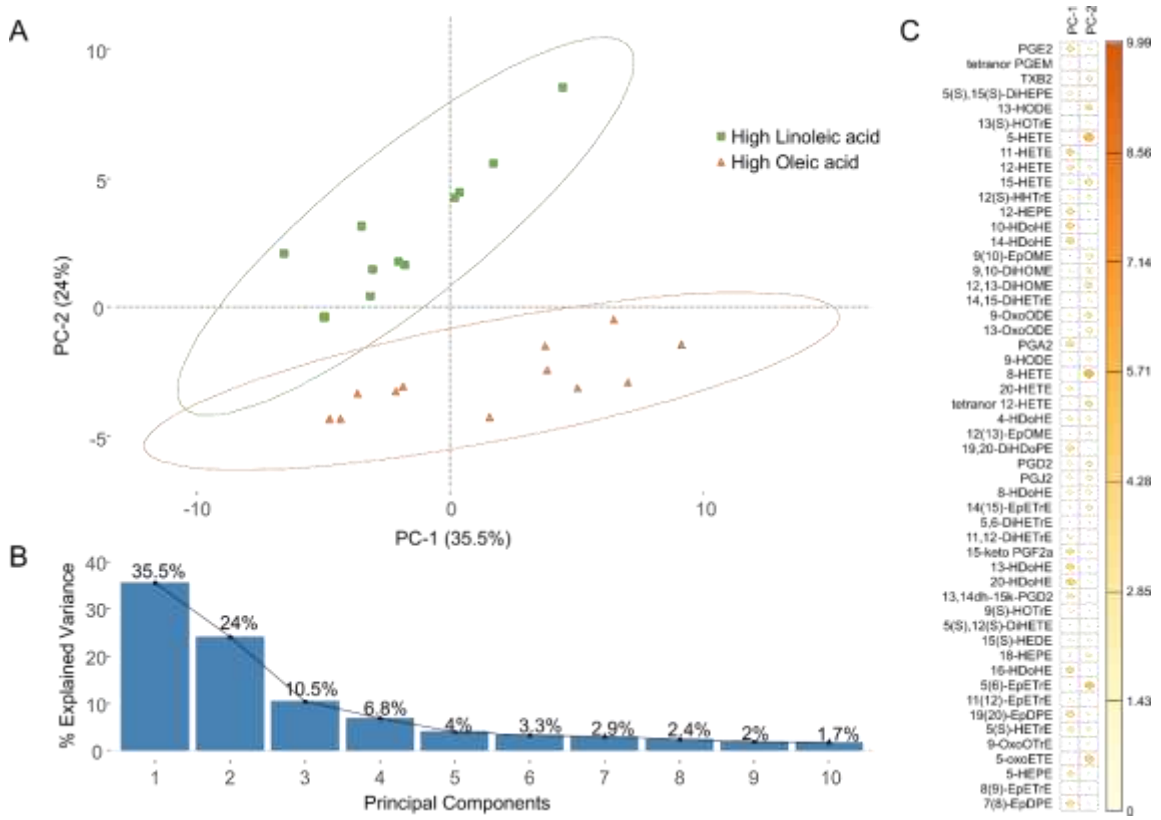

Figure 20. Dietary fatty acid composition determines circulating plasma LM profile. (A) PCA of rat plasma LMs after exposure to an LA-rich diet (green squares, N=11) or OA-rich diet (orange triangles, N=12). Samples are plotted on PC1 and PC2, which explain 35.5% and 24.0% of the total variance, respectively. Diet-dependent separation was primarily observed along PC2. (B) Proportion of variance explained by principal components PC1–PC10. (C) Factor map showing the contributions of individual LMs to PC1 and PC2; larger and darker points indicate stronger contributions to the respective component.

4.3.2. High linoleic acid dietary content promotes plasma accumulation of pro-inflammatory lipid mediators

As expected, rats maintained on the LA-rich diet displayed greater plasma accumulation of LMs derived from LA and its longer chain derivative AA, while accumulation of LMs derived from EPA and DHA was greater in rats maintained on the OA-rich diet. Univariate analysis detected 28 LMs with a p-value < 0.05 and a log2fold change > 1.5 (Figure 21), which we classified as “pro-inflammatory”, “anti-inflammatory”, or “unknown”.

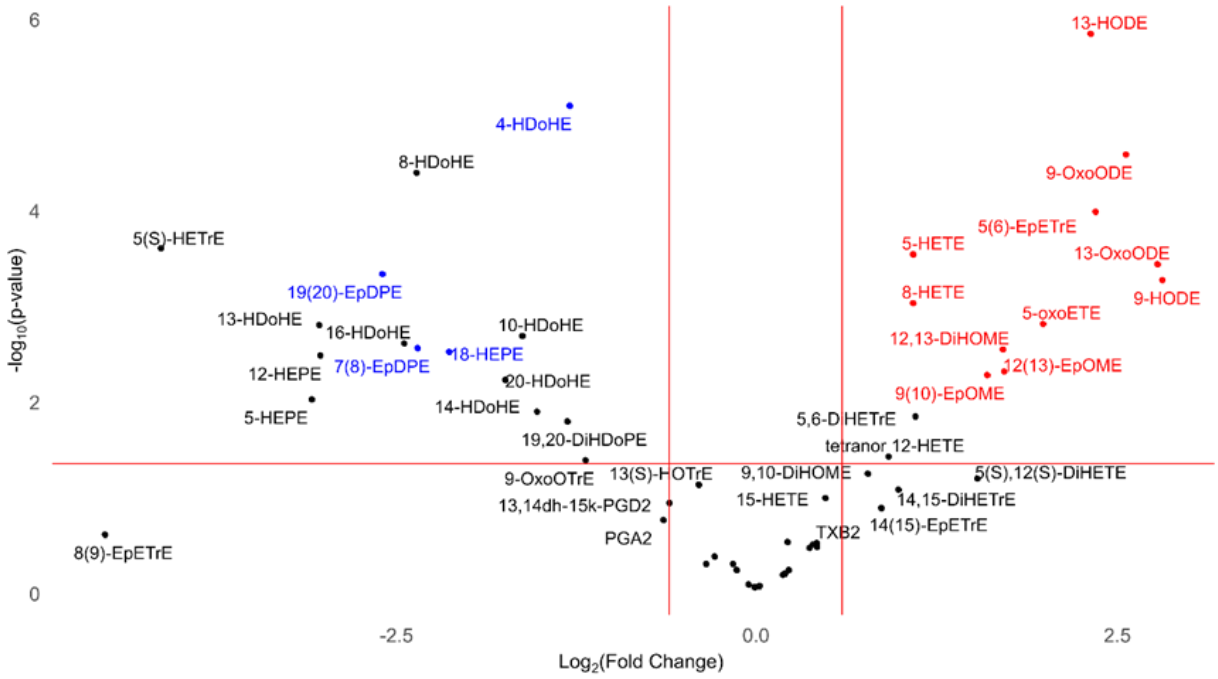

Figure 21. Excessive dietary linoleic acid promotes plasma accumulation of pro-inflammatory lipid mediators. Volcano plot of plasma LMs of rats fed LA-rich versus OA-rich diets. The x-axis represents the log2 fold change (LA-rich vs OA-rich diet) for each LM. Positive values indicate higher plasma concentrations in animals fed the LA-rich diet, whereas negative values indicate higher concentrations in animals fed the OA-rich diet. The y-axis shows statistical significance expressed as −log10 (p value). LMs with reported pro-inflammatory activity are highlighted in red, while those with reported anti-inflammatory activity are shown in blue.

4.4. TRPV1 channels as potential molecular targets of lipid mediators

Because the vanilloid binding pocket of TRPV1 represents a well-defined lipid-accessible regulatory site, it was used as a model system to evaluate whether circulating LMs possess the structural capacity to interact with TRP channels at the molecular level.

To assess this possibility, we performed molecular docking followed by molecular-dynamics simulations using the capsaicin-bound TRPV1 structure as a reference. A set of 13 endogenous LMs previously reported to modulate TRPV1 activity in vitro, 5-HETE, 20-HETE, LTB_4, 12-HpETE, 15-HpETE, 9-HODE, 13-HODE, 9-oxoODE, 13-oxoODE, 9(10)-EpOME, 12(13)-EpOME, 9,10-DiHOME, and 12,13-DiHOME, was selected for *in silico* interrogation together with AA and LA as negative controls. These ligands, derived from AA and LA, were docked into the vanilloid pocket, a region critical for TRPV1 activation and known to bind capsaicin as well as several endogenous lipid agonists.

The purpose of this computational approach was not to establish TRPV1 as the dominant mediator of lung injury, but rather to determine whether FP-associated LMs possess structural compatibility with TRPV1 ligand-binding architecture. This provides a molecular framework for interpreting whether circulating LMs could potentially modulate TRP channel activity during systemic inflammation.

4.4.1. Capsaicin docking

To validate the docking protocol, capsaicin was first docked into the vanilloid pocket of TRPV1 using both the closed (PDB: 7LPA) and open (PDB: 7LPE) channel conformations. In both structures, capsaicin adopted the characteristic head-down, tail-up orientation, with its vanillyl moiety directed toward the intracellular side and forming a persistent hydrogen bond between the keto group and Tyr511, accompanied by similar hydrophobic contacts. Subsequent 300-ns MD simulations confirmed that these interactions were stable over time and were not affected by modeling of the missing extracellular residues. Because the binding mode closely matched the cryo-EM reference pose, this validated the use of the closed TRPV1 structure for subsequent docking of endogenous LMs.

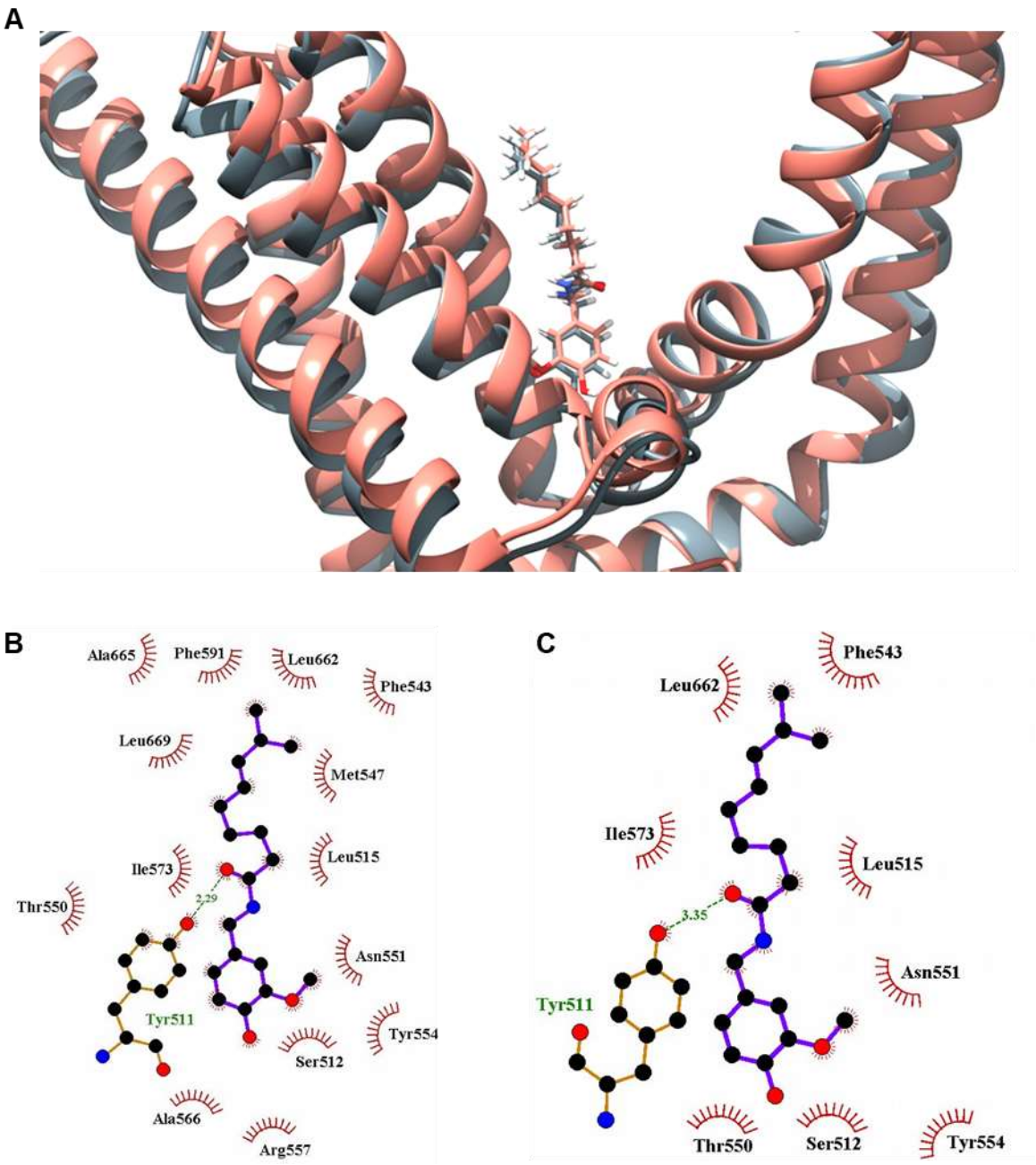

Figure 22. Capsaicin docking in the vanilloid pocket of TRPV1 in closed and open channel conformations. (A) Superposition of capsaicin docked into the closed (PDB: 7LPA) and opened (PDB: 7LPE) TRPV1 structures. Despite differences in global channel conformation, capsaicin occupies a nearly identical pose within the vanilloid pocket, adopting the characteristic head-down, tail-up orientation. (B) Interaction diagram illustrating capsaicin docked into the vanilloid pocket of the closed TRPV1 conformation. Capsaicin forms a stable hydrogen bond with Tyr511, supported by hydrophobic contacts with closest residues (C) Interaction diagram illustrating capsaicin binding within the vanilloid pocket of the open TRPV1 conformation. The binding poses and the major

stabilizing interactions, including the hydrogen bond with Tyr511 and hydrophobic contacts with surrounding residues, remain highly conserved relative to the closed state structure.

4.4.2. Docking of lipid mediators into the TRPV1 vanilloid pocket

After validating the docking protocol with capsaicin, the remaining LMs were docked into the vanilloid pocket using the capsaicin binding pose as a starting position. Clear differences emerged between simple ω-6 PUFAs (LA, AA) and their oxygenated derivatives.

LA and AA, which do not activate TRPV1, served as negative controls and showed minimal ability to interact with the pocket. Aside from transient contact between their terminal carboxyl group and Arg557, neither PUFA formed stable polar interactions (Figure 21A, Figure 22A). LA was particularly unstable and frequently shifted out of the binding site, consistent with its lack of TRPV1 agonist activity.

In contrast, all LM ligands displayed more defined and stable binding behavior, attributable to the presence of additional polar functional groups along the acyl chain. These groups enabled persistent hydrogen bonds and polar contacts with pocket residues, notably Tyr511, Thr550, and surrounding hydrophobic side chains, resulting in substantially improved stabilization relative to their parent PUFAs.

Here, we'll describe just some of the results obtained. Among LA derived LMs, 9-HODE adopted a twisted but stable conformation maintained by a weak hydrogen bond with Tyr511 (Figure 21B), whereas 9-oxoODE formed multiple (up to four) stable hydrogen bonds with Tyr511 and exhibited minimal movement, reflecting a strongly favored pose (Figure 21C).

Among AA derived LMs, LTB_4 formed an additional hydrogen bond through its C-12 hydroxyl group, improving pocket engagement compared with AA (Figure 22B). 15-HpETE also demonstrated stable binding, primarily via interactions with Thr550 rather than Tyr511, revealing an alternative but compatible binding mode (Figure 22C).

Collectively, these docking results demonstrate a clear distinction between parent PUFAs, which lack stable pocket engagement, and oxygenated LMs, which exhibit structurally favorable interactions consistent with their ability to modulate TRPV1 activity.

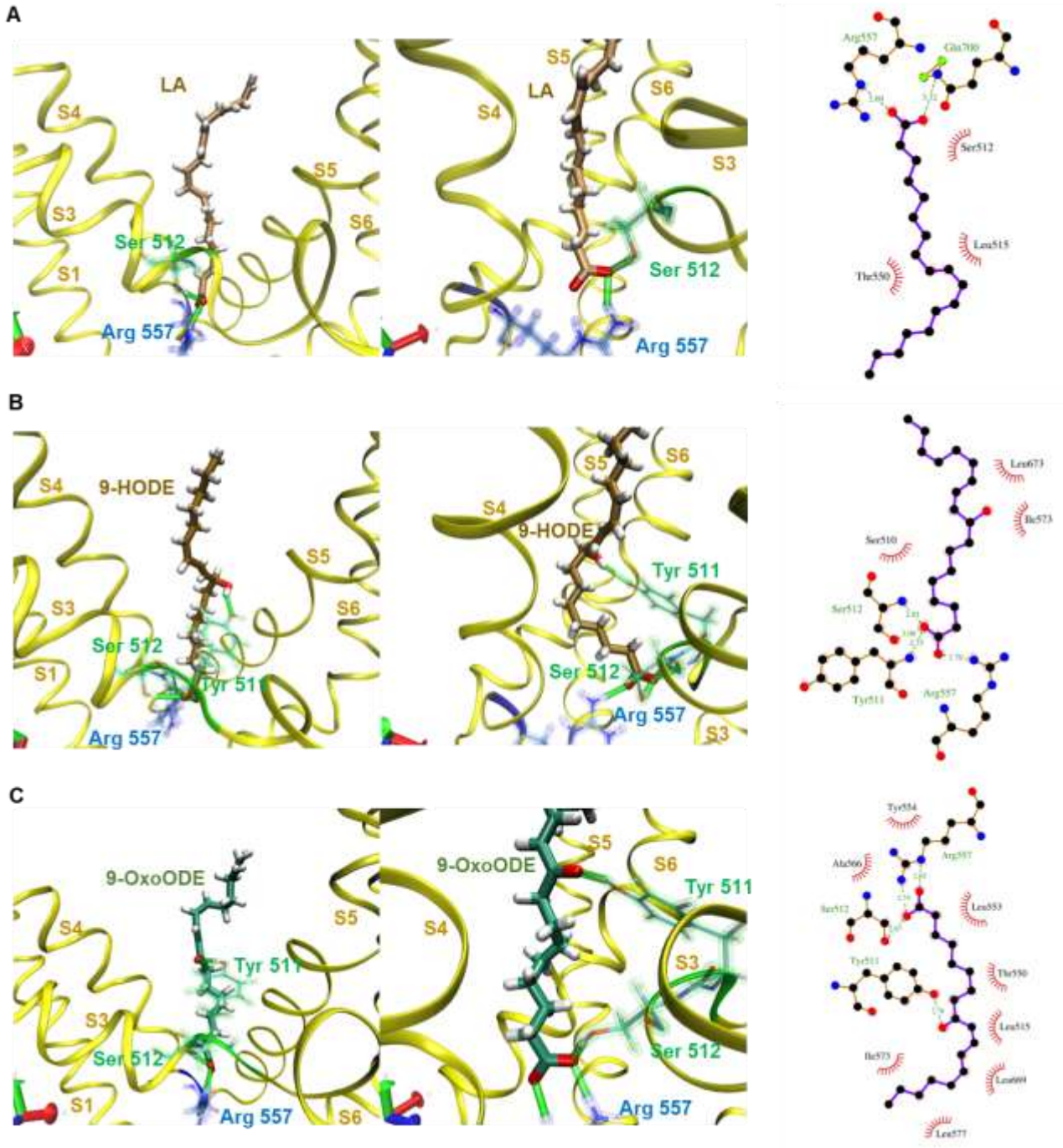

Figure 23. Binding interactions of linoleic acid and its derivatives 9-HODE and 9-OxoODE within the vanilloid pocket of the TRPV1 channel. (A) LA bound to the vanilloid pocket (left), with rotation of 90 (middle), and visual representation of all stable binding interactions (right). (B) 9-HODE bound to the vanilloid pocket (left), with rotation of 90 rotation of 90 (middle), and visual representation of all stable binding interactions (right). (C) 9-oxoODE bound to the vanilloid pocket (left), with (middle), and visual

representation of all stable binding interactions (right). Transmembrane domains of TRPV1 channel are noted as S1-S6.

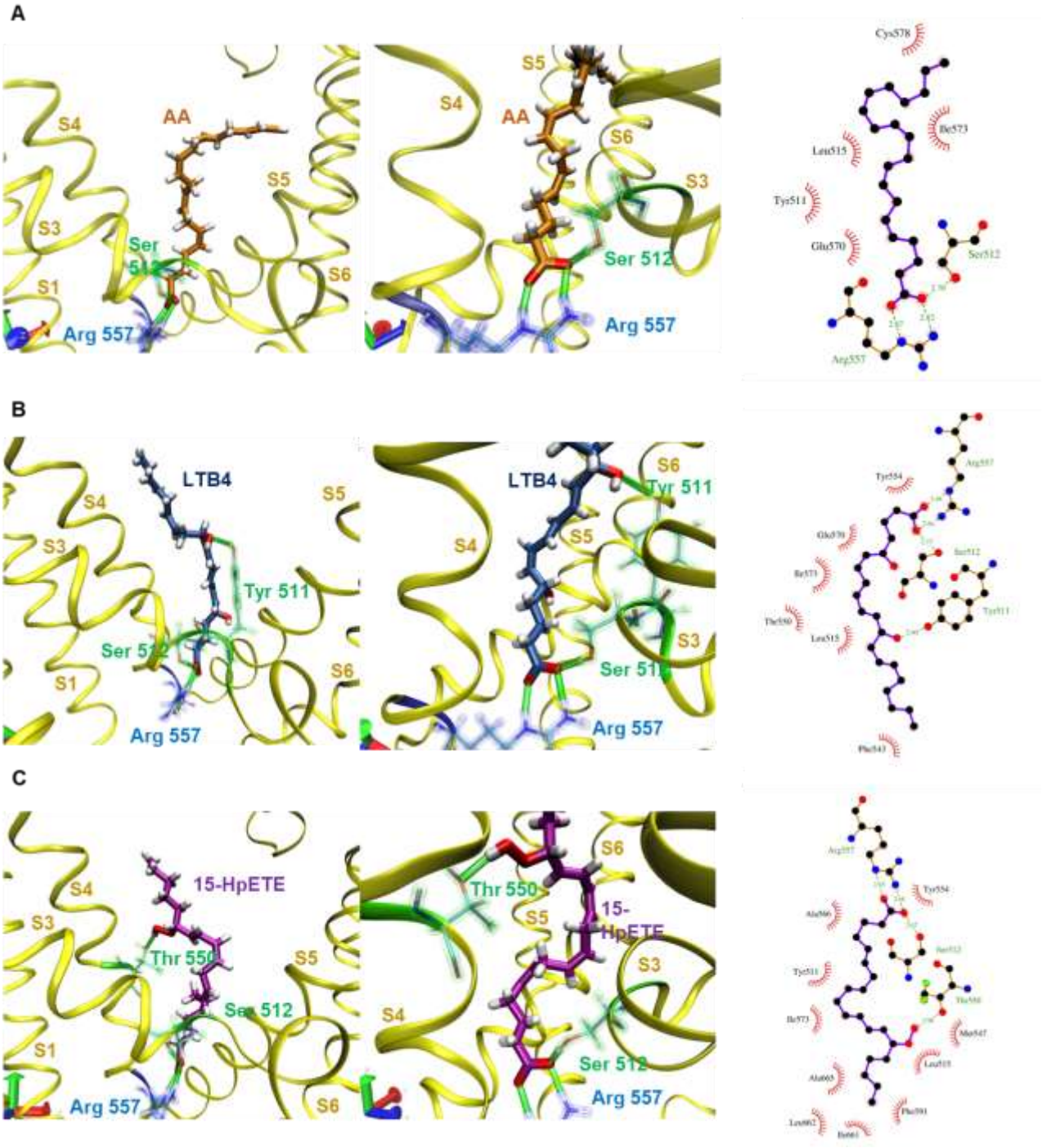

Figure 24. Binding interactions of arachidonic acid (AA) binding and its derivatives LTB4 and 15-HpETE within the vanilloid pocket of the TRPV1 channel. (A) AA bound to the vanilloid pocket (left), with rotation of 90(middle), and visual representation of all stable binding interactions (right). (B) LTB4 bound to the vanilloid pocket (left), with rotation of 90 rotation of 90 (middle), and visual representation of all stable binding interactions (right). (C) 15-HpETE bound to the vanilloid pocket (left), with (middle), and

visual representation of all stable binding interactions (right). Transmembrane domains of TRPV1 channel are noted as S1-S6**.**

4.4.3. Total free binding energy

After describing molecular interactions of LMs and TRPV1 we then calculated the total free binding energies (ΔG) of all LM ligands and compared them to that of capsaicin. Most LM ligands showed lower (more negative) binding free energies than capsaicin, indicating thermodynamically favorable binding to the TRPV1 vanilloid pocket. In contrast, 13-HODE and 9,10-DiHOME exhibited higher (less favorable) free binding energies, consistent with reduced compatibility with this binding site (Figure 23).

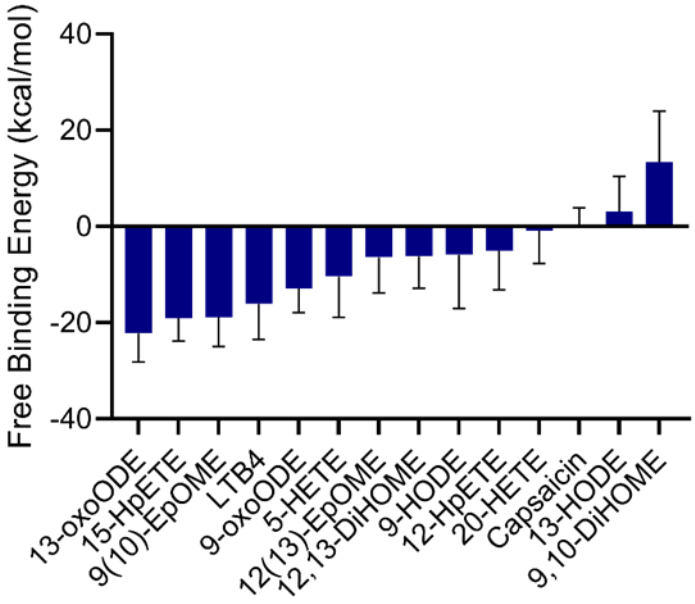

Figure 25. Docking-based estimates of free binding energy for lipid mediators in the TRPV1 vanilloid pocket. LM ligands were docked into the TRPV1 vanilloid pocket and their corresponding ΔG were calculated and expressed relative to capsaicin (each ΔG was normalized to the capsaicin reference). Values below the capsaicin baseline (negative ΔG values) indicate stronger, more favorable binding, whereas values above baseline (positive ΔG values) indicate weaker, less favorable binding. In addition, the spread of ΔG estimates was used as an indicator of binding stability, where greater dispersion suggests less consistent (i.e., less stable) binding.

4.4.4. Amino acid residues contribute to free binding energy

To further characterize LM–TRPV1 interactions, residue-specific contributions to the overall ΔG were evaluated (Figure 24A). Capsaicin exhibited predominantly favorable interactions across multiple amino acid residues, without pronounced repulsive contributions. In contrast, all LM ligands showed varying degrees of unfavorable (repulsive) interactions, with the most prominent repulsion observed for 9,10-DiHOME.

To explore similarities and differences in residue-level interaction patterns among ligands, principal component analysis (PCA) was applied to per-residue energy contributions and visualized in a two-dimensional space (Figure 24B). The first principal component (PC1), capturing the largest proportion of variance, was primarily driven by differences in polar repulsive interactions. The second principal component (PC2) reflected variations in ligand orientation and interactions with residues Ser510 and Ser512, located toward the intracellular region of the vanilloid pocket.

This analysis clearly distinguished capsaicin from all LM ligands, indicating a unique interaction profile. Additional separation was observed for 20-HETE and 9-HODE, consistent with their distinct binding conformations. Specifically, 20-HETE positioned its carboxyl group outside the vanilloid pocket (Figure 7), whereas 9-HODE inserted its carboxyl group deeper into the pocket, enabling interactions with Ser510 and Ser512 (Figure 25). Moreover, 13-oxoODE and 12-HpETE exhibited stable and persistent interactions with Ser510 (data not shown).

Finally, ligands sharing structural similarities, such as EpOMEs and DiHOMEs, clustered together in the PCA space, while AA derived LMs were preferentially distributed along PC2, reflecting common interaction features.

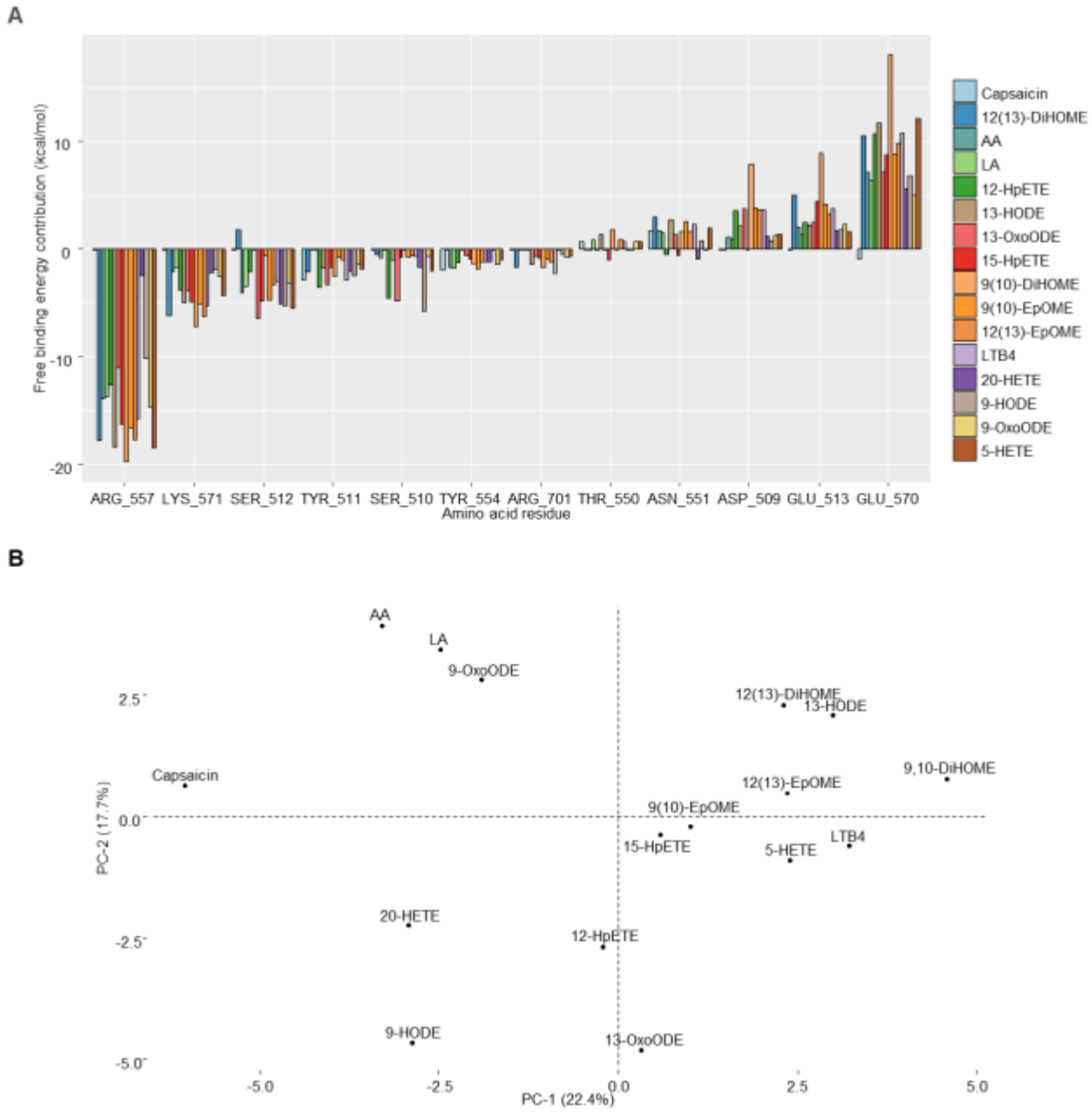

Figure 26. Estimated free binding energy contribution of amino acid residues in the vanilloid pocket to lipid mediator ligand binding. (A) Per-residue ΔG contributions for each LM ligand. Negative ΔG values indicate favorable residue-ligand interactions, with more negative values reflecting stronger contributions to binding. Positive ΔG values indicate unfavorable (repulsive) contributions, where larger positive values correspond to stronger repulsion. (B) PCA of per-residue ΔG contribution profiles across LM ligands. Ligands are projected onto PC1 and PC2, accounting for 24.0% and 16.3% of the total variance, respectively.

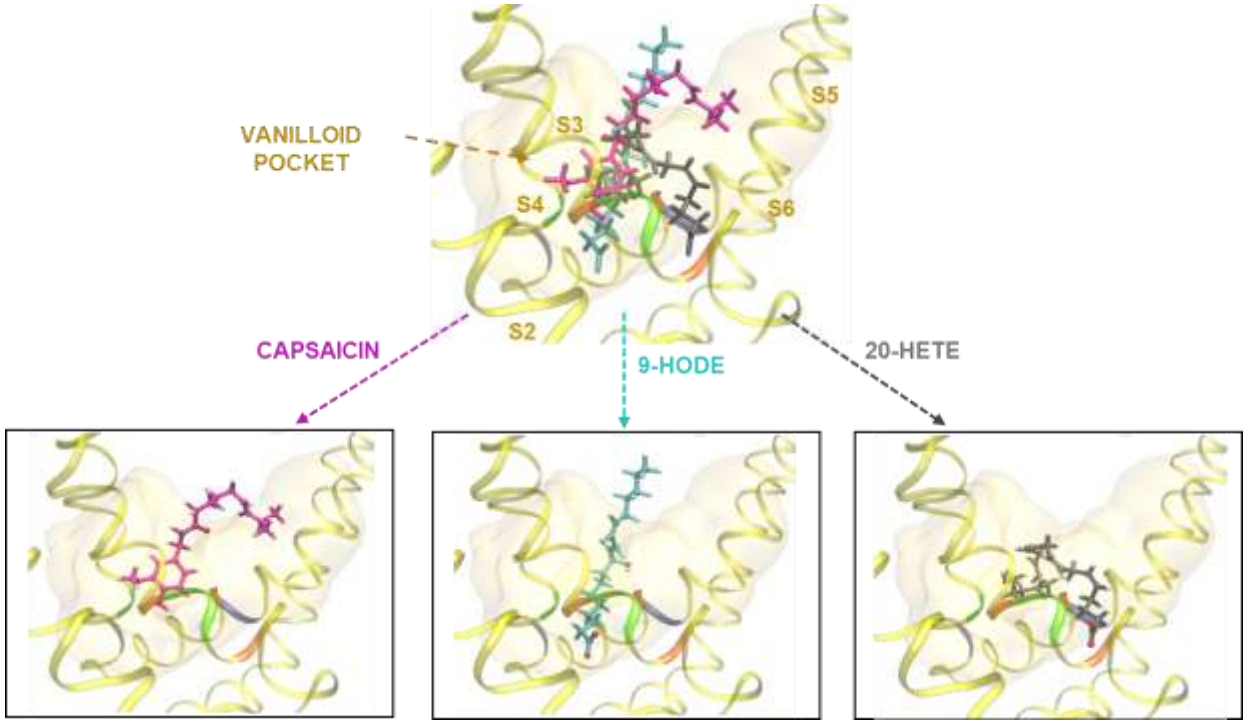

Figure 27. Superposition of the ligands bound within the vanilloid pocket of TRPV1. Capsaicin (purple), 9-HODE (cyan), and 20-HETE (grey) are shown overllaped within the vanilloid pocket (top). Bottom left: capsaicin adopts a head-down, tail-up orientation within the pocket. Bottom middle: 9-HODE is positioned deeper inside the vanilloid pocket. Bottom right: 20-HETE is oriented with its carboxyl group displaced toward the exterior of the vanilloid pocket. Ribbon coloring denotes negatively charged (red), positively charged (blue), and polar (green) amino acid residues. Transmembrane domains of the TRPV1 channel are labeled S1–S6.

4.4.5. Root mean square fluctuation

Across simulations, capsaicin showed very limited positional variability, reflected by consistently low root mean square fluctuation (RMSF) values (Figure 25). In contrast, selected LMs, including 12-HpETE and 9(10)-EpOME, exhibited higher RMSF, consistent with their ability to occupy two or more comparably stable binding poses within the TRPV1 vanilloid pocket. This conformational switching (“flipping”) between alternative stable orientations increased the apparent fluctuation.

Notably, 9,10-DiHOME also presented relatively low RMSF, however, this primarily resulted from pronounced repulsive interactions that constrained its mobility within the pocket, yielding restricted motion despite overall unfavorable binding. Overall, RMSF was influenced by both the position and number of polar functional groups on the LM, which

modulated hydrophobic tail stability. Therefore, atom-resolved RMSF analysis is required to more reliably evaluate LM binding stability.

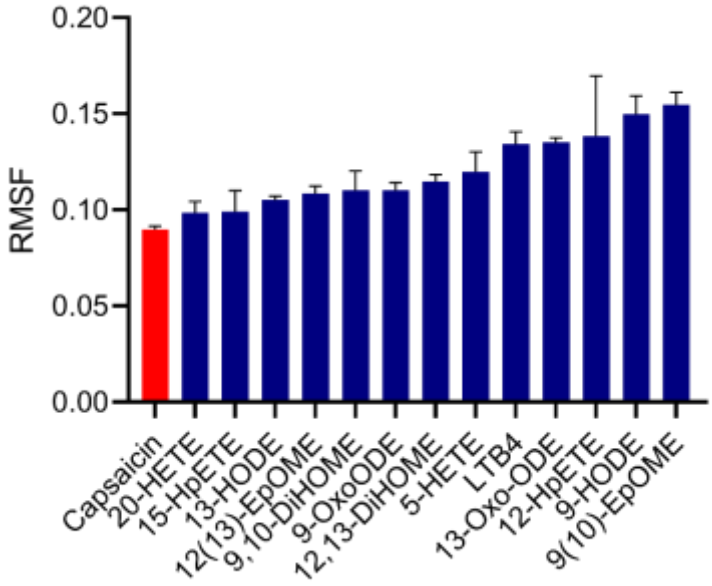

Figure 28. Distribution of root mean square fluctuation values for lipid mediator ligands bound in the TRPV1 vanilloid pocket. The histogram depicts RMSF values for all ligands over 45 ns of molecular dynamics simulations. RMSF was calculated as the mean fluctuation across all ligand atoms. Error bars indicate standard errors of the mean.

In summary, we used molecular dynamics simulations to examine how 13 LM ligands interact with the TRPV1 vanilloid pocket. The results indicate that a subset of LMs can adopt energetically favorable and stable binding within this site, whereas others may preferentially modulate TRPV1 via alternative interaction regions rather than the canonical vanilloid pocket. Overall, structurally related LMs tended to show comparable interaction profiles, although several clear exceptions emerged, which may help contextualize divergent *in vitro* and *in vivo* pharmacodynamic findings. Our study provides a novel starting point for future *in silico* studies investigating the binding interactions of LM ligands with TRPV1.

5. Discussion

Dysregulated LM signaling has been increasingly implicated in the lung pathogenesis including sALI, where it contributes to inflammatory amplification, endothelial dysfunction, and early tissue damage. Given these established associations, we sought to determine whether changes in LM profile could provide insight into the biochemical events that precede poor outcomes in sepsis. Using a rodent FP model, a widely used but biologically complex approach to mimic polymicrobial sepsis, we combined targeted LC-MS/MS profiling with biochemical markers of lung inflammation and *in silico* interrogation of LM-TRPV1 channel interactions. Although FP does not fully recapitulate the heterogeneity and clinical progression of human sALI, it robustly induces early systemic inflammation and therefore provides a suitable framework for studying upstream events.

Results of our study reveal an early shift in LA derived LMs and evidence of early neutrophil activation in lung tissue following FP. Moreover, our computational analyses demonstrate that several of this inflammation associated LMs are structurally capable of engaging the vanilloid binding pocket of TRPV1, suggesting a potential molecular mechanism linking circulating LMs with downstream cellular activation.

5.1. LC-MS/MS lipid mediator analysis

Accurate interpretation of LM dynamics critically depends on the analytical method used to quantify them. LMs are chemically heterogeneous, low abundant and highly reactive metabolites, and their reliable detection requires exceptional chromatographic resolution and MS sensitivity. Many species occur in the low pg/mL to low ng/mL range, also undergo rapid enzymatic turnover, and exhibit substantial structural similarity, particularly within regioisomeric pairs. As a result, LM quantification remains analytically demanding and often necessitates the use of high-performance MS platforms and carefully optimized acquisition strategies. An additional consideration is the markedly uneven endogenous abundance of different lipid classes. LA is the most abundant dietary PUFA in Western-type diets and is highly enriched in mammalian membrane PL. Consequently, LA derived metabolites such as DiHOMEs, EpOMEs and HODEs are often present at higher baseline concentrations and are therefore much easier to detect quantitatively than many AA or omega-3 derived mediators. Importantly, their apparent dominance in LM datasets should not be interpreted just as evidence of exclusive biological relevance, but also as a reflection of their favorable detectability. Conversely, structurally important but less abundant mediators may remain below LOD and LOQ even when biologically upregulated, indicating that analytical invisibility does not necessarily imply biological absence.

In this study, we optimized targeted LC-MS/MS for quantification of >100 structurally diverse LMs, including multiple regioisomers that are challenging to separate and

quantify. Several aspects of the method substantially strengthened the reliability of our findings. First, chromatographic optimization allowed baseline separation of key isomeric pairs, such as EpOMEs and DiHOMEs, which is essential given their identical precursor masses and overlapping fragmentation patterns. Without sufficient chromatographic resolution, quantitative interpretation of individual LA derived metabolites would not have been possible. Second, on-column optimization of MRM transitions improved signal stability and minimized in-source fragmentation, ensuring that the selected precursor-product ion pairs were truly analyte specific. Third, the use of a scheduled MRM acquisition strategy markedly increased dwell time and signal to noise ratio for low abundant analytes. This was particularly important for mediators present near the LOQ in biological matrices, where conventional unscheduled MRM would dilute signal across too many transitions and compromise peak definition.

In addition to instrumental optimization, sample preparation was a critical determinant of analytical performance. SPE was used to remove polar interferents that suppress ionization of low abundant LMs. SPE enrichment increases analytical sensitivity and reproducibility, however, recovery varies across lipid panels. The recovery differences highlight a limitation of LM analysis suggesting that no single extraction protocol uniformly recovers all lipid families, necessitating the use of IS to correct for class specific losses. To address this, we incorporated multiple deuterated IS distributed across the chromatographic run, enabling accurate normalization of analytes to the nearest eluting IS. Because deuterated IS standards co-elute with their non-labeled analogues and experience the same extraction losses and matrix effects, this approach corrected for variability in SPE recovery, matrix effect and day to day instrument drift. Using several IS rather than one was essential given the chemical diversity of the LM panel.

Despite these optimizations, only a minority of the >100 targeted LMs was reliably quantified, while the rest remained below the LOQ, particularly in lung tissue, even after sample pre-concentration. Rather than representing a failure of the analytical approach, this pattern reflects the intrinsically low endogenous abundance, rapid turnover and matrix-dependent recovery of many LMs.

Together, these methodological considerations highlight both the strengths and unavoidable constraints of LC-MS/MS based LM profiling and provide important context for interpreting the observed predominance of LA derived LMs in our dataset.

5.2. Rodent fecal peritonitis model

The FP model used in this study represents one of the most widely employed and physiologically relevant experimental systems for inducing polymicrobial sepsis in rodents. Its major strength lies in its ability to reproduce the early systemic inflammatory surge characteristic of human sepsis, including rapid cytokine release, metabolic

reprogramming, circulatory disturbances and multi-organ stress responses. FP also triggers complex and dynamic host-pathogen interaction, involving bacterial products, damage-associated molecules and innate immune activation, thereby providing an appropriate context in which to study upstream biochemical signals such as LMs.

However, FP does not fully replicate the heterogeneity or treatment-modified trajectories of sALI in humans. Lung injury in this model often develops later and may remain subtle within short observational windows, and species-specific differences in immune responses and LM metabolism can further limit direct translation. Thus, while FP offers a biologically informative framework for probing early systemic LM shifts and lung-directed inflammatory activation, validation in complementary models and human cohorts will be essential for fully understanding their relevance to sALI.

5.3. Interpretation of systemic lipid mediator dynamics

The plasma LM profile following FP revealed a rapid and selective shift dominated by LA derived metabolites, particularly both DiHOME diols. We observed a rapid and sustained increase in plasma LA derived 12,13-DiHOME, 9,10-DiHOME, 9-OxoODE and ALA derived 9,10-DiHODE, whereas lung tissue concentrations remained unchanged. Although LA derived mediators are generally easier to detect due to their higher endogenous abundance, the magnitude and consistency of the early DiHOME rise indicate that this signal reflects genuine biological activation rather than a simple analytical bias. Indeed, similar early systemic increases in LA diols have been reported during acute inflammation and correlate with poor outcomes in trauma and sepsis (Bergmann et al., 2022). A comparable elevation of DiHOMEs has been observed in bronchoalveolar lavage fluid of asthmatic patients (Larsson et al., 2014). Elevated DiHOME/EpOME ratios and nonlinear EpOME-DiHOME relationships further support the presence of an early metabolic shift within the LA metabolic pathway. Functionally, such DiHOME accumulation has been associated with endothelial barrier dysfunction, impaired mitochondrial bioenergetics and neutrophil priming, all processes relevant to the pathogenesis of sALI.

In contrast, other PUFA derived mediators that were detected, remained comparatively stable across time points. This divergence between LM classes may indicate pathway prioritization early in sepsis, where LA derived signals dominate the circulating LM landscape. Importantly, however, the relative stability of other PUFA metabolites does not imply a lack of involvement. Their low baseline concentrations and rapid intracellular turnover make systemic detection considerably more challenging. Likewise, CYP450 dependent pathways are known to be activated during systemic inflammation and may contribute to broader LM dysregulation beyond what is analytically visible in circulation.

By 48 h, most elevated metabolites exhibited partial normalization, consistent with a transient systemic inflammatory pulse rather than ongoing accumulation. This temporal profile aligns with reported shifts from early hyperinflammatory to later immunomodulatory phases in sepsis, where acute LM bursts are followed by metabolic adaptation or exhaustion of biosynthetic capacity.

Overall, the observed systemic LM dynamics support a model in which early sepsis is characterized by a rapid and preferential activation of LA metabolic pathways, producing a distinct plasma signature. These findings highlight the sensitivity of circulating LMs as early indicators of systemic inflammatory activation.

5.4. Plasma-lung dissociation: why systemic LM shifts do not mirror lung tissue levels

Although plasma LMs showed a clear early shift following FP, corresponding changes in lung tissue were not detected. This discrepancy is not unexpected and reflects inherent differences between circulating and tissue derived LMs. Plasma LM concentrations integrate systemic production from multiple organs and therefore respond rapidly to whole-body inflammatory activation. In contrast, lung tissue LMs are produced and metabolized locally, and often remain confined to specific cellular compartments rather than accumulating in bulk tissue.

Another contributing factor is that many LMs in solid organs occur at extremely low concentrations, frequently near or below analytical quantification limits, even when biologically active. This is particularly relevant for early time points, where molecular activation may precede measurable lipid accumulation. Consistent with this, only a small subset of targeted LMs was quantifiable in lung homogenates despite adequate analytical sensitivity.

Importantly, the absence of detectable LM changes in lung tissue does not rule out their involvement in sALI. Taken together, these findings suggest that systemic LM shifts occur earlier and more robustly than detectable changes in lung tissue and may represent upstream inflammatory events that precede or modulate local biochemical responses in the lung.

5.5. Early biochemical activation of neutrophils in lung tissue

Although lung LM concentrations did not show measurable changes within the first 48 hours of FP, biochemical markers of neutrophil activity revealed evidence of early inflammatory activation in the lung. MPO, a marker of neutrophil activation was significantly elevated in septic animals, whereas CD16, a marker associated with

neutrophil recruitment, remained unchanged. This pattern suggests that neutrophils were activated but not yet substantially accumulated within lung tissue, reflecting an early inflammatory stage preceding structural injury. These findings are consistent with established models of sepsis induced acute lung injury, in which neutrophil activation occurs hours before overt infiltration or edema. MPO elevation indicates enhanced oxidative potential and release of granule enzymes, processes known to impair endothelial integrity and contribute to barrier dysfunction. In contrast, unchanged CD16 levels suggest that widespread neutrophil recruitment into the parenchyma had not yet occurred, aligning with the lack of significant changes in the lung wet to dry weight ratio.

Together, these results indicate that the lung has entered a biochemical phase of injury, characterized by early neutrophil activation without detectable structural alteration. This supports the concept that systemic inflammatory signals, including circulating LMs, may prime or activate pulmonary immune cells before measurable tissue-level remodeling occurs. The timing of these events further aligns with the observed plasma LM dynamics, suggesting that systemic LM disturbances may contribute to early neutrophil dependent processes in the lung.

5.6. Influence of dietary linoleic acid on lipid mediator biosynthesis

With this experiment we demonstrated that exposure to a LA rich diet increases plasma accumulation of pro-inflammatory LMs derived from LA and AA. Moreover, exposure to a diet with reduced LA is associated with increased plasma accumulation of anti-inflammatory LMs derived from EPA and DHA. The latter observation is somewhat unexpected given that these fatty acids were not components of either diet and the concentration of their precursor, ALA, was equal in both diets (Table 8). It is likely that excess LA interferes with production of anti-inflammatory LMs derived from the less abundant EPA and DHA. These findings are consistent with finding of Taha et al., which demonstrated that lowering dietary LA in humans increased the plasma concentrations of the omega-3 PUFAs, EPA and DHA (Taha et al., 2014). Excess dietary LA likely competes with ALA for elongation-desaturation enzymes that convert ALA to long-chain omega-3 PUFAs. Additionally, excess dietary LA likely competes with omega-3 PUFAs for enzymes involved in LM production. This further raises the possibility that high LA intake may reduce the benefits of EPA and DHA supplementation based on substrate competition.

The diets used in the present study were manufactured using purified triglycerides, and the only source of dietary PUFA were the essential FA, LA and ALA. This allowed for the dietary FA content to be precisely controlled, beyond what can be done with commercially available oils. An additional strength of this study was the breadth of the panel of quantified LMs, which included most LMs derived from COX, LOX and CYP pathways, for which standards are commercially available. Limitation of our study is the single timepoint of sample collection, which occurred at nine weeks of age. It remains unclear if diet-dependent differences in LM profiles are exaggerated in older rats.

A recent meta-analysis by Li et. al., indicates that higher LA intake is associated with modest reductions in cardiovascular disease risk and mortality (Li et al., 2020). However, as the authors accurately highlight as a major limitation, the default comparison for most of the studies included in their analysis compared high LA intake to high saturated fatty acid intake. It is unclear whether widespread dietary campaigns aimed at reducing cardiovascular disease risk by reducing dietary intake of saturated fat may have inadvertently promoted hyper-inflammatory states in the population, by increasing LA consumption.

Our findings suggest that dietary LA content may be a modifiable lifestyle factor that can regulate accumulation of pro-inflammatory LMs and support the notion that LMs can be valuable biomarkers for poor pulmonary outcomes in sepsis.

5.7. Structural compatibility of lipid mediators with TRPV1

To explore whether circulating LMs have the structural capacity to modulate ion channels involved in inflammatory signaling, we examined the ability of selected LMs to bind the vanilloid pocket of TRPV1 using molecular docking and molecular dynamics simulations. This pocket is the best-defined ligand binding region of TRPV1, responsible for capsaicin recognition and gating transitions, and therefore represents a suitable site for probing potential lipid-channel interactions.

Using capsaicin as a starting ligand, we first validated the docking protocol by demonstrating highly conserved binding geometries and residue interactions in both open and closed TRPV1 conformations. We then docked a panel of 13 endogenous LMs previously reported to influence TRPV1 activity *in vitro*. Most ligands adopted stable pose within the vanilloid pocket and exhibited favorable binding free energies, often more negative than those of capsaicin, indicating that several LMs possess strong structural compatibility with TRPV1. In contrast, only a few ligands, such as 13-HODE and 9,10-DiHOME, showed less favorable binding energies, suggesting that not all LMs share the same capacity to engage in this pocket.

Analysis of per-residue energy contributions revealed that capsaicin formed uniformly stabilizing interactions with no relevant repulsive components, whereas all LMs displayed varying degrees of repulsion within the pocket. Certain ligands, such as 20-HETE and 9-HODE, adopted distinct binding geometries driven by the position of their terminal carboxyl groups, which either extended toward the pocket entrance or interacted more deeply with intracellularly oriented residues. Principal component analysis further demonstrated clustering of structurally related LMs, such as EpOMEs and DiHOMEs, indicating that shared structural motifs guide their interaction behavior.

These computational findings do not prove TRPV1 activation in sALI, but they show that several inflammation-associated LMs have the structural prerequisites to bind a key

regulatory site of TRPV1. This raises the possibility that LM surges observed during early sepsis could influence TRP channel activity, either directly or indirectly, thereby contributing to inflammatory signaling pathways relevant to lung injury. Future functional studies will be necessary to determine whether these structurally compatible LMs act as agonists, partial agonists, or modulators of TRPV1 gating under physiological conditions.

5.8. Integrated interpretation of lipid mediator dynamics, lung responses and TRPV1 interactions

Taken together, our findings outline a coherent sequence of early events that connect systemic LM dysregulation with biochemical signs of lung injury. The rapid and selective surge of LA derived metabolites in plasma, particularly DiHOMEs, indicates activation of LA pathways within hours of FP. These metabolites have been implicated in endothelial dysfunction, mitochondrial impairment, and neutrophil priming, suggesting that their early rise may contribute to inflammatory activation in lungs even before structural damage becomes apparent.

Consistent with this interpretation, lung tissue did not yet show detectable LM accumulation or fluid imbalance, but exhibited clear biochemical evidence of neutrophil activation, reflected by increased MPO levels. This dissociation between systemic lipid level and tissue level suggests that early LM perturbations function as upstream inflammatory signals, capable of priming pulmonary immune responses ahead of measurable edema or lipid remodeling in the lung parenchyma.

Our *in silico* analyses further demonstrate that several LMs that were found elevated in plasma possess the structural capacity to bind the vanilloid pocket of TRPV1, a lipid-sensitive ion channel expressed in pulmonary cell types. Although docking does not establish functional activation, the observed binding compatibilities highlight a plausible molecular interface through which circulating LMs could modulate cellular excitability, calcium flux, or inflammatory signaling pathways relevant to lung injury. These computational results, together with the biological data, suggest that TRP channels may represent downstream targets of early LM accumulation during sepsis.

In summary, the integration of plasma lipidomic, lung biochemical markers, and TRPV1 structural modeling supports a model in which systemic LA derived LMs participate in pulmonary injury pathways. This framework provides mechanistic insight into early sALI and identifies potential lipid-TRP channel interactions worthy of further experimental validation.

5.9. Limitations of the study

Several limitations of this study should be acknowledged when interpreting the findings.

First, although the LC-MS/MS method was extensively optimized, only a minority of the >100 targeted LMs could be reliably quantified, particularly in lung tissue. This reflects the intrinsically low endogenous abundance, rapid turnover, and matrix-dependent recovery of many LMs, but nonetheless restricts the breadth of tissue level conclusions that can be drawn. Second, lung tissue was analyzed as whole homogenate, which may obscure microdomain-specific lipid signaling; biologically meaningful LM fluctuations occurring at endothelial or epithelial interfaces may not be detectable in bulk tissue. Third, the assessment of lung inflammation was limited to MPO and CD16, which capture early neutrophil activation but do not fully represent the complexity of pulmonary immune responses. A more comprehensive panel, including markers of endothelial injury, oxidative stress, and cytokine signaling, may reveal additional mechanistic layers as well as histological evaluation.

In addition, although molecular docking provides valuable structural insight, it cannot establish whether LMs functionally activate or inhibit TRPV1 channels *in vivo*. Functional electrophysiological or calcium-imaging assays are required to determine whether structurally compatible LMs exert physiological effects on TRP channel gating. Finally, the FP model represents a clinically relevant form of polymicrobial sepsis but may not capture the full spectrum of immune and metabolic responses seen in human sALI. Extension to additional models or human samples will therefore be important for broader translational interpretation.

6. Conclusion

For this study, we established and optimized a targeted LC-MS/MS method for quantitative profiling of LMs in plasma and lung tissue.

Investigating the role of LMs in sALI pathophysiology in the FP rat model of sepsis, we found that:

- FP induced a rapid and selective systemic shift in plasma LMs, dominated by LA derived metabolites
- Plasma 12,13-DiHOME and 9,10-DiHOME increased markedly at 6 h and 24 h, with partial normalization by 48 h while other metabolites remained comparatively stable
- Lung tissue LM concentrations showed no significant group differences, indicating a plasma-lung dissociation in early LM dynamics
- Despite the absence of overt pulmonary edema (wet/dry ratio), lung MPO was elevated, consistent with early neutrophil activation preceding measurable structural injury
- Plasma 12,13-DiHOME correlated strongly with lung MPO, linking systemic LA derived LM dysregulation to early pulmonary inflammation

These findings suggest that early sepsis is characterized by a transient systemic surge of LA derived LMs that precedes overt edema yet aligns with early neutrophil activation in the lung.

Investigating LM-TRPV1 interactions by *silico* analyses, we found that:

- Multiple endogenous LMs displayed stable binding within the TRPV1 vanilloid pocket during molecular dynamics simulations, frequently engaging key residues implicated in activation of the channel
- Overall binding energetics and interaction patterns support structural compatibility of several LMs with TRPV1

These computational results suggest that several inflammation-associated LMs possess the structural prerequisites to interact with a key regulatory site of TRPV1, warranting future functional validation.

Investigating if dietary interventions modulate circulatory LM profiles, we found that:

- Dietary FA composition strongly shapes the circulating LM profile
- High dietary LA promoted accumulation of LA and AA derived pro-inflammatory LMs and reduced omega-3 derived anti-inflammatory mediators.

These findings suggest diet as a major upstream determinant of systemic LM balance and an important modifiable lifestyle factor for lowering the risk of hyperinflammatory states.

Based on our findings, our ongoing study aims to assess how dietary intervention affects pulmonary outcomes, including markers of lung injury, in the FP model.

7. References

Abraham, E. (2016). New Definitions for Sepsis and Septic Shock: Continuing Evolution but With Much Still to Be Done. *JAMA*, *315*(8), 757–759. https://doi.org/10.1001/JAMA.2016.0290

Alvarez, D. F., King, J. A., Weber, D., Addison, E., Liedtke, W., & Townsley, M. I. (2006). Transient receptor potential vanilloid 4-mediated disruption of the alveolar septal barrier: A novel mechanism of acute lung injury. *Circulation Research*, *99*(9), 988–995. https://doi.org/10.1161/01.RES.0000247065.11756.19

Aoyama, H., Suzuki, K., Izawa, Y., Kobashashi, M., & Ozawa, T. (1982). Mitochondria-toxic activity in burned human skin: relation to severity of burn and period after burn. *Burns*, *9*(1), 13–16. https://doi.org/https://doi.org/10.1016/0305-4179(82)90129-2

Astarita, G., Kendall, A. C., Dennis, E. A., & Nicolaou, A. (2015). Targeted lipidomic strategies for oxygenated metabolites of polyunsaturated fatty acids. In *Biochimica et Biophysica Acta - Molecular and Cell Biology of Lipids* (Vol. 1851, Issue 4, pp. 456–468). Elsevier B.V. https://doi.org/10.1016/j.bbalip.2014.11.012

Bang, S., Yoo, S., Yang, T. J., Cho, H., & Hwang, S. (2012). 17(R)-resolvin D1 specifically inhibits transient receptor potential ion channel vanilloid 3 leading to peripheral antinociception. *British Journal of Pharmacology*, *165*(3), 683–692. https://doi.org/10.1111/j.1476-5381.2011.01568.x

Bang, S., Yoo, S., Yang, T. J., Cho, H., Kim, Y. G., & Hwang, S. W. (2010). Resolvin D1 attenuates activation of sensory transient receptor potential channels leading to multiple anti-nociception. *British Journal of Pharmacology*, *161*(3), 707–720. https://doi.org/10.1111/j.1476-5381.2010.00909.x

Bastarache, J. A., Smith, K., Jesse, J. J., Putz, N. D., Meegan, J. E., Bogart, A. M., Schaaf, K., Ghosh, S., Shaver, C. M., & Ware, L. B. (2022). A two-hit model of sepsis plus hyperoxia causes lung permeability and inflammation. *American Journal of Physiology - Lung Cellular and Molecular Physiology*, *322*(2), L273–L282. https://doi.org/10.1152/AJPLUNG.00227.2021

Bellani, G., Laffey, J. G., Pham, T., Fan, E., Brochard, L., Esteban, A., Gattinoni, L., Van Haren, F. M. P., Larsson, A., McAuley, D. F., Ranieri, M., Rubenfeld, G., Thompson, B. T., Wrigge, H., Slutsky, A. S., & Pesenti, A. (2016). Epidemiology, patterns of care, and mortality for patients with acute respiratory distress syndrome in intensive care units in 50 countries. *JAMA - Journal of the American Medical Association*, *315*(8), 788–800. https://doi.org/10.1001/jama.2016.0291

Belvisi, M. G., & Birrell, M. A. (2017). The emerging role of transient receptor potential channels in chronic lung disease. *The European Respiratory Journal*, *50*(2). https://doi.org/10.1183/13993003.01357-2016

Blasbalg, T. L., Hibbeln, J. R., Ramsden, C. E., Majchrzak, S. F., & Rawlings, R. R. (2011). Changes in consumption of omega-3 and omega-6 fatty acids in the United States during the 20th century. *The American Journal of Clinical Nutrition*, *93*(5), 950–962. https://doi.org/10.3945/AJCN.110.006643

Bone, R. C., Balk, R. A., Cerra, F. B., Dellinger, R. P., Fein, A. M., Knaus, W. A., Schein, R. M. H., & Sibbald, W. J. (1992). Definitions for sepsis and organ failure and guidelines for the use of innovative therapies in sepsis. *Chest*, *101*(6), 1644–1655. https://doi.org/10.1378/chest.101.6.1644

Boomer, J. S., To, K., Chang, K. C., Takasu, O., Osborne, D. F., Walton, A. H., Bricker, T. L., Jarman, S. D., Kreisel, D., Krupnick, A. S., Srivastava, A., Swanson, P. E., Green, J. M., & Hotchkiss, R. S. (2011). Immunosuppression in patients who die of sepsis and multiple organ failure. *JAMA*, *306*(23), 2594–2605. https://doi.org/10.1001/jama.2011.1829

Brash, A. R. (1999). Lipoxygenases: Occurrence, functions, catalysis, and acquisition of substrate. In *Journal of Biological Chemistry* (Vol. 274, Issue 34, pp. 23679–23682). https://doi.org/10.1074/jbc.274.34.23679

Buczynski, M. W., Dumlao, D. S., & Dennis, E. A. (2009). An integrated omics analysis of eicosanoid biology. In *Journal of Lipid Research* (Vol. 50, Issue 6, pp. 1015–1038). https://doi.org/10.1194/jlr.R900004-JLR200

Burney, M., Underwood, J., McEvoy, S., Nelson, G., Dzierba, A., Kauari, V., & Chong, D. (2012). Early Detection and Treatment of Severe Sepsis in the Emergency Department: Identifying Barriers to Implementation of a Protocol-based Approach. *Journal of Emergency Nursing*, *38*(6), 512–517. https://doi.org/10.1016/j.jen.2011.08.011

Cai, L., Rodgers, E., Schoenmann, N., & Raju, R. P. (2023). Advances in Rodent Experimental Models of Sepsis. *International Journal of Molecular Sciences*, *24*(11). https://doi.org/10.3390/IJMS24119578

Calfee, C. S., Delucchi, K., Parsons, P. E., Thompson, B. T., Ware, L. B., & Matthay, M. A. (2014). Subphenotypes in acute respiratory distress syndrome: Latent class analysis of data from two randomised controlled trials. *The Lancet Respiratory Medicine*, *2*(8), 611–620. https://doi.org/10.1016/S2213-2600(14)70097-9

Cao, E., Liao, M., Cheng, Y., & Julius, D. (2013). TRPV1 structures in distinct conformations reveal mechanisms of activation. *Nature*, *504*(7478), 113. https://doi.org/10.1038/NATURE12823

Caterina, M. J., Schumacher, M. A., Tominaga, M., Rosen, T. A., Levine, J. D., & Julius, D. (1997). The capsaicin receptor: A heat-activated ion channel in the pain pathway. *Nature*, *389*(6653), 816–824. https://doi.org/10.1038/39807

Chen, H., Zhang, Y., Zhang, W., Liu, H., Sun, C., Zhang, B., Bai, B., Wu, D., Xiao, Z., Lum, H., Zhou, J., Chen, R., & Liang, G. (2019). Inhibition of myeloid differentiation factor 2 by baicalein protects against acute lung injury. *Phytomedicine*, *63*. https://doi.org/10.1016/j.phymed.2019.152997

Chiamvimonvat, N., Ho, C.-M., Tsai, H.-J., & Hammock, B. D. (2007). The Soluble Epoxide Hydrolase as a Pharmaceutical Target for Hypertension. *Journal of Cardiovascular Pharmacology*, *50*(3), 225–237. https://doi.org/10.1097/FJC.0b013e3181506445

Chousterman, B. G., Swirski, F. K., & Weber, G. F. (2017). Cytokine storm and sepsis disease pathogenesis. In *Seminars in Immunopathology* (Vol. 39, Issue 5, pp. 517–528). Springer Verlag. https://doi.org/10.1007/s00281-017-0639-8

Dalli, J., Colas, R. A., Quintana, C., Barragan-Bradford, D., Hurwitz, S., Levy, B. D., Choi, A. M., Serhan, C. N., & Baron, R. M. (2017). Human Sepsis Eicosanoid and Proresolving Lipid Mediator Temporal Profiles: Correlations with Survival and Clinical Outcomes. *Critical Care Medicine*, *45*(1), 58–68. https://doi.org/10.1097/CCM.0000000000002014

Damann, N., Owsianik, G., Li, S., Poll, C., & Nilius, B. (2009). The calcium-conducting ion channel transient receptor potential canonical 6 is involved in macrophage inflammatory protein-2-induced migration of mouse neutrophils. *Acta Physiologica*, *195*(1), 3–11. https://doi.org/10.1111/j.1748-1716.2008.01918.x

De Petrocellis, L., Schiano Moriello, A., Imperatore, R., Cristino, L., Starowicz, K., & Di Marzo, V. (2012). A re-evaluation of 9-HODE activity at TRPV1 channels in comparison with anandamide: Enantioselectivity and effects at other TRP channels and in sensory neurons. *British Journal of Pharmacology*, *167*(8), 1643–1651. https://doi.org/10.1111/j.1476-5381.2012.02122.x

Dejager, L., Pinheiro, I., Dejonckheere, E., & Libert, C. (2011). Cecal ligation and puncture: The gold standard model for polymicrobial sepsis? *Trends in Microbiology*, *19*(4), 198–208. https://doi.org/10.1016/j.tim.2011.01.001

Delano, M. J., & Ward, P. A. (2016). The immune system's role in sepsis progression, resolution, and long-term outcome. In *Immunological Reviews* (Vol. 274, Issue 1, pp. 330–353). Blackwell Publishing Ltd. https://doi.org/10.1111/imr.12499

Dennis, E. A., & Norris, P. C. (2015). Eicosanoid storm in infection and inflammation. In *Nature Reviews Immunology* (Vol. 15, Issue 8, pp. 511–523). Nature Publishing Group. https://doi.org/10.1038/nri3859

Dibekoğlu, C., Kemertaş, K., Aygun, H., & Erbas, O. (2025). Methylene Blue Alleviates Inflammatory and Oxidative Lung Injury in a Rat Model of Feces-Induced Peritonitis. *Medicina (Lithuania)*, *61*(8). https://doi.org/10.3390/medicina61081456

Dietrich, A. (2019). Modulators of transient receptor potential (TRP) channels as therapeutic options in lung disease. In *Pharmaceuticals* (Vol. 12, Issue 1). MDPI AG. https://doi.org/10.3390/ph12010023

Englert, J. A., Bobba, C., & Baron, R. M. (2019). Integrating molecular pathogenesis and clinical translation in sepsis-induced acute respiratory distress syndrome. In *JCI Insight* (Vol. 4, Issue 2). American Society for Clinical Investigation. https://doi.org/10.1172/jci.insight.124061

Evans, L., Rhodes, A., Alhazzani, W., Antonelli, M., Coopersmith, C. M., French, C., Machado, F. R., Mcintyre, L., Ostermann, M., Prescott, H. C., Schorr, C., Simpson, S., Wiersinga, W. J., Alshamsi, F., Angus, D. C., Arabi, Y., Azevedo, L., Beale, R., Beilman, G., … Levy, M. (2021). Surviving sepsis campaign: international guidelines for management of sepsis and septic shock 2021. *Intensive Care Medicine*, *47*(11), 1181–1247. https://doi.org/10.1007/s00134-021-06506-y

Fallon, E. A., Chung, C. S., Heffernan, D. S., Chen, Y., De Paepe, M. E., & Ayala, A. (2021). Survival and Pulmonary Injury After Neonatal Sepsis: PD1/PDL1's Contributions to Mouse and Human Immunopathology. *Frontiers in Immunology*, *12*. https://doi.org/10.3389/fimmu.2021.634529

Festic, E., Carr, G. E., Cartin-Ceba, R., Hinds, R. F., Banner-Goodspeed, V., Bansal, V., Asuni, A. T., Talmor, D., Rajagopalan, G., Frank, R. D., Gajic, O., Matthay, M. A., & Levitt, J. E. (2017). Randomized Clinical Trial of a Combination of an Inhaled Corticosteroid and Beta Agonist in Patients at Risk of Developing the Acute Respiratory Distress Syndrome. *Critical Care Medicine*, *45*(5), 798. https://doi.org/10.1097/CCM.0000000000002284

Fisher, B. J., Kraskauskas, D., Martin, E. J., Farkas, D., Wegelin, J. A., Brophy, D., Ward, K. R., Voelkel, N. F., Fowler, A. A., & Natarajan, R. (2012). Mechanisms of attenuation of abdominal sepsis induced acute lung injury by ascorbic acid. *American Journal of Physiology - Lung Cellular and Molecular Physiology*, *303*(1). https://doi.org/10.1152/ajplung.00300.2011

Fredenburgh, L. E., Perrella, M. A., Barragan-Bradford, D., Hess, D. R., Peters, E., Welty-Wolf, K. E., Kraft, B. D., Harris, R. S., Maurer, R., Nakahira, K., Oromendia, C., Davies, J. D., Higuera, A., Schiffer, K. T., Englert, J. A., Dieffenbach, P. B., Berlin, D. A., Lagambina, S., Bouthot, M., … Choi, A. M. (2018). A phase I trial of low-dose inhaled carbon monoxide in sepsis-induced ARDS. *JCI Insight*, *3*(23). https://doi.org/10.1172/JCI.INSIGHT.124039

Funk, C. D. (2001). Prostaglandins and leukotrienes: Advances in eicosanoid biology. In *Science* (Vol. 294, Issue 5548, pp. 1871–1875). https://doi.org/10.1126/science.294.5548.1871

G J Slotman, K W Burchard, A D'Arezzo, & D S Gann. (1988). Ketoconazole Prevents Acute Respiratory Failure in Critically ill surgical patients. *The Journal of Trauma*, *28*(5), 648–654. https://doi.org/10.1097/00005373-198805000-00015

Ganter, M. T., Roux, J., Miyazawa, B., Howard, M., Frank, J. A., Su, G., Sheppard, D., Violette, S. M., Weinreb, P. H., Horan, G. S., Matthay, M. A., & Pittet, J. F. (2008). Interleukin-1β causes acute lung injury via αvβ5 and αvβ6 integrin-dependent mechanisms. *Circulation Research*, *102*(7), 804–812. https://doi.org/10.1161/CIRCRESAHA.107.161067

Gonnert, F. A., Recknagel, P., Seidel, M., Jbeily, N., Dahlke, K., Bockmeyer, C. L., Winning, J., Lösche, W., Claus, R. A., & Bauer, M. (2011). Characteristics of Clinical Sepsis Reflected in a Reliable and Reproducible Rodent Sepsis Model. *Journal of Surgical Research*, *170*(1), e123–e134. https://doi.org/10.1016/J.JSS.2011.05.019

Grailer, J. J., Kalbitz, M., Zetoune, F. S., & Ward, P. A. (2014). Persistent neutrophil dysfunction and suppression of acute lung injury in mice following cecal ligation and puncture sepsis. *Journal of Innate Immunity*, *6*(5), 695–705. https://doi.org/10.1159/000362554

Green, D. P., Ruparel, S., Gao, X., Ruparel, N., Patil, M., Akopian, A., & Hargreaves, K. M. (2016). Central activation of TRPV1 and TRPA1 by novel endogenous agonists contributes to mechanical and thermal allodynia after burn injury. *Molecular Pain*, *12*. https://doi.org/10.1177/1744806916661725

Guillou, H., Zadravec, D., Martin, P. G. P., & Jacobsson, A. (2010). The key roles of elongases and desaturases in mammalian fatty acid metabolism: Insights from transgenic mice. *Progress in Lipid Research*, *49*(2), 186–199. https://doi.org/10.1016/J.PLIPRES.2009.12.002

Herold, S., Becker, C., Ridge, K. M., & Budinger, G. R. S. (2015). Influenza virus-induced lung injury: Pathogenesis and implications for treatment. *European Respiratory Journal*, *45*(5), 1463–1478. https://doi.org/10.1183/09031936.00186214

Hildreth, K., Kodani, S. D., Hammock, B. D., & Zhao, L. (2020). Cytochrome P450-derived linoleic acid metabolites EpOMEs and DiHOMEs: a review of recent studies. In *Journal of Nutritional Biochemistry* (Vol. 86). Elsevier Inc. https://doi.org/10.1016/j.jnutbio.2020.108484

Hotchkiss, R. S., & Karl, I. E. (2003). *The Pathophysiology and Treatment of Sepsis*. www.nejm.org

Hotchkiss, R. S., Moldawer, L. L., Opal, S. M., Reinhart, K., Turnbull, I. R., & Vincent, J. L. (2016). Sepsis and septic shock. In *Nature Reviews Disease Primers* (Vol. 2). Nature Publishing Group. https://doi.org/10.1038/nrdp.2016.45

Hotchkiss, R. S., Monneret, G., & Payen, D. (2013). Sepsis-induced immunosuppression: From cellular dysfunctions to immunotherapy. In *Nature Reviews Immunology* (Vol. 13, Issue 12, pp. 862–874). https://doi.org/10.1038/nri3552

Huang, M., Cai, S., & Su, J. (2019). The pathogenesis of sepsis and potential therapeutic targets. In *International Journal of Molecular Sciences* (Vol. 20, Issue 21). MDPI AG. https://doi.org/10.3390/ijms20215376

Hulbert, A. J., Kelly, M. A., & Abbott, S. K. (2014). Polyunsaturated fats, membrane lipids and animal longevity. In *Journal of Comparative Physiology B: Biochemical, Systemic, and Environmental Physiology* (Vol. 184, Issue 2, pp. 149–166). https://doi.org/10.1007/s00360-013-0786-8

Hwang, S. W., Cho, H., Kwak, J., Lee, S. Y., Kang, C. J., Jung, J., Cho, S., Min, K. H., Suh, Y. G., Kim, D., & Oh, U. (2000). Direct activation of capsaicin receptors by products of lipoxygenases: Endogenous capsaicin-like substances. *Proceedings of the National Academy of Sciences*, *97*(11), 6155–6160. https://doi.org/10.1073/PNAS.97.11.6155

Izquierdo-Garcia, J. L., Nin, N., Jimenez-Clemente, J., Horcajada, J. P., Del Mar Arenas-Miras, M., Gea, J., Esteban, A., Ruiz-Cabello, J., & Lorente, J. A. (2018). Metabolomic profile of ards by nuclear magnetic resonance spectroscopy in patients with h1n1 influenza virus pneumonia. *Shock*, *50*(5), 504–510. https://doi.org/10.1097/SHK.0000000000001099

Jain, P. P., Lai, N., Xiong, M., Chen, J., Babicheva, A., Zhao, T., Parmisano, S., Zhao, M., Paquin, C., Matti, M., Powers, R., Balistrieri, A., Kim, N. H., Valdez-Jasso, D., Thistlethwaite, P. A., Shyy, J. Y. J., Wang, J., Garcia, J. G. N., Makino, A., & Yuan, J. X. J. (2021). TRPC6, a therapeutic target for pulmonary hypertension. *American Journal of Physiology. Lung Cellular and Molecular Physiology*, *321*(6), L1161–L1182. https://doi.org/10.1152/AJPLUNG.00159.2021

JD, T., GR, B., J, S., MA, M., KD, L., TE, A., RG, B., C, S., P, R., IS, D., BP, deBoisblanc, CL, H., RD, H., & BT, T. (2014). Rosuvastatin for sepsis-associated acute respiratory distress syndrome. *The New England Journal of Medicine*, *370*(23), 2191–2200. https://doi.org/10.1056/NEJMOA1401520

Jian, M. Y., King, J. A., Al-Mehdi, A. B., Liedtke, W., & Townsley, M. I. (2008). High vascular pressure-induced lung injury requires P450 epoxygenase-dependent activation of TRPV4. *American Journal of Respiratory Cell and Molecular Biology*, *38*(4), 386–392. https://doi.org/10.1165/rcmb.2007-0192OC

Jia-Ning, H., Taki, F., Sugiyama, S., Asai, J., Izawa, Y., Satake, T., & Ozawa, T. (1988). Neutrophil-Derived Epoxide, 9,10-Epoxy-12-Octadecenoate, Induces Pulmonary Edema. *Lung*, *166*(6), 327–337. https://doi.org/10.1007/BF02714065

Karu, N., Kindt, A., Lamont, L., van Gammeren, A. J., Ermens, A. A. M., Harms, A. C., Portengen, L., Vermeulen, R. C. H., Dik, W. A., Langerak, A. W., van der Velden, V. H. J., & Hankemeier, T. (2022). Plasma Oxylipins and Their Precursors Are Strongly Associated with COVID-19 Severity and with Immune Response Markers. *Metabolites*, *12*(7). https://doi.org/10.3390/metabo12070619

Kor, D. J., Carter, R. E., Park, P. K., Festic, E., Banner-Goodspeed, V. M., Hinds, R., Talmor, D., Gajic, O., Ware, L. B., & Gong, M. N. (2016). Effect of Aspirin on Development of ARDS in At-Risk Patients Presenting to the Emergency Department: The LIPS-A Randomized Clinical Trial. *JAMA*, *315*(22), 2406. https://doi.org/10.1001/JAMA.2016.6330

Kosaka, K., Suzuki, K., Hayakawa, M., Sugiyama, S., & Ozawa, T. (1994). Leukotoxin, a linoleate epoxide: Its implication in the late death of patients with extensive burns. In *Molecular and Cellular Biochemistry* (Vol. 139). Kluwer Academic Publishers.

Kumar, H., Kawai, T., & Akira, S. (2009). Pathogen recognition in the innate immune response. In *Biochemical Journal* (Vol. 420, Issue 1, pp. 1–16). https://doi.org/10.1042/BJ20090272

Kumar, S., Ingle, H., Prasad, D. V. R., & Kumar, H. (2013). Recognition of bacterial infection by innate immune sensors. In *Critical Reviews in Microbiology* (Vol. 39, Issue 3, pp. 229–246). https://doi.org/10.3109/1040841X.2012.706249

Kumar, V. (2020). Pulmonary Innate Immune Response Determines the Outcome of Inflammation During Pneumonia and Sepsis-Associated Acute Lung Injury. In *Frontiers in immunology* (Vol. 11, p. 1722). NLM (Medline). https://doi.org/10.3389/fimmu.2020.01722

Kuo, Y. W., Chang, H. T., Wu, P. C., Chen, Y. F., Lin, C. K., Wen, Y. F., & Jerng, J. S. (2012). Compliance and barriers to implementing the sepsis resuscitation bundle for patients developing septic shock in the general medical wards. *Journal of the Formosan Medical Association*, *111*(2), 77–82. https://doi.org/10.1016/j.jfma.2011.01.004

Lamkanfi, M., & Dixit, V. M. (2014). Mechanisms and functions of inflammasomes. In *Cell* (Vol. 157, Issue 5, pp. 1013–1022). Elsevier B.V. https://doi.org/10.1016/j.cell.2014.04.007

Langley, R. J., Tsalik, E. L., Van Velkinburgh, J. C., Glickman, S. W., Rice, B. J., Wang, C., Chen, B., Carin, L., Suarez, A., Mohney, R. P., Freeman, D. H., Wang, M., You, J., Wulff, J., Will Thompson, J., Arthur Moseley, M., Reisinger, S., Edmonds, B. T., Grinnell, B., … Kingsmore, S. F. (2013). Sepsis: An integrated clinico-metabolomic

model improves prediction of death in sepsis. *Science Translational Medicine*, *5*(195). https://doi.org/10.1126/scitranslmed.3005893

Le, H. D., Fallon, E. M., Kalish, B. T., De Meijer, V. E., Meisel, J. A., Gura, K. M., Nose, V., Pan, A. H., Bistrian, B. R., & Puder, M. (2013). The effect of varying ratios of docosahexaenoic acid and arachidonic acid in the prevention and reversal of biochemical essential fatty acid deficiency in a murine model. *Metabolism: Clinical and Experimental*, *62*(4), 499–508. https://doi.org/10.1016/j.metabol.2012.10.003

Levy, M. M., Fink, M. P., Marshall, J. C., Abraham, E., Angus, D., Cook, D., Cohen, J., Opal, S. M., Vincent, J. L., & Ramsay, G. (2003). 2001 SCCM/ESICM/ACCP/ATS/SIS International Sepsis Definitions Conference. *Critical Care Medicine*, *31*(4), 1250–1256. https://doi.org/10.1097/01.CCM.0000050454.01978.3B

Li, J., Guasch-Ferré, M., Li, Y., & Hu, F. B. (2020). Dietary intake and biomarkers of linoleic acid and mortality: systematic review and meta-analysis of prospective cohort studies. *The American Journal of Clinical Nutrition*, *112*(1), 150–167. https://doi.org/10.1093/AJCN/NQZ349

Limaye, A. P., Stapleton, R. D., Peng, L., Gunn, S. R., Kimball, L. E., Hyzy, R., Exline, M. C., Files, D. C., Morris, P. E., Frankel, S. K., Mikkelsen, M. E., Hite, D., Enfield, K. B., Steingrub, J., O'Brien, J., Parsons, P. E., Cuschieri, J., Wunderink, R. G., Hotchkin, D. L., … Boeckh, M. (2017). Effect of Ganciclovir on IL-6 Levels Among Cytomegalovirus-Seropositive Adults With Critical Illness: A Randomized Clinical Trial. *JAMA*, *318*(8), 731–740. https://doi.org/10.1001/JAMA.2017.10569

Lindemann, O., Umlauf, D., Frank, S., Schimmelpfennig, S., Bertrand, J., Pap, T., Hanley, P. J., Fabian, A., Dietrich, A., & Schwab, A. (2013). TRPC6 Regulates CXCR2-Mediated Chemotaxis of Murine Neutrophils. *The Journal of Immunology*, *190*(11), 5496–5505. https://doi.org/10.4049/jimmunol.1201502

Luostarinen, S., Hämäläinen, M., Pemmari, A., & Moilanen, E. (2023). The regulation of TRPA1 expression and function by Th1 and Th2-type inflammation in human A549 lung epithelial cells. *Inflammation Research : Official Journal of the European Histamine Research Society ... [et Al.]*, *72*(7), 1327–1339. https://doi.org/10.1007/S00011-023-01750-Y

M Yu, & G Tomasa. (1993). A double-blind, prospective, randomized trial of ketoconazole a thromboxane synthetase inhibitor in the prophylaxis of the adult respiratory distress syndrome. *Critical Care Medicine*, *21*(11), 1635–1641. https://doi.org/10.1097/00003246-199311000-00010

Majno, G. (1991). The Ancient Riddle of Sepsis. *The Journal of Infectious Diseases*, *163*(5), 937–945. https://academic.oup.com/jid/article-abstract/163/5/937/900710

Marszalek, J. R., & Lodish, H. F. (2005). Docosahexaenoic acid, fatty acid-interacting proteins, and neuronal function: Breastmilk and fish are good for you. In *Annual*

Review of Cell and Developmental Biology (Vol. 21, pp. 633–657). https://doi.org/10.1146/annurev.cellbio.21.122303.120624

Mayr, F. B., Yende, S., & Angus, D. C. (2014). Epidemiology of severe sepsis. In *Virulence* (Vol. 5, Issue 1, pp. 4–11). Taylor and Francis Inc. https://doi.org/10.4161/viru.27372

McReynolds, C. B., Cortes-Puch, I., Ravindran, R., Khan, I. H., Hammock, B. G., Shih, P. an B., Hammock, B. D., & Yang, J. (2021). Plasma Linoleate Diols Are Potential Biomarkers for Severe COVID-19 Infections. *Frontiers in Physiology*, *12*. https://doi.org/10.3389/fphys.2021.663869

Melissa Gabbs, Leng, S., Devassy, J. G., Monirujjaman, M., & Aukema, H. M. (2015). Advances in our understanding of oxylipins derived from dietary PUFAs 1,2. In *Advances in Nutrition* (Vol. 6, Issue 5, pp. 513–540). American Society for Nutrition. https://doi.org/10.3945/an.114.007732

Mortadza, S. A. S., Wang, L., Li, D., & Jiang, L. H. (2015). TRPM2 Channel-Mediated ROS-Sensitive Ca(2+) Signaling Mechanisms in Immune Cells. *Frontiers in Immunology*, *6*(JUL). https://doi.org/10.3389/FIMMU.2015.00407

Müller, I., Alt, P., Rajan, S., Schaller, L., Geiger, F., & Dietrich, A. (2022). Transient Receptor Potential (TRP) Channels in Airway Toxicity and Disease: An Update. *Cells*, *11*(18). https://doi.org/10.3390/CELLS11182907

Muniz, B. F., Netto, G. M., Jr Ferreira, M., Prata, L. O., Mayrink, C. C., Guimarães, Y. L., Caliari, M. V, & Duval-Araujo, I. (2015). Neutrophilic infiltration in lungs of mice with peritonitis in acid or basic medium. In *Int J Clin Exp Med* (Vol. 8, Issue 4). www.ijcem.com/

Narváez-Rivas, M., & León-Camacho, M. (2015). Fats: Classification and Analysis. In *Encyclopedia of Food and Health* (pp. 596–603). Elsevier Inc. https://doi.org/10.1016/B978-0-12-384947-2.00274-9

Nassini, R., Pedretti, P., Moretto, N., Fusi, C., Carnini, C., Facchinetti, F., Viscomi, A. R., Pisano, A. R., Stokesberry, S., Brunmark, C., Svitacheva, N., McGarvey, L., Patacchini, R., Damholt, A. B., Geppetti, P., & Materazzi, S. (2012). Transient receptor potential ankyrin 1 channel localized to non-neuronal airway cells promotes non-neurogenic inflammation. *PLoS ONE*, *7*(8). https://doi.org/10.1371/journal.pone.0042454

Norris, P. C., Gosselin, D., Reichart, D., Glass, C. K., & Dennis, E. A. (2014). Phospholipase A2 regulates eicosanoid class switching during inflammasome activation. *Proceedings of the National Academy of Sciences of the United States of America*, *111*(35), 12746–12751. https://doi.org/10.1073/pnas.1404372111

Park, C. K. (2015). Maresin 1 Inhibits TRPV1 in Temporomandibular Joint-Related Trigeminal Nociceptive Neurons and TMJ Inflammation-Induced Synaptic Plasticity

in the Trigeminal Nucleus. *Mediators of Inflammation*, *2015*. https://doi.org/10.1155/2015/275126

Park, C. K., Lü, N., Xu, Z. Z., Liu, T., Serhan, C. N., & Ji, R. R. (2011). Resolving TRPV1- and TNF-α-mediated spinal cord synaptic plasticity and inflammatory pain with neuroprotectin D1. *Journal of Neuroscience*, *31*(42), 15072–15085. https://doi.org/10.1523/JNEUROSCI.2443-11.2011

Park, C. K., Xu, Z. Z., Liu, T., Lü, N., Serhan, C. N., & Ji, R. R. (2011). Resolvin D2 is a potent endogenous inhibitor for transient receptor potential subtype V1/A1, inflammatory pain, and spinal cord synaptic plasticity in mice: Distinct roles of resolvin D1, D2, and E1. *Journal of Neuroscience*, *31*(50), 18433–18438. https://doi.org/10.1523/JNEUROSCI.4192-11.2011

Patwardhan, A. M., Akopian, A. N., Ruparel, N. B., Diogenes, A., Weintraub, S. T., Uhlson, C., Murphy, R. C., & Hargreaves, K. M. (2010). Heat generates oxidized linoleic acid metabolites that activate TRPV1 and produce pain in rodents. *Journal of Clinical Investigation*, *120*(5), 1617–1626. https://doi.org/10.1172/JCI41678

Patwardhan, A. M., Scotland, P. E., Akopian, A. N., Hargreaves, K. M., Designed, K. M. H., & Performed, A. N. A. (2009). Activation of TRPV1 in the spinal cord by oxidized linoleic acid metabolites contributes to inflammatory hyperalgesia. In *PNAS November* (Vol. 3, Issue 44).

Peralta, J. G., Barnard, M. L., & Turrens, J. F. (1993). CHARACTERISTICS OF NEUTROPHIL INFLUX IN RAT LUNGS FOLLOWING FECAL PERITONITIS. In *Inflammation* (Vol. 1, Issue 3).

Peters, J. I., Bell, R. C., Prihoda, T. J., Harris, G., Andrews, C., & Johanson, W. G. (1989). Clinical Determinants of Abnormalities in Pulmonary Functions in Survivors of the Adult Respiratory Distress Syndrome. *American Review of Respiratory Disease*, *139*(5), 1163–1168. https://doi.org/10.1164/ajrccm/139.5.1163

Prandini, P., De Logu, F., Fusi, C., Provezza, L., Nassini, R., Montagner, G., Materazzi, S., Munari, S., Gilioli, E., Bezzerri, V., Finotti, A., Lampronti, I., Tamanini, A., Dechecchi, M. C., Lippi, G., Ribeiro, C. M., Rimessi, A., Pinton, P., Gambari, R., … Cabrini, G. (2016). Transient receptor potential ankyrin 1 channels modulate inflammatory response in respiratory cells from patients with cystic fibrosis. *American Journal of Respiratory Cell and Molecular Biology*, *55*(5), 645–656. https://doi.org/10.1165/rcmb.2016-0089OC

Prescott, H. C., Iwashyna, T. J., Blackwood, B., Calandra, T., Chlan, L. L., Choong, K., Connolly, B., Dark, P., Ferrucci, L., Finfer, S., Girard, T. D., Hodgson, C., Hopkins, R. O., Hough, C. L., Jackson, J. C., Machado, F. R., Marshall, J. C., Misak, C., Needham, D. M., … Angus, D. C. (2019). Understanding and enhancing sepsis survivorship priorities for research and practice. In *American Journal of Respiratory*

and Critical Care Medicine (Vol. 200, Issue 8, pp. 972–981). American Thoracic Society. https://doi.org/10.1164/rccm.201812-2383CP

Qiao, X., Yin, J., Zheng, Z., Li, L., & Feng, X. (2024). Endothelial cell dynamics in sepsis-induced acute lung injury and acute respiratory distress syndrome: pathogenesis and therapeutic implications. In *Cell Communication and Signaling* (Vol. 22, Issue 1). BioMed Central Ltd. https://doi.org/10.1186/s12964-024-01620-y

Quesnel, C., Nardelli, L., Piednoir, P., Leçon, V., Marchal-Somme, J., Lasocki, S., Bouadma, L., Philip, I., Soler, P., Crestani, B., & Dehoux, M. (2010). Alveolar fibroblasts in acute lung injury: Biological behaviour and clinical relevance. *European Respiratory Journal*, *35*(6), 1312–1321. https://doi.org/10.1183/09031936.00074709

Rajan, S., Shalygin, A., Gudermann, T., Chubanov, V., & Dietrich, A. (2024). TRPM2 channels are essential for regulation of cytokine production in lung interstitial macrophages. *Journal of Cellular Physiology*, *239*(11), e31322. https://doi.org/10.1002/JCP.31322;REQUESTEDJOURNAL:JOURNAL:10974652;JOURNAL:JOURNAL:15530809;WGROUP:STRING:PUBLICATION

Rogers, A. J., Leligdowicz, A., Contrepois, K., Jauregui, A., Vessel, K., Deiss, T. J., Belzer, A., Liu, T., Lippi, M., Ke, S., Ross, E., Zhou, H., Hendrickson, C., Gomez, A., Sinha, P., Kangelaris, K. N., Liu, K. D., Calfee, C. S., & Matthay, M. A. (2021). Plasma Metabolites in Early Sepsis Identify Distinct Clusters Defined by Plasma Lipids. *Critical Care Explorations*, *3*(8), E0478. https://doi.org/10.1097/CCE.0000000000000478

Rogers, A. J., McGeachie, M., Baron, R. M., Gazourian, L., Haspel, J. A., Nakahira, K., Fredenburgh, L. E., Hunninghake, G. M., Raby, B. A., Matthay, M. A., Otero, R. M., Fowler, V. G., Rivers, E. P., Woods, C. W., Kingsmore, S., Langley, R. J., & Choi, A. M. K. (2014). Metabolomic derangements are associated with mortality in critically ill adult patients. *PLoS ONE*, *9*(1). https://doi.org/10.1371/journal.pone.0087538

Rubenfeld, G. D., Caldwell, E., Peabody, E., Weaver, J., Martin, D. P., Neff, M., Stern, E. J., & Hudson, L. D. (2005). Incidence and Outcomes of Acute Lung Injury From the Division of Pulmonary and Criti-cal Care Medicine (G. In *n engl j med* (Vol. 16, Issue 20). www.nejm.org

Rudd, K. E., Johnson, S. C., Agesa, K. M., Shackelford, K. A., Tsoi, D., Kievlan, D. R., Colombara, D. V., Ikuta, K. S., Kissoon, N., Finfer, S., Fleischmann-Struzek, C., Machado, F. R., Reinhart, K. K., Rowan, K., Seymour, C. W., Watson, R. S., West, T. E., Marinho, F., Hay, S. I., … Naghavi, M. (2020). Global, regional, and national sepsis incidence and mortality, 1990–2017: analysis for the Global Burden of Disease Study. *The Lancet*, *395*(10219), 200–211. https://doi.org/10.1016/S0140-6736(19)32989-7

Sanders, Y. Y., Kumbla, P., & Hagood, J. S. (2007). Enhanced myofibroblastic differentiation and survival in thy-1(-) lung fibroblasts. *American Journal of*

Respiratory Cell and Molecular Biology, *36*(2), 226–235. https://doi.org/10.1165/rcmb.2006-0178OC

Saraiva-Santos, T., Zaninelli, T. H., Manchope, M. F., Andrade, K. C., Ferraz, C. R., Bertozzi, M. M., Artero, N. A., Franciosi, A., Badaro-Garcia, S., Staurengo-Ferrari, L., Borghi, S. M., Ceravolo, G. S., Andrello, A. C., Zanoveli, J. M., Rogers, M. S., Casagrande, R., Pinho-Ribeiro, F. A., & Verri, W. A. (2023). Therapeutic activity of lipoxin A4 in TiO2-induced arthritis in mice: NF-κB and Nrf2 in synovial fluid leukocytes and neuronal TRPV1 mechanisms. *Frontiers in Immunology*, *14*. https://doi.org/10.3389/fimmu.2023.949407

Schaller, L., Gudermann, T., & Dietrich, A. (2024). TRPV4 Mediates Alveolar Epithelial Barrier Integrity and Induces ADAM10-Driven E-Cadherin Shedding. *Cells*, *13*(20). https://doi.org/10.3390/CELLS13201717

Schmitz, G., & Ecker, J. (2008). The opposing effects of n-3 and n-6 fatty acids. In *Progress in Lipid Research* (Vol. 47, Issue 2, pp. 147–155). Elsevier Ltd. https://doi.org/10.1016/j.plipres.2007.12.004

Serhan, C. N., Dalli, J., Karamnov, S., Choi, A., Park, C., Xu, Z., Ji, R., Zhu, M., & Petasis, N. A. (2012a). Macrophage proresolving mediator maresin 1 stimulates tissue regeneration and controls pain. *The FASEB Journal*, *26*(4), 1755–1765. https://doi.org/10.1096/fj.11-201442

Serhan, C. N., Dalli, J., Karamnov, S., Choi, A., Park, C., Xu, Z., Ji, R., Zhu, M., & Petasis, N. A. (2012b). Macrophage proresolving mediator maresin 1 stimulates tissue regeneration and controls pain. *The FASEB Journal*, *26*(4), 1755–1765. https://doi.org/10.1096/fj.11-201442

Sevanian, A., Mead, J. F., & Stein, R. A. (1979). Epoxides as Products of Lipid Autoxidation in Rat Lungs. *Lipids*, *14*(7), 634–643. https://doi.org/10.1007/BF02533449

Sharma, N., Chen, A., Heinen, L., Liu, R., Dwivedi, D. J., Zhou, J., Lalu, M. M., Mendelson, A. A., McDonald, B., Kretz, C. A., Fox-Robichaud, A. E., & Liaw, P. C. (2024). Impact of age on the host response to sepsis in a murine model of fecal-induced peritonitis. *Intensive Care Medicine Experimental* , *12*(1). https://doi.org/10.1186/s40635-024-00609-8

Shi, Y., Wang, L., Yu, S., Ma, X., & Li, X. (2022). Risk factors for acute respiratory distress syndrome in sepsis patients: a retrospective study from a tertiary hospital in China. *BMC Pulmonary Medicine*, *22*(1). https://doi.org/10.1186/s12890-022-02015-w

Shimazui, T., Oami, T., Shimada, T., Tomita, K., & Nakada, T. A. (2025). Age-dependent differences in the association between blood interleukin-6 levels and mortality in patients with sepsis: a retrospective observational study. *Journal of Intensive Care*, *13*(1). https://doi.org/10.1186/s40560-025-00775-1

Simopoulos A P. (1999). Essential fatty acids in health and chronic disease. *The American Journal of Clinical Nutrition*, *70*(3), 560–569. https://doi.org/10.1093/ajcn/70.3.560s

Singer, M., Deutschman, C. S., Seymour, C., Shankar-Hari, M., Annane, D., Bauer, M., Bellomo, R., Bernard, G. R., Chiche, J. D., Coopersmith, C. M., Hotchkiss, R. S., Levy, M. M., Marshall, J. C., Martin, G. S., Opal, S. M., Rubenfeld, G. D., Poll, T. Der, Vincent, J. L., & Angus, D. C. (2016). The third international consensus definitions for sepsis and septic shock (sepsis-3). In *JAMA - Journal of the American Medical Association* (Vol. 315, Issue 8, pp. 801–810). American Medical Association. https://doi.org/10.1001/jama.2016.0287

Singh, C., Rai, R. K., Azim, A., Sinha, N., Ahmed, A., Singh, K., Kayastha, A. M., Baronia, A. K., Gurjar, M., Poddar, B., & Singh, R. K. (2015). Metabolic profiling of human lung injury by 1H high-resolution nuclear magnetic resonance spectroscopy of blood serum. *Metabolomics*, *11*(1), 166–174. https://doi.org/10.1007/s11306-014-0688-0

Sinha, P., Delucchi, K. L., McAuley, D. F., O'Kane, C. M., Matthay, M. A., & Calfee, C. S. (2020). Development and validation of parsimonious algorithms to classify acute respiratory distress syndrome phenotypes: a secondary analysis of randomised controlled trials. *The Lancet Respiratory Medicine*, *8*(3), 247–257. https://doi.org/10.1016/S2213-2600(19)30369-8

Sinuff, T., Cook, D. J., Peterson, J. C., & Fuller, H. D. (1999). Development, Implementation, and Evaluation of a Ketoconazole Practice Guideline for ARDS Prophylaxis. *Journal of Critical Care*, *14*(1), 1–6. https://doi.org/10.1016/s0883-9441(99)90001-1

Sisignano, M., Park, C. K., Angioni, C., Zhang, D. D., von Hehn, C., Cobos, E. J., Ghasemlou, N., Xu, Z. Z., Kumaran, V., Lu, R., Grant, A., Fischer, M. J. M., Schmidtko, A., Reeh, P., Ji, R. R., Woolf, C. J., Geisslinger, G., Scholich, K., & Brenneis, C. (2012). 5,6-EET is released upon neuronal activity and induces mechanical pain hypersensitivity via TRPA1 on central afferent terminals. *Journal of Neuroscience*, *32*(18), 6364–6372. https://doi.org/10.1523/JNEUROSCI.5793-11.2012

Sonkusare, S. K., & Laubach, V. E. (2022). Endothelial TRPV4 channels in lung edema and injury. In *Current Topics in Membranes* (Vol. 89, pp. 43–62). Academic Press Inc. https://doi.org/10.1016/bs.ctm.2022.07.001

Stamme, C., Bundschuh, D. S., Hartung, T., Gebert, U., Wollin, L., Nu¨sing, R., Nu¨sing, N., Wendel, A., & Uhlig, S. (1999). Temporal Sequence of Pulmonary and Systemic Inflammatory Responses to Graded Polymicrobial Peritonitis in Mice. In *INFECTION AND IMMUNITY* (Vol. 67, Issue 11).

Stapleton, R. D., Wang, B. M., Hudson, L. D., Rubenfeld, G. D., Caldwell, E. S., & Steinberg, K. P. (2005). Causes and timing of death in patients with ARDS. *Chest*, *128*(2), 525–532. https://doi.org/10.1378/chest.128.2.525

Stephenson, D. J., Hoeferlin, L. A., & Chalfant, C. E. (2017). Lipidomics in translational research and the clinical significance of lipid-based biomarkers. In *Translational Research* (Vol. 189, pp. 13–29). Mosby Inc. https://doi.org/10.1016/j.trsl.2017.06.006

Stone, M. J. (2017). Regulation of chemokine-receptor interactions and functions. In *International Journal of Molecular Sciences* (Vol. 18, Issue 11). MDPI AG. https://doi.org/10.3390/ijms18112415

Stringer, K. A., Serkova, N. J., Karnovsky, A., Guire, K., Paine, R., & Standiford, T. J. (2011). Metabolic consequences of sepsis-induced acute lung injury revealed by plasma 1 H-nuclear magnetic resonance quantitative metabolomics and computational analysis. *Am J Physiol Lung Cell Mol Physiol*, *300*, 4–11. https://doi.org/10.1152/ajplung.00231.2010.-Metabolomics

Sun, B., Lei, M., Zhang, J., Kang, H., Liu, H., & Zhou, F. (2023). Acute lung injury caused by sepsis: how does it happen? In *Frontiers in Medicine* (Vol. 10). Frontiers Media SA. https://doi.org/10.3389/fmed.2023.1289194

Suzuki, K., Aoyama, H., Izawa, Y., Kobayashi, M., & Ozawa, T. (1981). Isolation of a substance toxic to mitochondrial function from the burned skin of rats. *Burns*, *8*(2), 110–117. https://doi.org/https://doi.org/10.1016/0305-4179(81)90031-0

Taha, A. Y., Cheon, Y., Faurot, K. F., MacIntosh, B., Majchrzak-Hong, S. F., Mann, J. D., Hibbeln, J. R., Ringel, A., & Ramsden, C. E. (2014). Dietary omega-6 fatty acid lowering increases bioavailability of omega-3 polyunsaturated fatty acids in human plasma lipid pools. *Prostaglandins, Leukotrienes and Essential Fatty Acids*, *90*(5), 151–157. https://doi.org/10.1016/J.PLEFA.2014.02.003

Takayuki Ozawa, Satoru Sugiyama, Mika Hayakawa, Tatsuo Satake, Fumio Taki, Masaru Iwata, & Kazumi Taki. (1988). Existence of Leukotoxin 9,10-Epoxy-12-0ctadecenoate in Lung Lavages from Rats Breathing Pure Oxygen and from Patients with the Adult Respiratory Distress Syndrome 1-3. *American Review of Respiratory Disease*, *137*(3). https://doi.org/10.1164/ajrccm/137.3.535

Takeuchi, O., & Akira, S. (2010). Pattern Recognition Receptors and Inflammation. In *Cell* (Vol. 140, Issue 6, pp. 805–820). Elsevier B.V. https://doi.org/10.1016/j.cell.2010.01.022

Tang, M., Tian, Y., Li, D., Lv, J., Li, Q., Kuang, C., Hu, P., Wang, Y., Wang, J., Su, K., & Wei, L. (2014). TNF-α mediated increase of HIF-1α inhibits VASP expression, which reduces alveolar-capillary barrier function during Acute Lung Injury (ALI). *PLoS ONE*, *9*(7). https://doi.org/10.1371/journal.pone.0102967

Tauseef, M., Farazuddin, M., Sukriti, S., Rajput, C., Meyer, J. O., Ramasamy, S. K., & Mehta, D. (2016). Transient receptor potential channel 1 maintains adherens junction plasticity by suppressing sphingosine kinase 1 expression to induce endothelial hyperpermeability. *FASEB Journal : Official Publication of the Federation of American*

Societies for Experimental Biology, *30*(1), 102–110. https://doi.org/10.1096/FJ.15-275891

Tauseef, M., Knezevic, N., Chava, K. R., Smith, M., Sukriti, S., Gianaris, N., Obukhov, A. G., Vogel, S. M., Schraufnage, D. E., Dietrich, A., Birnbaumer, L., Malik, A. B., & Mehta, D. (2012). TLR4 activation of TRPC6-dependent calcium signaling mediates endotoxininduced lung vascular permeability and inflammation. *Journal of Experimental Medicine*, *209*(11), 1953–1968. https://doi.org/10.1084/jem.20111355

Thompson, B. T. (2000). Ketoconazole for early treatment of acute lung injury and acute respiratory distress syndrome: a randomized controlled trial. The ARDS Network. *JAMA*, *283*(15), 1995–2002. https://doi.org/10.1001/JAMA.283.15.1995

Tominaga, M., Caterina, M. J., Malmberg, A. B., Rosen, T. A., Gilbert, H., Skinner, K., Raumann, B. E., Basbaum, A. I., & Julius, D. (1998). The cloned capsaicin receptor integrates multiple pain-producing stimuli. *Neuron*, *21*(3), 531–543. https://doi.org/10.1016/S0896-6273(00)80564-4

Tsangaris, H., Lekka, M. E., & Nakos, G. (2005). Mechanically Ventilated Lung and Response to Pseudomonas Aeruginosa. *Critical Care Medicine*, *33*(8), 1887. https://doi.org/10.1097/01.ccm.0000170195.16137.88

van der Poll, T., Shankar-Hari, M., & Wiersinga, W. J. (2021). The immunology of sepsis. In *Immunity* (Vol. 54, Issue 11, pp. 2450–2464). Cell Press. https://doi.org/10.1016/j.immuni.2021.10.012

Van Der Poll, T., Van De Veerdonk, F. L., Scicluna, B. P., & Netea, M. G. (2017). The immunopathology of sepsis and potential therapeutic targets. In *Nature Reviews Immunology* (Vol. 17, Issue 7, pp. 407–420). Nature Publishing Group. https://doi.org/10.1038/nri.2017.36

Varga, N. I., Bagiu, I. C., Vulcanescu, D. D., Lazureanu, V., Turaiche, M., Rosca, O., Bota, A. V., & Horhat, F. G. (2025). IL-6 Baseline Values and Dynamic Changes in Predicting Sepsis Mortality: A Systematic Review and Meta-Analysis. In *Biomolecules* (Vol. 15, Issue 3). Multidisciplinary Digital Publishing Institute (MDPI). https://doi.org/10.3390/biom15030407

Varisco, B. M. (2011). The pharmacology of acute lung injury in sepsis. In *Advances in Pharmacological Sciences* (Vol. 2011). https://doi.org/10.1155/2011/254619

Vincent, J. L. (2022). Current sepsis therapeutics. In *eBioMedicine* (Vol. 86). Elsevier B.V. https://doi.org/10.1016/j.ebiom.2022.104318

Viswan, A., Ghosh, P., Gupta, D., Azim, A., & Sinha, N. (2019). Distinct Metabolic Endotype Mirroring Acute Respiratory Distress Syndrome (ARDS) Subphenotype and its Heterogeneous Biology. *Scientific Reports*, *9*(1). https://doi.org/10.1038/s41598-019-39017-4

Wallis, J. G., Watts, J. L., & Browse, J. (2002). Polyunsaturated fatty acid synthesis: What will they think of next? *Trends in Biochemical Sciences*, *27*(9), 467–473. https://doi.org/10.1016/S0968-0004(02)02168-0

Wang, M., Zhang, X., Guo, J., Yang, S., Yang, F., & Chen, X. (2023). TRPC6 Deletion Enhances eNOS Expression and Reduces LPS—Induced Acute Lung Injury. *International Journal of Molecular Sciences*, *24*(23). https://doi.org/10.3390/ijms242316756

Wang, Y., Tang, Z., Huang, H., Li, J., Wang, Z., Yu, Y., Zhang, C., Li, J., Dai, H., Wang, F., Cai, T., & Tang, N. (2018). Pulmonary alveolar type I cell population consists of two distinct subtypes that differ in cell fate. *Proceedings of the National Academy of Sciences of the United States of America*, *115*(10), 2407–2412. https://doi.org/10.1073/pnas.1719474115

Ward, P. A. (2004). The dark side of C5a in sepsis. In *Nature Reviews Immunology* (Vol. 4, Issue 2, pp. 133–142). Nature Publishing Group. https://doi.org/10.1038/nri1269

Watanabe, H., Vriens, J., Prenen, J., Droogmans, G., Voets, T., & Nillus, B. (2003). Anandamide and arachidonic acid use epoxyeicosatrienoic acids to activate TRPV4 channels. *Nature 2003 424:6947*, *424*(6947), 434–438. https://doi.org/10.1038/nature01807

Weissmann, N., Sydykov, A., Kalwa, H., Storch, U., Fuchs, B., Mederos Y Schnitzler, M., Brandes, R. P., Grimminger, F., Meissner, M., Freichel, M., Offermanns, S., Veit, F., Pak, O., Krause, K. H., Schermuly, R. T., Brewer, A. C., Schmidt, H. H. H. W., Seeger, W., Shah, A. M., … Dietrich, A. (2012). Activation of TRPC6 channels is essential for lung ischaemia-reperfusion induced oedema in mice. *Nature Communications*, *3*. https://doi.org/10.1038/NCOMMS1660

Wen, H., Östman, J., Bubb, K. J., Panayiotou, C., Priestley, J. V., Baker, M. D., & Ahluwalia, A. (2012a). 20-Hydroxyeicosatetraenoic acid (20-HETE) is a novel activator of transient receptor potential vanilloid 1 (TRPV1) channel. *Journal of Biological Chemistry*, *287*(17), 13868–13876. https://doi.org/10.1074/jbc.M111.334896

Wen, H., Östman, J., Bubb, K. J., Panayiotou, C., Priestley, J. V., Baker, M. D., & Ahluwalia, A. (2012b). 20-Hydroxyeicosatetraenoic acid (20-HETE) is a novel activator of transient receptor potential vanilloid 1 (TRPV1) channel. *Journal of Biological Chemistry*, *287*(17), 13868–13876. https://doi.org/10.1074/jbc.M111.334896

West, J. B. (2009). Comparative physiology of the pulmonary blood-gas barrier: the unique avian solution. *Am J Physiol Regul Integr Comp Physiol*, *297*, 1625–1634. https://doi.org/10.1152/ajpregu.00459.2009.-Two

Wook Hwang, S., Cho, H., Kwak, J., Lee, S.-Y., Kang, C.-J., Jung, J., Cho, S., Hoon Min, K., Suh, Y.-G., Kim, D., & Oh, U. (2000). Direct activation of capsaicin receptors by products of lipoxygenases: Endogenous capsaicin-like substances. In *National Institutes of Health*. www.pnas.org

Xu, M., Zhang, Y., Wang, M., Zhang, H., Chen, Y., Adcock, I. M., Chung, K. F., Mo, J., Zhang, Y., & Li, F. (2019). TRPV1 and TRPA1 in Lung Inflammation and Airway Hyperresponsiveness Induced by Fine Particulate Matter (PM2.5). *Oxidative Medicine and Cellular Longevity*, *2019*. https://doi.org/10.1155/2019/7450151

Xu, Z. Z., Zhang, L., Liu, T., Park, J. Y., Berta, T., Yang, R., Serhan, C. N., & Ji, R. R. (2010). Resolvins RvE1 and RvD1 attenuate inflammatory pain via central and peripheral actions. *Nature Medicine*, *16*(5), 592–597. https://doi.org/10.1038/nm.2123

YOKOO, K., HAYAKAWA, M., SUGIYAMA, S., OZAWA, T., AOYAMA, H., IZAWA, Y., KONDO, T., & HAYAKAWA, Y. (1986). A Novel Uncoupler of Mitochondrial Respiration, 9, 10-Epoxy-12-octadecenoate, Exists in Human Burned Skin. *Journal of Clinical Biochemistry and Nutrition*, *1*(2), 121–127. https://doi.org/10.3164/jcbn.1.121

Yue, L., & Xu, H. (2021). TRP channels in health and disease at a glance. *Journal of Cell Science*, *134*(13). https://doi.org/10.1242/jcs.258372

Zhang, J., Shao, Y., Wu, J., Zhang, J., Xiong, X., Mao, J., Wei, Y., Miao, C., & Zhang, H. (2025). Dysregulation of neutrophil in sepsis: recent insights and advances. In *Cell Communication and Signaling* (Vol. 23, Issue 1). BioMed Central Ltd. https://doi.org/10.1186/s12964-025-02098-y

Zhang, L., Tian, Y., Yang, J., Li, J., Tang, H., & Wang, Y. (2018). Colon Ascendens Stent Peritonitis (CASP) Induces Excessive Inflammation and Systemic Metabolic Dysfunction in a Septic Rat Model. *Journal of Proteome Research*, *17*(1), 680–688. https://doi.org/10.1021/acs.jproteome.7b00730

Zheng, J., Plopper, C. G., Lakritz, J., Storms, D. H., & Hammock, B. D. (2001). Leukotoxin-Diol A Putative Toxic Mediator Involved in Acute Respiratory Distress Syndrome. In *Am. J. Respir. Cell Mol. Biol* (Vol. 25). www.atsjournals.org

Zhou, G., Dada, L. A., Wu, M., Kelly, A., Trejo, H., Zhou, Q., Varga, J., Sznajder, J. I., & Hypoxia, S. J. (2009). Hypoxia-induced alveolar epithelial-mesenchymal transition requires mitochondrial ROS and hypoxia-inducible factor 1. *Am J Physiol Lung Cell Mol Physiol*, *297*. https://doi.org/10.1152/ajplung.00007.2009.-Pa

Zhou, X., & Liao, Y. (2021). Gut-Lung Crosstalk in Sepsis-Induced Acute Lung Injury. In *Frontiers in Microbiology* (Vol. 12). Frontiers Media S.A. https://doi.org/10.3389/fmicb.2021.779620

8. List of figures

9. List of tables

10. List of abbreviations

AA	Arachidonic acid
ALA	Alpha-linolenic acid
ALI	Acute lung injury
ARDS	Acute respiratory distress syndrome
AT1	Alveolar type 1 cells
AT2	Alveolar type 2 cells
BAL	Bronchoalveolar lavage
CE	Collision energy
CLP	Cecal ligation and puncture
CMV	Cytomegalovirus
CP	Cecal peritonitis
CYP	Cytochrome P450 epoxygenases
DAMPs	Damage associated molecular patterns
DHA	Docosahexaenoic acid
DiHOME	Dihydroxy-octadecenoic acid
DRG	Dorsal root ganglion
EET	Epoxyeicosatrienoic acid
EPA	Eicosapentaenoic acid
EpOME	Epoxy-octadecenoic acid
ESICM	European Society of Intensive Care Medicine

FA	Fatty acid
FiO_2	Fraction of inspired oxygen
FP	Fecal peritonitis
GCS	Glasgow Coma Scale
HETE	Hydroxyeicosatetraenoic acid
HODE	Hydroxyoctadecadienoic acid
iCO	Inhaled carbon monoxide
IS	Internal standards
IL-1	Interleukin-1
LA	Linoleic acid
LC	Liquid chromatography
LC-MS/MS	Liquid chromatography-tandem mass spectrometry
LIRE	Lung ischemia-reperfusion-induced edema
LMs	Lipid mediators
LOD	Limit of detection
LOQ	Limit of quantification
LOX	Lipoxygenases
LPS	Lipopolysaccharide
LTB_4	Leukotriene B_4
MAP	Mean arterial pressure
MaR1	Maresin 1

MPO	Myeloperoxidase
MRM	Multiple reaction monitoring
MS	Mass spectrometry
MUFA	Monounsaturated fatty acids
NSAIDs	Non-steroidal anti-inflammatory drugs
OxoODE	Oxo-octadecadienoic acid
PAMPs	Pathogen associated molecular patterns
PaO_2	Partial pressure of oxygen
PL	Phospholipids
PRRs	Pathogen recognition receptors
PUFA	Polyunsaturated fatty acids
qSOFA	Quick Sequential Organ Failure Assessment score
ROS	Reactive oxygen species
Rt	Retention time
RvD2	Resolvin D2
RvE1	Resolvin E1
sALI	Sepsis associated lung injury
SCCM	Society of Critical Care Medicine
sEH	Soluble epoxy hydrolase
SFA	Saturated fatty acids
SIRS	Systemic inflammatory response syndrome

SPE	Solid phase extraction
SOFA	Sequential Organ Failure Assessment score
TG	Triglycerides
TGF-β	Tumor growth factor β
TLRs	Toll-like receptors
TNF-α	Tumor necrosis factor-α
TRP	Transient receptor potential
TRPV1	Transient receptor potential vanilloid 1

11. Biography

PERSONAL INFORMATION

Name: Nada Birkić

Date of birth: 15-03-1998

Address: Milana Rustambega 10, 51 000 Rijeka (Croatia)

Phone number: +385 99 432 7030

Email: nada.birkic1@gmail.com

EDUCATION AND QUALIFICATIONS

2021 – Present **PhD student - PhD program *Medicinal chemistry***

Faculty of biotechnology and drug development, University of Rijeka (Rijeka, Croatia)

Working on PhD thesis as a part of a Croatian science foundation (HRZZ) project *Diet derived eicosanoids and phenotype in sepsis (UIP-2020-02-2476)* under menthorship of dr. Christian A. Reynolds in a Laboratory for mass spectrometry

Relevant experience:

HPLC and Mass Spectrometry: extensive hands-on experience with LC-MS and LC-MS/MS techniques

Instruments:

Waters: Acquity UPLC I-Class system coupled to a Xevo TQD Triple Quadrupole Mass Spectrometer, SYNAPT G2-Si HDMS

Agilent: Agilent 1260 Infinity HPLC system coupled to a Triple Quadrupole Mass Spectrometer (QQQ), Agilent 1290 infinity II UPLC system coupled to a 6550 iFunnel Q-TOF Mass Spectrometer

Bruker: MALDI-TOF Mass Spectrometer

Software: proficient in MassLynx and TargetLynx (Waters) and MassHunter (Agilent) for qualitative and quantitative data acquisition, processing and reporting

2019 – 2021 **Master of Drug research and development**

Faculty of biotechnology and drug development, University of Rijeka (Rijeka, Croatia)

Master thesis title: *Antioxidant activity and stability of 6-amino-6-deoxy-L-ascorbic acid and N-methyl-6-amino-6-deoxy-L-ascorbic acid and their potential use in the cosmetic industry* under menthorship of dr. Karlo Wittine

Relevant experience: Exposure to multiple research laboratories, working as part of a research team, hands-on experience with spectrophotometric and mass spectrometry techniques, scientific writing and presentation, critical reading of the literature, experimental design and data analysis

2016 – 2019 **Bachelor of biotechnology and drug research**

Faculty of biotechnology and drug development, University of Rijeka (Rijeka, Croatia)

WORK EXPERIENCE

2021 – Present **Research and teaching assistant**

Faculty of biotechnology and drug development, University of Rijeka (Rijeka, Croatia); Laboratory for high throughput screening (Mass spectrometry)

Nov – Dec 2023 **Erasmus+ visiting PhD student**

Instituto De Fundació de Recerca Clínic Barcelona Institut d'Investigacions Biomèdiques August Pi i Sunyer (FRCB-IDIBAPS), University of Barcelona, (Barcelona, Spain)

Jul – Oct 2021 **Research trainee**

Faculty of biotechnology and drug development, University of Rijeka (Rijeka, Croatia); Laboratory for high throughput screening (Mass spectrometry)

2018 – 2020 **Chemistry instructor for elementary and high school education**

Mathrix, Rijeka (Rijeka, Croatia)

2019 **Professional practice**

Jadran Galenski Laboratory - JGL d.d., Rijeka (Rijeka, Croatia)

TEACHING EXPERIENCE

2021 – Present Faculty of biotechnology and drug development, University of Rijeka (Rijeka, Croatia)

BIL305 Bioassays in drug research

Giving lectures and supervising laboratory exercises on HPLC, mass spectrometry, and other instrumental techniques. Combining theoretical principles with practical training to familiarize students with modern analytical workflows

BIL107 Analytical chemistry

Conducting seminars focused on solving calculation-based problems and supervised laboratory classes, helping students apply theoretical concepts to analytical practice

BUM101 Systems biomedicine

Taught the use of the R programming language for biomedical data analysis, focusing on statistical approaches and data visualization

TRAINING AND ADDITIONAL EDUCATION

Jan – Jun 2025 **Pedagogical, Psychological, Didactic and Teaching Methodology Training Programme**

Faculty of Humanities and Social Sciences, Josip Juraj Strossmayer University of Osijek (Osijek, Croatia)

Oct 2023 **Transmission electron microscopy course**

Faculty of medicine, University of Rijeka (Rijeka, Croatia)

Jul 2023 **15th Mass Spectrometry in Biotechnology & Medicine Summer School**

Center for advanced academic studies, Dubrovnik (Dubrovnik, Croatia); Certificate in MSBM examination

Sep 2023 **Staff training for work with experimental animals (C category)**

Veterinarian faculty, University of Zagreb (Zagreb, Croatia); Certificate

Nov 2021 **Winter School Innovation Leaders in BioMed & Health**

Faculty of Pharmacy and biochemistry, University of Zagreb (Zagreb, Croatia)

CONFERENCE AND SEMINAR PARTICIPATIONS

2025 **Lipids in diet and health**. London, UK, 27-28 November; *Temporal changes in plasma 12,13-DiHOME concentrations following the induction of fecal peritonitis: a biomarker of sepsis-associated lung injury* (Oral presentation)

20th Waters Users Meeting. Lovran, Croatia, 10-12 June

2024 **FEBS3+ Meeting: Exploring Molecular Frontiers.** Pula, Croatia 25 – 28 September; **Birkić N**., Novak A., Ivanov A. M., Reynolds CA. *A Tandem mass spectrometry in combination with ion mobility for characterization of cardiolipin molecular diversity* (Poster presentation)

The 9th European Workshop on Lipid Mediators. Edinburgh, Scotland, 26-28 June

2nd Workshop on Mass Spectrometry in Life Sciences. Zagreb, Croatia, 19-20 September; **Birkic N**., Reynolds CA. *LC-MS/MS method development for quantification of omega-6 polyunsaturated fatty acid (PUFA)-derived lipid mediators* (Poster presentation)

2023

18th Waters Users Meeting. Opatija, Croatia, 13-15 June

15th Mass Spectrometry School in Biotechnology and Medicine. Dubrovnik, Croatia 02 - 08 July; Soldatić K., **Birkić N**., Minić Ž., Reynolds CA. *Development of an LC-MS/MS method for quantification of plasma short-chain fatty acids in a rat model of spinal cord injury* (Poster presentation)

2022

1st Workshop on Mass Spectrometry in Life Sciences. Zagreb, Croatia, 24-26 November

The 8th European Workshop on Lipid Mediators. Stockholm, Sweden, 29 June - 01 July; **Birkić N**., Svedružić Ž., Reynolds CA. *A molecular dynamics workflow for interrogating PUFA derived lipid mediator interactions with the TRPV1 channel* (Poster presentation)

Lipid yeast conference. Gothenburg, Sweden, 01-03 June

"SCIENCE AND US" 1st biomedicine and health PhD students congress with international participation. Rijeka, Croatia 19 - 20 May; **Birkić N**., Minić Ž., Azar T., Maddipati K. R., Reynolds CA. *Excessive dietary linoleic acid promotes plasma accumulation of pronociceptive fatty acyl lipid mediators* (Poster presentation)

Publications

2025

Saftić Martinović, Lara, **Birkic, Nada** et al.,Pavlešić, Tomislav; Planinić, Ana; Gobin, Ivana; Mišetić Ostojić, Dijana; Pedisić, Sandra, Chemical Characterization of Rare Unifloral Honeys of Ailanthus (Ailanthus altissima), Fennel (Foenicum vulgare), and Raspberry (Rubus idaeus) and their Antimicrobial and Antioxidant Activity Agricultural Research 14, 130–142 (2025). https://doi.org/10.1007/s40003-024-00754-2

2024 **Birkic, Nada**; Ožbolt, Eva; Reynolds, A. Christian; Pavlešić, Tomislav; Lučin, Ivana; Andabaka, Željko; Saftić Martinović, Lara. *Maturation of wine in underwater springs as a novel wine production process*. European Food Research and Technology, 2024, 250, 615–622 (2024). https://doi.org/10.1007/s00217-023-04410-x

2023 **Birkic**, **Nada**; Visentin, David; Svedružić, Željko; Reynolds, A. Christian. *Binding interactions of fatty acyl lipid mediators within the vanilloid pocket of TRPV1: A molecular dynamics study*. Prostaglandins & Other Lipid Mediators, 30;169:10677 (2023).

https://doi.org/10.1016/j.prostaglandins.2023.106771

Saftić Martinović, Lara; **Birkić, Nada**; Miletić, Vedran; Antolović, Roberto; Štanfel, Danijela; Wittine, Karlo. *Antioxidant Activity, Stability in Aqueous Medium and Molecular Docking/Dynamics Study of 6-Amino- and N-Methyl-6-amino-L-ascorbic Acid.* International journal of molecular sciences, 2023, 24: 1410; 24021410, 18. https://doi.org/10.3390/ijms24021410

2022 **Birkic, Nada**; Azar, Toni; Maddipati, Rao Krishna; Minic, Zeljka; Reynolds, A. Christian. *Excessive dietary linoleic acid promotes plasma accumulation of pronociceptive fatty acyl lipid mediators*. Scientific reports 12, 17832 (2022). https://doi.org/10.1038/s41598-022-21823-y

Language skills

Mother tongue(s): Croatian

Other language(s):

	Understanding		Speaking		Writing
	Leasening	Reading	Spoken interaction	Spoken production	
English	B2	B2	B2	B2	B2

Levels: A1 and A2: Basic user; B1 and B2: Independent user; C1 and C2: Proficient user

Digital skills

Competent with the Windows operating system, Graph-Pad Prism, lipid/protein databases, molecular modeling and visualization tools (e.g. PyMOL, UCSF Chimera, VMD) and R studio